NASA/TM–2017-219794

Greased Lightning (GL-10) Performance Flight Research – Flight Data Report

Robert G. McSwain and Louis J. Glaab
Langley Research Center, Hampton, Virginia

Colin R. Theodore
Ames Research Center, Moffett Field, California

November 2017

NASA STI Program . . . in Profile

Since its founding, NASA has been dedicated to the advancement of aeronautics and space science. The NASA scientific and technical information (STI) program plays a key part in helping NASA maintain this important role.

The NASA STI program operates under the auspices of the Agency Chief Information Officer. It collects, organizes, provides for archiving, and disseminates NASA's STI. The NASA STI program provides access to the NTRS Registered and its public interface, the NASA Technical Reports Server, thus providing one of the largest collections of aeronautical and space science STI in the world. Results are published in both non-NASA channels and by NASA in the NASA STI Report Series, which includes the following report types:

- TECHNICAL PUBLICATION. Reports of completed research or a major significant phase of research that present the results of NASA Programs and include extensive data or theoretical analysis. Includes compilations of significant scientific and technical data and information deemed to be of continuing reference value. NASA counter-part of peer-reviewed formal professional papers but has less stringent limitations on manuscript length and extent of graphic presentations.

- TECHNICAL MEMORANDUM. Scientific and technical findings that are preliminary or of specialized interest, e.g., quick release reports, working papers, and bibliographies that contain minimal annotation. Does not contain extensive analysis.

- CONTRACTOR REPORT. Scientific and technical findings by NASA-sponsored contractors and grantees.

- CONFERENCE PUBLICATION. Collected papers from scientific and technical conferences, symposia, seminars, or other meetings sponsored or co-sponsored by NASA.

- SPECIAL PUBLICATION. Scientific, technical, or historical information from NASA programs, projects, and missions, often concerned with subjects having substantial public interest.

- TECHNICAL TRANSLATION. English-language translations of foreign scientific and technical material pertinent to NASA's mission.

Specialized services also include organizing and publishing research results, distributing specialized research announcements and feeds, providing information desk and personal search support, and enabling data exchange services.

For more information about the NASA STI program, see the following:

- Access the NASA STI program home page at http://www.sti.nasa.gov

- E-mail your question to help@sti.nasa.gov

- Phone the NASA STI Information Desk at 757-864-9658

- Write to:
  NASA STI Information Desk
  Mail Stop 148
  NASA Langley Research Center
  Hampton, VA 23681-2199

NASA/TM–2017-219794

Greased Lightning (GL-10) Performance Flight Research – Flight Data Report

Robert G. McSwain and Louis J. Glaab
Langley Research Center, Hampton, Virginia

Colin R. Theodore
Ames Research Center, Moffett Field, California

National Aeronautics and
Space Administration

Langley Research Center
Hampton, Virginia 23681-2199

November 2017

Acknowledgments

The authors gratefully acknowledges the Aeronautics Research Mission Directorate Convergent Aeronautics Solutions Design Environment for Novel Vertical Lift Vehicles (CAS DELIVER) project which supported this work through NASA Langley Research Center. Special appreciation goes to the hard working team members who supported the collection of this flight research data:

DELIVER Principle Investigator
Colin Theodore, Ames Research Center, Moffett Field, California

DELIVER GL-10 Project Manager
Robert McSwain, Langley Research Center, Hampton, Virginia

Flight System Support
Arthur White, Dave Hare, Greg Howland, Lou Glaab, Michael Langford,
Scott Sealey, and Toby Comeaux
Langley Research Center, Hampton, Virginia

Flight Data System Support
Christine Odenwald, Jeff Brandt, Josh Carbonneau, Mark Jones, Mike Cooney,
Neil Coffey, and Sean Laughter
Langley Research Center, Hampton, Virginia

Operations Support
Brian Beaton, Jeff Hill, Mark Motter and Ryan Hammitt
Langley Research Center, Hampton, Virginia

Expertise and Council
Bill Fredericks, Dave North, David Christhilf, Nik Zawodny and Paul Rothhaar
Langley Research Center, Hampton, Virginia

Available from:

NASA STI Program / Mail Stop 148
NASA Langley Research Center
Hampton, VA 23681-2199
Fax: 757-864-6500

Contents

List of Figures

List of Tables

Abstract

Modern aircraft design methods have produced acceptable designs for large conventional aircraft performance. With revolutionary electronic propulsion technologies fueled by the growth in the small UAS (Unmanned Aerial Systems) industry, these same prediction models are being applied to new smaller, and experimental design concepts requiring a VTOL (Vertical Take Off and Landing) capability for ODM (On Demand Mobility). A 50% sub-scale GL-10 flight model was built and tested to demonstrate the transition from hover to forward flight utilizing DEP (Distributed Electric Propulsion)[1][2]. In 2016 plans were put in place to conduct performance flight testing on the 50% sub-scale GL-10 flight model to support a NASA project called DELIVER (Design Environment for Novel Vertical Lift Vehicles). DELIVER was investigating the feasibility of including smaller and more experimental aircraft configurations into a NASA design tool called NDARC (NASA Design and Analysis of Rotorcraft)[3]. This report covers the performance flight data collected during flight testing of the GL-10 50% sub-scale flight model conducted at Beaver Dam Airpark, VA. Overall the flight test data provides great insight into how well our existing conceptual design tools predict the performance of small scale experimental DEP concepts. Low fidelity conceptual design tools estimated the L/D_{max} of the GL-10 50% sub-scale flight model to be 16. Experimentally measured L/D_{max} for the GL-10 50% scale flight model was 7.2. The aerodynamic performance predicted versus measured highlights the complexity of wing and nacelle interactions which is not currently accounted for in existing low fidelity tools.

Introduction

The GL-10 flight model which was designed and built for demonstrating the feasibility of the tilt-wing/tilt-tail VTOL concept provided NASA with an opportunity to collect experimental flight data to use in verification of our current performance prediction models/tools. Performance flight research of the GL-10 was conducted in June 2017 to support the DELIVER project. A total of 22 flights were conducted which included: Functional Check Flights, Instrument Check Flights and Research Flights. In addition to providing data for NDARC, testing provided detailed transition flight data which has not been previously acquired for this unique phase of flight. After a series of ground system check-outs were completed, the GL-10 was flown on a vertical tether at the NASA Langley Landing Loads Facility. Once a hover flight was completed on tether, functional check flights and instrument check flights were conducted at Beaver Dam Airpark located in Elberon Virginia to ensure all systems were ready to begin performance research flights.

Nomenclature

AGL	Above Ground Level
Alpha	Angle of Attack
CAS	Convergent Aeronautics Solutions
CG	Center of Gravity
DEP	Distributed Electric Propulsion
DELIVER	Design Environment for Novel Vertical Lift Vehicles
ESC	Electronic Speed Controller
GL	Greased Lightning
LaRC	Langley Research Center
L/D	Lift to Drag Ratio
MAC	Mean Aerodynamic Chord
NDARC	NASA Design and Analysis of Rotorcraft
PWM	Pulse Width Modulation
UAS	Unmanned Aerial System
VTOL	Vertical Take Off and Landing

a	Glide Angle
$C_{L\ max}$	Maximum Lift Coefficient
h	Vertical Height
V_{stall}	Stall Speed
y	Flight Path Distance
α_f	Fuselage Angle of Attack
$\alpha_{w,stall}$	Wing Angle of Attack Stall
β_f	Fuselage Angle of Sideslip
θ_w	Wing Angle of Incidence
θ_t	Tail Angle of Incidence

Flight Model Specifications

The GL-10 flight model which can be seen in [Figure 1] is described in [Table 1].

Figure 1. GL-10 N528NU Hovering During Flight Tests

Table 1. NASA GL-10 N528NU Flight Model Specifications

sUAS Type	VTOL, 10 Motor, Brushless Motor
Propellers	Aeronaut CAM Carbon 16x8”
Motors	Scorpion SII-4020-360KV
Wingspan	124.8 in
Wing Area	1141.7 in^2
Mean Chord	9.67 in
MAC Leading Edge	25.9 in
Datum Reference	Nose
CG Station	32 in
Allowable CG Envelope	30-33 in
C.G. Relative to MAC	5.85 in Aft of Leading Edge (64%)
Maximum Take Off Weight	62 lbs
Empty Weight	46 lbs
Flight Research Weight	57.11 lbs
Flight Research CG in Forward Flight	31.75 in

A side view perspective of the GL-10 can be seen in [Figure 2]. A rear view perspective can be seen in [Figure 3]. A top view perspective can be seen in [Figure 4]. An isometric view perspective can be seen in [Figure 5].

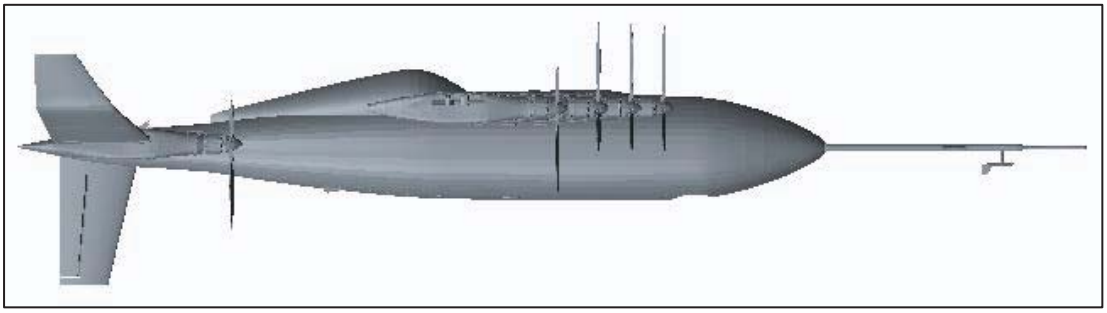

Figure 2. GL-10 CAD Side Model View

Figure 3. GL-10 CAD Rear Model View

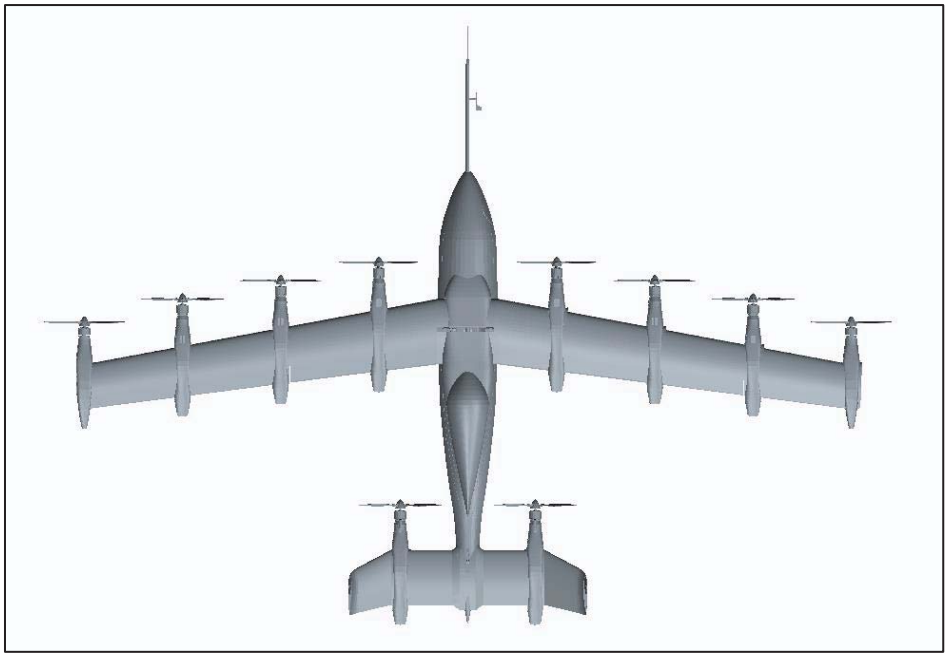

Figure 4. GL-10 CAD Top Model View

Figure 5. GL-10 CAD Isometric Model View

The MAC and associated reference dimensions can be seen in [Figure 6]. Utilizing CAD software a geometric method was used for determining the MAC [1].

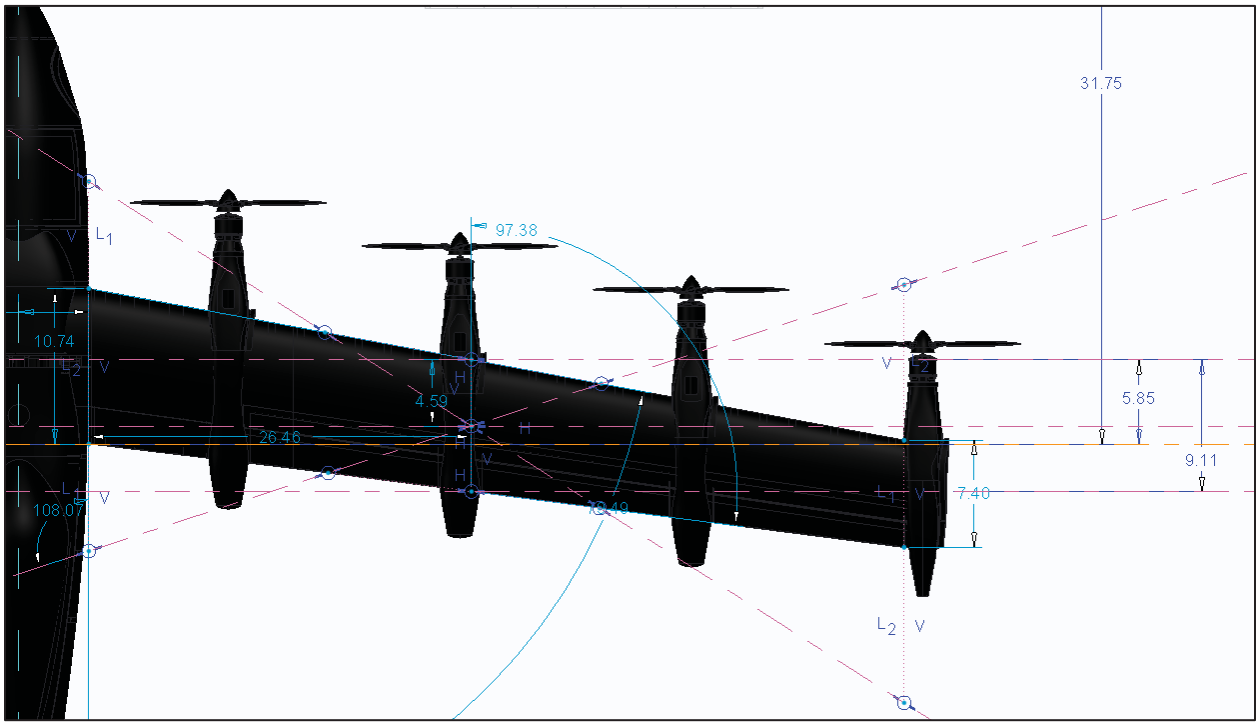

Figure 6. GL-10 MAC

The total weight of the aircraft during testing is broken down into several components in [Table 2]. This shows 13% of total take-off weight was used for batteries.

Table 2. GL-10 Weight Table

Empty Weight (lbs)	46
Battery Weight (lbs)	7.2
Data System Weight (lbs)	4.3
Take Off Weight (lbs)	57.5

The desired location of the CG along the longitudinal axis (CG_x) can be seen in [Figure 7]. The actual CG was measured by utilizing two weight scales. The permitted CG range was determined during the initial design work which can be seen in [Table 3].

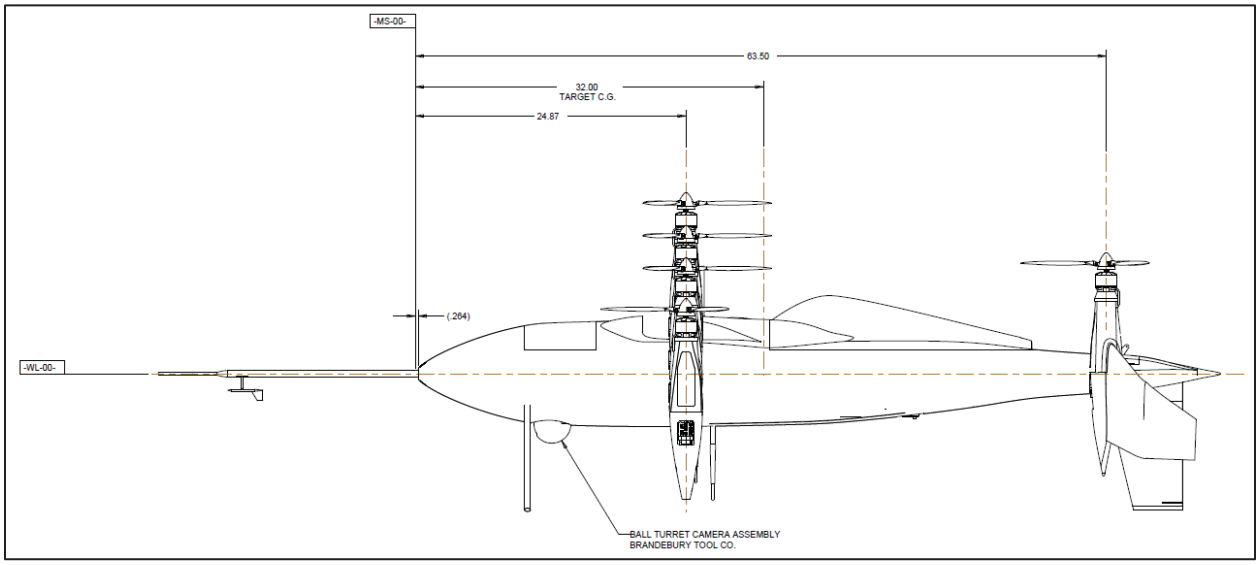

Figure 7. GL-10 CG_x Forward Flight Target

Table 3. GL-10 Forward Flight CG_x Range

CG_x Forward Limit (in)	30
CG_x Target Location (in)	32
CG_x Aft Limit (in)	33

The naming convention for motors and control surfaces can be seen in [Figure 8]. The red areas indicate the motor nacelles, and the blue areas indicate the control surfaces. This can be referenced to identify the specific motors either in the flight data, or throughout this report.

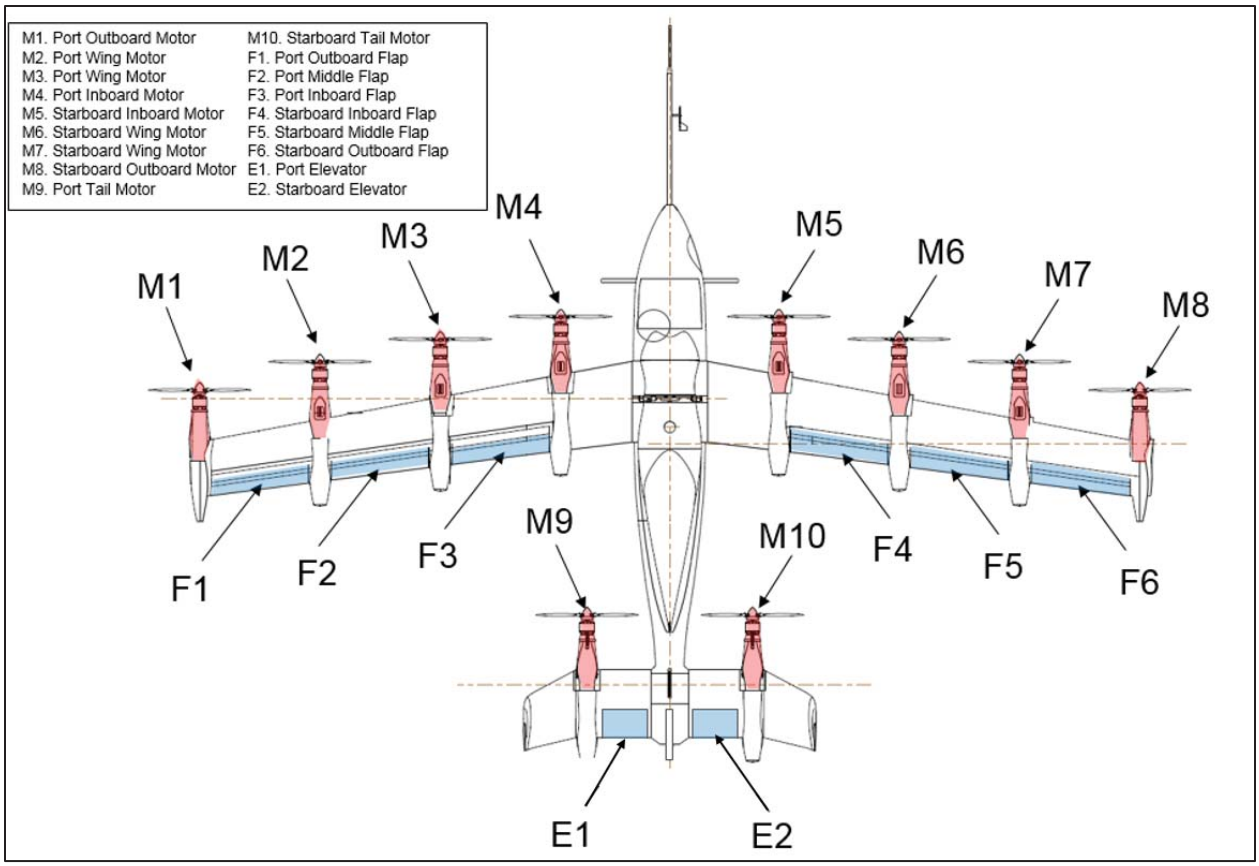

Figure 8. Top View of Motor and Control Surface Assignments

Flight Test Overview

To support performance research, the GL-10 which had only been used as a tilt wing/tail DEP VTOL demonstrator required instrumentation to be designed, fabricated, integrated, and tested to support data requirements. The performance metrics to be measured were power required during various modes of flight and L/D in forward flight. The data system also had the capability to record flight dynamics, which was desired to help provide insight into the transition dynamics for future tilt wing concepts. The modes tested included hover flight, outbound transition, powered straight and level forward flight, turning maneuvers, unpowered glide forward flight, and inbound transition.

Research Data Sensors

Flight Data System hardware on the aircraft consisted mostly of low cost commercial components. For propulsion data Castle Creations 50A Edge ESC's [Figure 9] combined with Castle Creations Castle Serial Links [Figure 10] were used to measure RPM and Battery Voltage. For power data Allegro ACS770KCB-150U-PFF-T current sensors [Figure 11] were used to measure battery current. For airspeed data a Honeywell HSCDRRD001PDAA5 pressure sensor was used to measure dynamic pressure. For air data a SpaceAge Control Alpha/Beta Pitot Probe [Figure 12] was used to measure angle of attack and angle of sideslip. For attitude, altitude and location data an Advanced Navigation Spatial INS was used to measure position, attitude and time. Betatronics Inc 25413 Potentiometers as seen in [Figure 13] were used to measure the wing and tail angle of incidence.

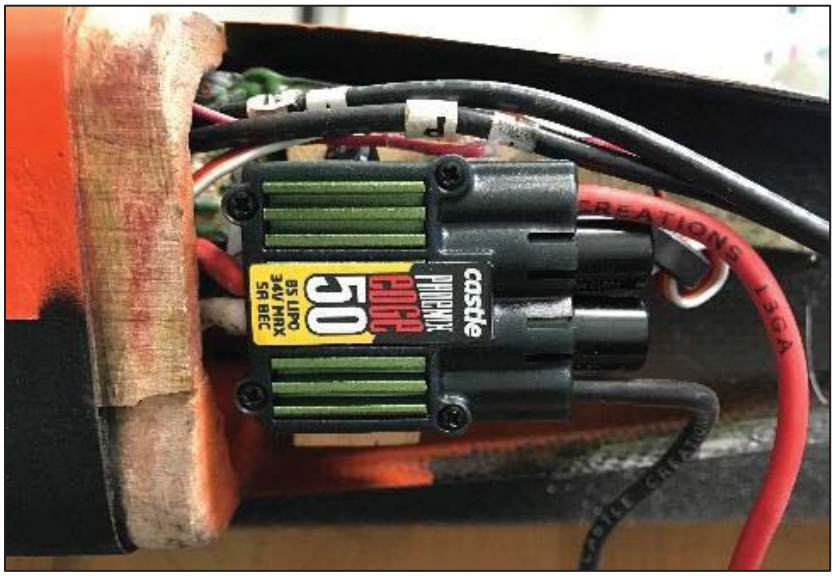

Figure 9. Motor 1 Nacelle w/Integrated ESC

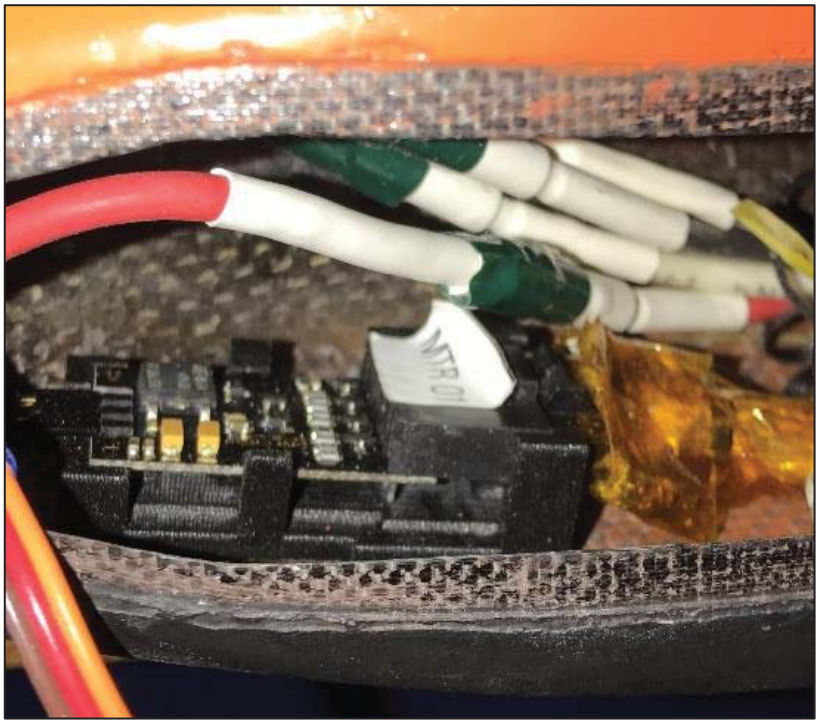

Figure 10. Motor 1 Nacelle w/Integrated Serial Link

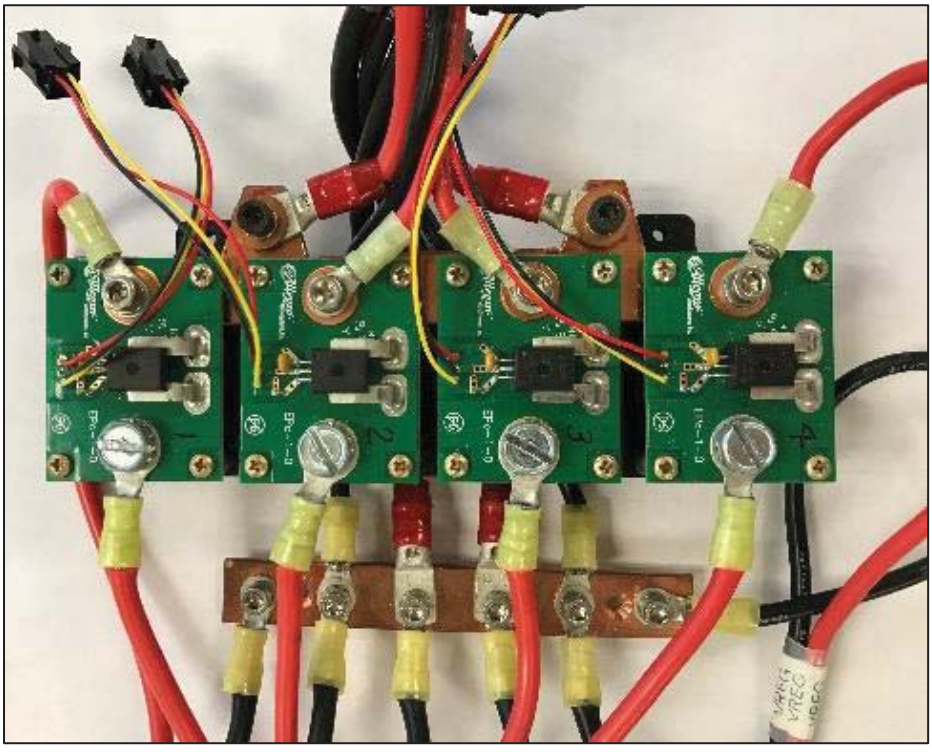

Figure 11. Power Bus w/Integrated Allegro 150A Current Sensors

Figure 12. SpaceAge Controls Alpha/Beta Pitot Tube


Figure 13. Tail Actuator Arm w/Integrated Potentiometer

Sensor Calibration

After installation of the data system, several data measurements were checked against calibrated sources to verify the data recorded produced expected engineering values. The alpha and beta vanes were calibrated using a 3D printed tool [Figure 14] which provided three reference points (-30°,0°,30°). The airspeed was calibrated using a Mensor Automated Pressure Calibrator [Figure 15]. It is worth noting that there is a low-end of airspeed around 22 kts, which was based on the sensor measured values below this airspeed producing imaginary numbers due to signal noise. The wing and tail angle potentiometers were referenced using a handheld digital angle meter application, a calibrated reference source was not available. The battery current sensors were calibrated using a West Mountain Radio Computerized Battery Analyzer [Figure 16]. The ESC RPM measurements were verified using a laser tachometer. The ESC Voltage measurement was verified using a DC power supply. The Spatial measurements were verified in the lab using an indoor GPS repeater and a handheld digital angle meter application.

Figure 14. Alpha/Beta Potentiometer Calibration Tool (-30°, 0°, 30°)

Figure 15. Pitot Probe Calibration Tool (Static/Dynamic)

Figure 16. 150A Current Sensor Calibration Tool

The following information in [Table 4] shows the measured data compared to the calibrated sources. It is worth noting that airspeed data was not filtered, so the measured value is the top of the noise band. This band was due to the supply voltage noise. The airspeed data used in plots throughout this report were smoothed and adjusted to compensate for the measured offset. The current data is only accurate when a load was being measured above 20A.

Table 4. Research Data Compared to Calibrated Sources

	Calibrated Source	Measured	Accuracy
Airspeed (kts)	45	46	+/- 1 *
Current (A)	150	150	+/- 1 **
Voltage (V)	29	28.9	+/- 0.1
AOA (deg)	0	0	+/- 1
AOS (deg)	0	0	+/- 1
RPM	3248	3628	+/-25***

* Recorded airspeed data not filtered, the top of the noise band measured 46 kts

** Recorded current accuracy valid above 20A

***Recorded RPM accuracy varied, this is valid during steady or small command signals changes

Test Site Location

Prior to DELIVER research activities the GL-10 had only conducted flights in restricted airspace at Fort A.P. Hill VA. To enable more flexibility in scheduling the research flights for DELIVER, a COA (Certificate of Authorization) was established at Beaver Dam Airpark, Elberon Virginia [Figure 17]. [Figure18] shows Beaver Dam is located about 1 hours from Langley Research Center. Local testing allowed for schedule flexibility based on personnel availability, weather, system availability, and UAS operations support equipment. It is worth noting that Beaver Dam Airpark offers a Class-G ceiling of 1,200 ft AGL, which can be seen in [Figure 19].

Figure 17. Google Earth View of Test Site

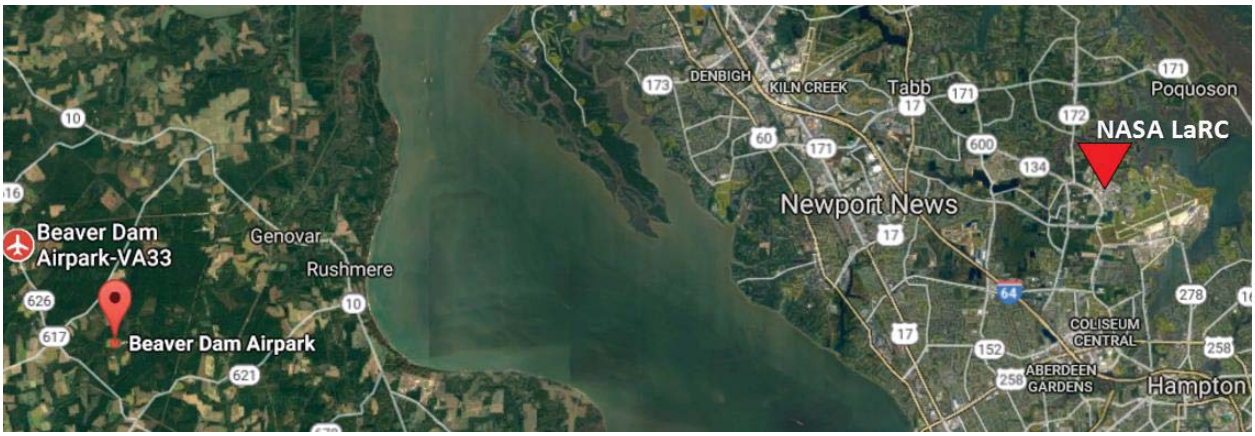

Figure 18. Google Earth View of Test Site Location Relative to NASA Langley

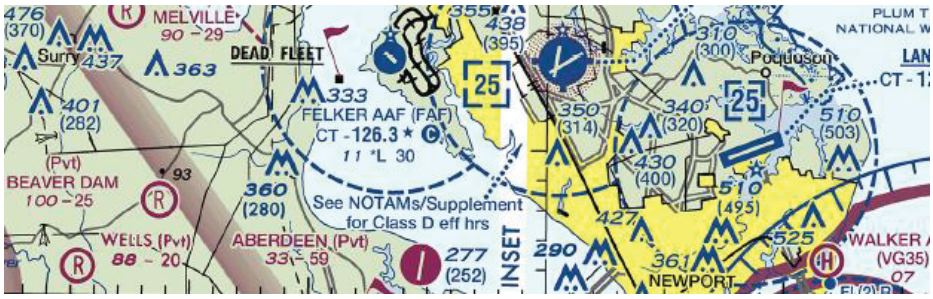

Figure 19. FAA Sectional Chart of Test Site

Support for flight operations required several personnel on-site, personnel in [Figure 20] from left to right included: Gregory Howland (GL-10 Technician), Dave Hare (GL-10 Technician), Robert McSwain (GL-10 Test Engineer), Lou Glaab (GL-10 External Pilot), Josh Carbonneau (GL-10 Software Engineer), Mark Agate (Intern), and Ryan Hammitt (Range Safety Officer).


Figure 20. Group Picture Taken at Beaver Dam Airpark, VA

Flight Test Cards

During the initial planning of the project, data was labeled as required vs. desired. The primary factor which determined if the data was required was based on resources, schedule and minimum success criteria. The performance data required for the research activity was determined by the DELIVER project and the following test cards were conducted:

Required:

- Hover Mode: Hover - Power required to sustain a constant altitude hover.
- Hover Mode: Climb – Power required during a various climb rates.
- Hover Mode: Descent – Power required during at various descent rates.
- Hover Mode: Forward Translation – Power required during forward translation in hover at various ground speeds.
- Fast Forward Flight Mode: Straight and Level – Power required during forward flight holding altitude with wings level at various airspeeds.
- Fast Forward Flight Mode: Climb – Power required during a climb at various airspeeds.
- Fast Forward Flight Mode: Descent – Power required during a descent at various airspeeds.

The performance data desired for the research activity was determined by the DELIVER project and the following test cards were conducted:

Desired:

- Fast Forward Flight Mode: Unpowered Glide – Glide with all motors off and propellers folded at various airspeeds.

It is worth noting that for Hover Mode, the wing and tail are at a 90° angle of incidence; For Fast Forward Flight Mode the wing is at a +4° angle of incidence, the tail neutral point is +2°, and the external pilot could command the tail +/- 12°.

Data requirements established by the project which were referenced in generating the flight test cards included:

Required:

- Airspeed
- Angle of Attack
- Angle of Sideslip
- Battery Current
- Power Bus Voltage
- Altitude
- Geographic Position
- Attitude
- Acceleration
- Angular Acceleration
- Aircraft Velocity
- Propeller RPM (4 Required, All Desired)

- Motor Power (4 Required, All Desired)

Desired:

- Wing Angle
- Tail Angle
- Wing Actuator Current
- Tail Actuator Current
- ESC Temperature
- Pilot Input
- Controller Output

Flight Data System

The flight data system consisted of the following hardware:

- Labjack T7
- Advanced Navigation Spatial INS
- Odriod XU4
- Odriod Shield
- Atmel XMEGAA3BU-XPLD-ND
- Castle Creations Phoenix Edge 50A ESC
- Castle Creations Serial Link
- Freewave MM2-T Radio
- Allegro 150A Current Sensor
- Allegro 50A Current Sensor
- SpaceAge Controls Alpha/Beta & Pitot Probe
- Honeywell Differential Pressure Sensor (HSCDRRD001PDAA5)
- Honeywell Static Pressure Sensor (SSCDANN015PAAA5)

A data system diagram is provided in [Figure 21]. This diagram is accurate with the exception of the airspeed and altitude air pressure sensors. The I2C pressure sensors were replaced with Honeywell analog sensors to allow the I2C bus to only deliver motor ESC data. This was based on the difficulties implementing the I2C bus throughout the vehicle, and not wanting to rely on the I2C bus for airspeed data in the event we had bandwidth issues.

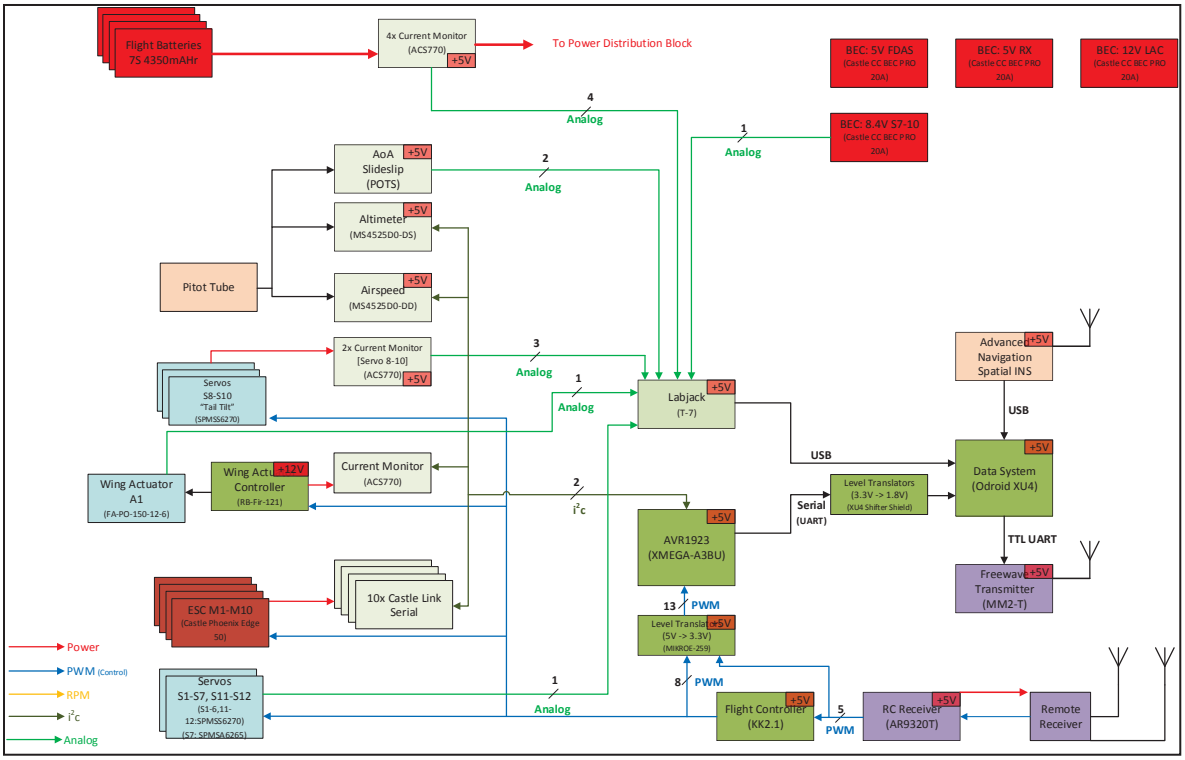

Figure 21. Data System Diagram

Flight Model Hybrid Electric Development

The full scale GL-10 concept was based on utilizing a hybrid electric propulsion system in conjunction with DEP. Although the GL-10 50% Scale flight model was originally built to demonstrate DEP and VTOL transitions of this concept, a generator was designed and built via a NASA Small Business Innovative Research Project based on GL-10 requirements. Launchpoint Technologies developed a 1.5kW generator [Figure 22] called a “Genset”. This generator was designed for the GL-10 to be used in forward flight to enable long endurance missions. The Genset was delivered to Langley Research Center on November 2016. DELIVER GL-10 performance flight testing provided experimentally measured power requirements for the GL-10, which can be referenced for making future decisions to integrate and develop the GL-10 50% Scale flight model into a hybrid electric testbed.

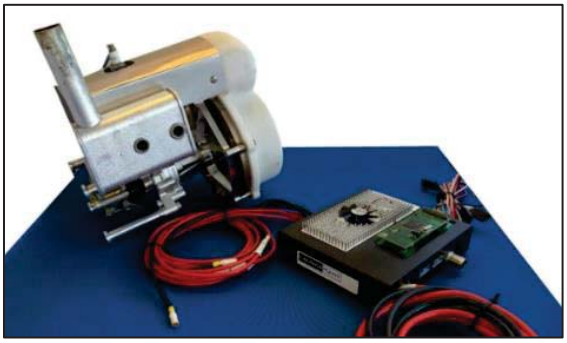

Figure 22. LaunchPoint Technologies 1500W Hybrid UAV Power System

Results

Transitions Flight Dynamics

A large amount of data were collected during flight testing which can be used to better understand the transition corridor and provide improvements in future tilt wing/tail DEP VTOL research activities. The transitions are handled by a flight controller through the use of RC control signal mixing and a programmed schedule for the wing and tail rotation between two modes of flight. The flight controller provides closed-loop feedback control utilizing body-axis angular rates and attitudes to help control the vehicle. During hover there are PID gains assigned, and there are separate PID gains assigned during forward flight. The settings to control the feedback gains for hover and FFF are blended linearly during transition. During hover the pilot input is mixed to assigned motor and servo outputs which correspond to a "Y-copter" multi-rotor configuration. During forward flight the pilot input is assigned as per the normal RC airplane configuration (aileron, elevator, throttle, and rudder). The scheduled rotation of the wing and tail [Figure 23] are set to a 10 second transition period where the mixing is slowly transferred from the Y-copter control (Mode 1) to the wing-borne forward flight control (Mode 2). The transition time of 10 seconds was based on the maximum speed of the main wing actuator, which required at least 10 seconds to translate the wing from 90° to 4°. Since the tail actuators could rotate faster than the wing actuators, the tail rotation schedule was adjusted to account for balancing pitch moments during transition. [Table 5] provides a high level summary of the controller outputs for the two different flight modes.

Table 5. Flight Controller Output RC Mixing

Controller Output Channel	OUT1	OUT2	OUT3	OUT4	OUT5	OUT6	OUT7	OUT8
Signal Destination	Tail Motors	Elevator Servos	Tail Rotation Servos	Aileron Servos	Port Motors	Wing Rotation Actuator	Starboard Motors	Rudder Servos
RC Input for Hover Mode	Throttle Elevator	Not Used	Programmed Schedule*	Rudder	Throttle Aileron	Programmed Schedule*	Throttle Aileron	Not Used
RC Input for Forward Flight Mode	Throttle	Elevator	Programmed Schedule*	Aileron	Throttle	Programmed Schedule*	Throttle	Rudder

*See [Figure 22] for schedule

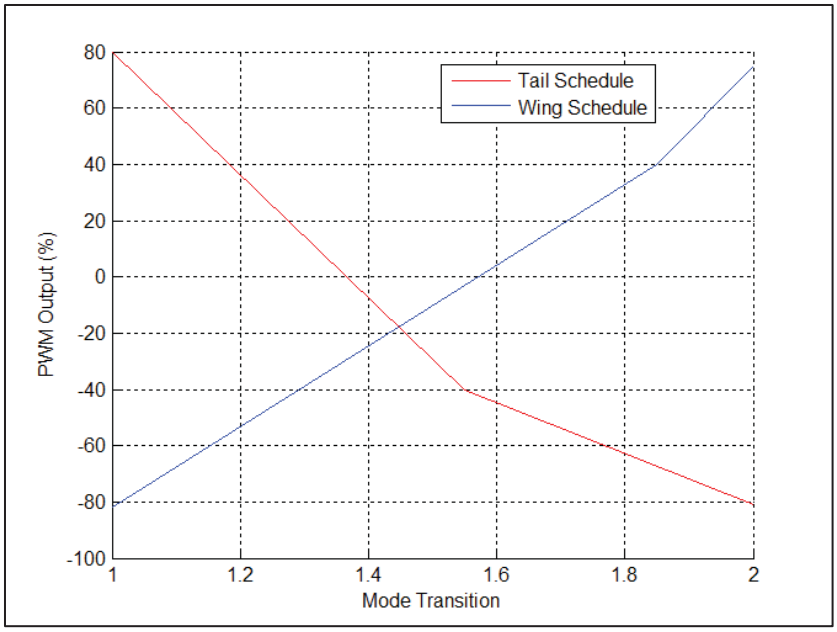

Figure 23. Wing/Tail Rotation Schedule

During research flights the most dynamic transitions were observed during outbound transitions. This can be seen in [Figure 24-25] where inbound transitions have a nice consistent slope indicating a controlled decrease in airspeed while wing angle of attack increased. The wing angle of attack is the sum of the air data probe angle of attack measurement and the wing angle of incidence measurement. During outbound transitions there is an uncontrolled variability in airspeed which is likely due to motor thrust not being adequate to overcome drag during segments of the transition. This deceleration would lead to stalls in the last half of transition. For analysis one method of comparison was to look at the differences between inbound and outbound initial conditions. Inbound transitions the wing angle of attack is low and airspeed is high. The motors primary function is attitude control during this transition since drag is providing the needed deceleration. The opposite case is observed during outbound transitions where motors have to provide thrust to overcome the drag to continue accelerating throughout the transition. The net moment from the motors needs to be carefully balanced to achieve smooth outbound transitions. This can be seen on the Flight 14 (Cyan Color) outbound transition as the airspeed begins to decrease, then the airspeed increases after a significant decrease in the wing angle of attack. Given the DEP, propulsion integration effects were significant.

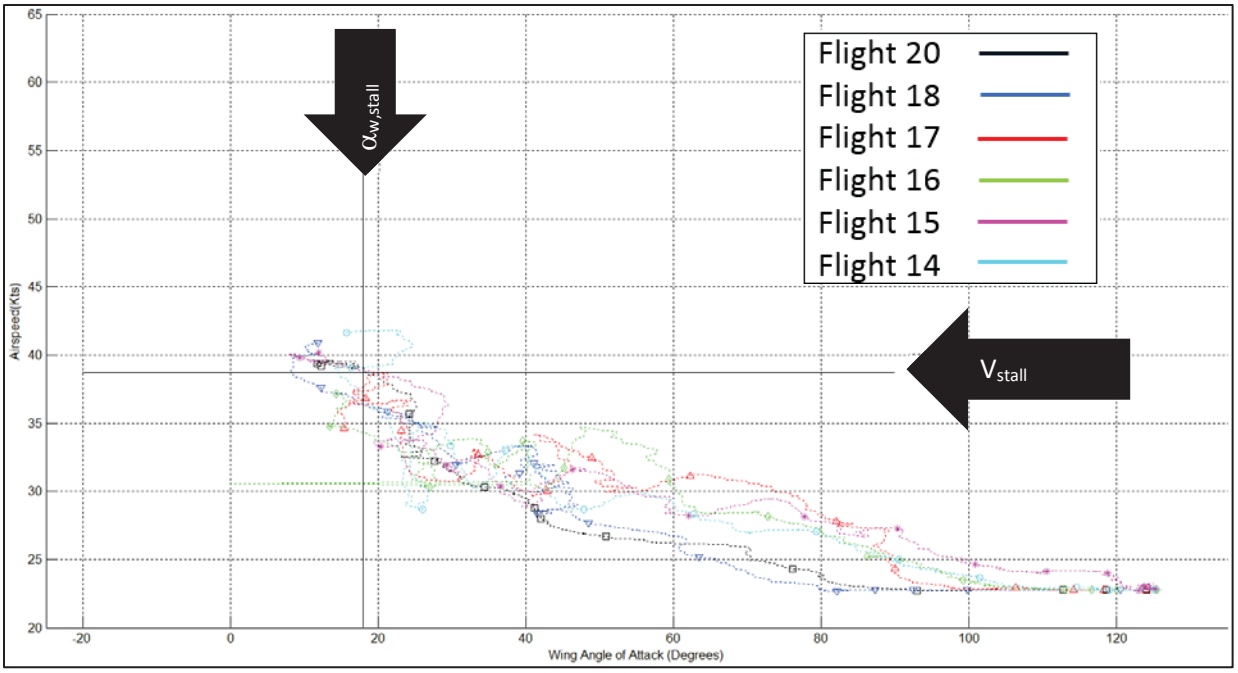

Figure 24. Inbound Transition Comparisons

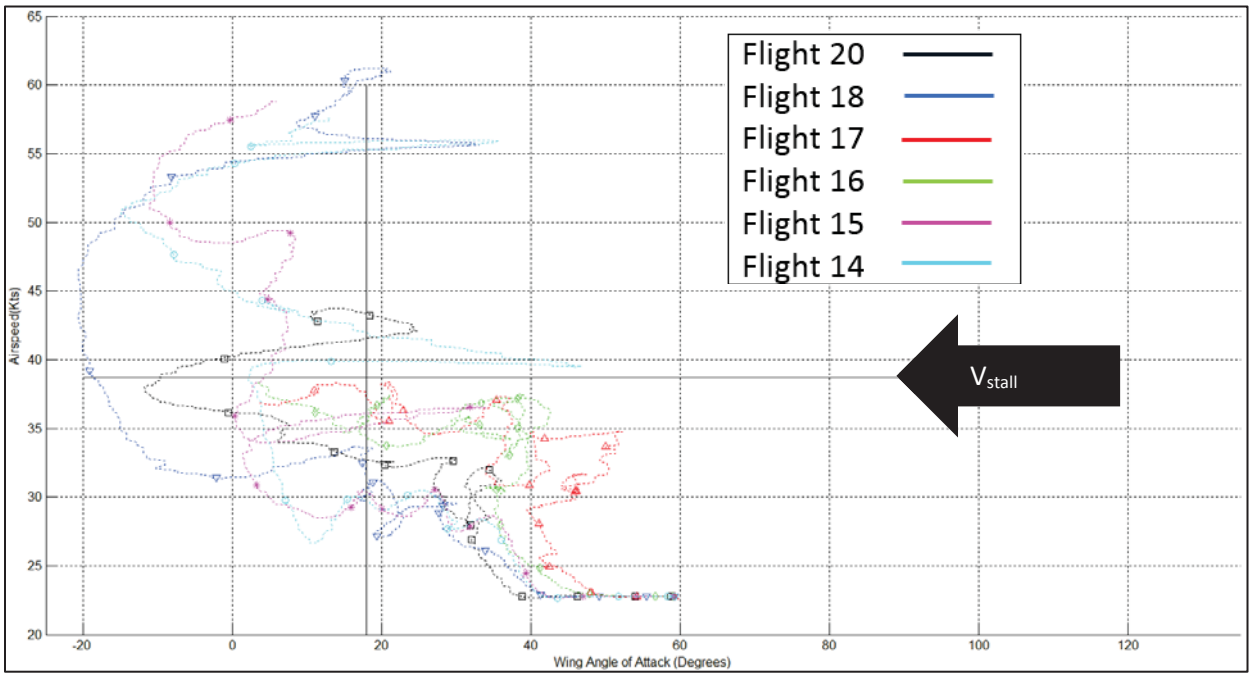

Figure 25. Outbound Transition Comparisons

Two reference lines are provided in the transition comparison plots: Wing stall alpha ($\alpha_{w,stall}$), and stall speed (V_{stall}). These values are based on wind tunnel data in [Figure 26] from a 30% sub-scale model shown in [Figure 27]. Specifically the $\alpha_{w,stall}$ was determined from an angle of attack of 14° at a $C_{l,max}$ of 1.37 plus 4° due to the wing angle of incidence totaling 18°. Wind tunnel data also provides a reference

for comparison with aerodynamic performance later in this report. The wind tunnel test conducted was during the previous research activity [4][5][6] which was focused on demonstrating the GL-10 concept transition. Test 164 run 175 in this figure was used as a baseline reference to compare the DELIVER data results with.

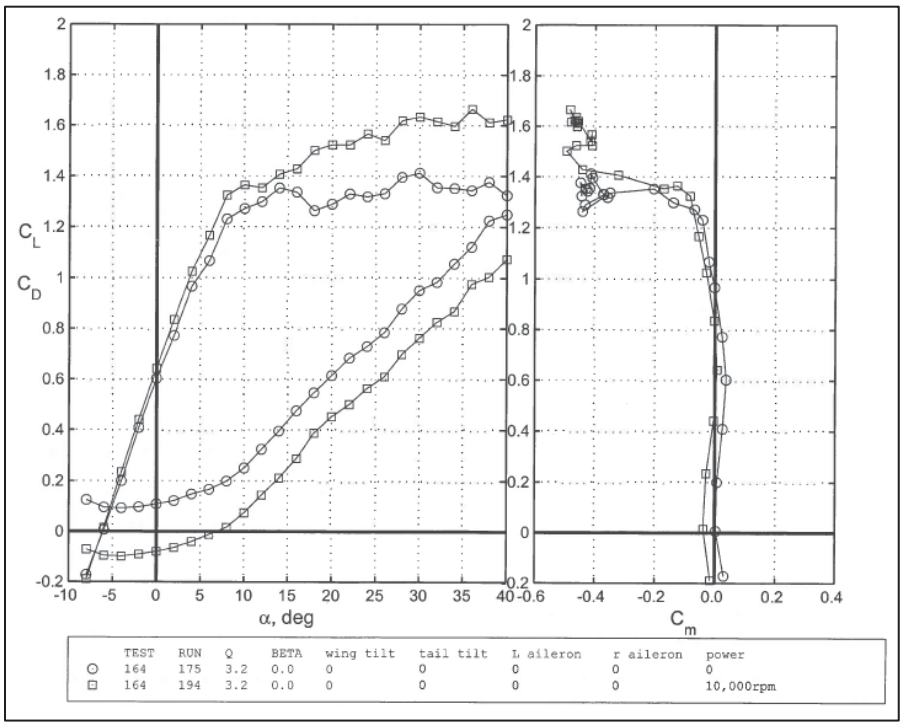

Figure 26. Wind Tunnel Model Aerodynamic Performance Reference (Q~30.7kts)

Figure 27. Design of Experiments GL-10 Controls 30% Scale Wind Tunnel Model

The aircraft stall alpha was based on the $C_{L\,max}$ observed in the wind tunnel data plot. The maximum lift coefficient recorded before a decrease in lift is 1.43, which occurs at an alpha of 14 degrees. This establishes a $C_{L\,max}$ of 1.43 and a stall alpha of 14°. The wing alpha stall is determined by adding the wing angle of incidence (+4°) which is 18°. This is only used since during the transition we are looking at the wing alpha in plots, rather than the fuselage. The wing stall speed was calculated by [Equation 1] utilizing this $C_{L\,max}$.

$$V_{stall} = \sqrt{\frac{2Wg}{\rho S C_{L_{max}}}} \tag{1}$$

Mass	W=25.9 kg
Gravity Acceleration	g=9.8 m/s^2
Air Density	ρ=1.255 kg/m^3
Wing Area	S=.737 m^3
Max Coefficient of Lift	$C_{L\,max}$ =1.43
Stall Speed	V_{stall} = 19.6 m/s (38.1 kts)

A challenge to tilt wing concepts like the GL-10 is the physical connection between propulsion thrust and wing lift. The angle between the thrust vector and the wing lift vector is constant because they are both rotated by the same actuator. This implies that thrust needs to be managed to both produce zero moments on the vehicle while also providing a total lift force (i.e. aerodynamic lift and propulsive lift) equal to the vehicle's weight. During initial stages of the transition, the amount of thrust provide for acceleration is very low due to the angles involved. During outbound transitions, it was observed that vehicle acceleration was very low as a result. This led to the situation where inadequate speed was developed leading to risks of stalls. An example of this dependence would be during the outbound transition, you cannot increase motor thrust to accelerate forward without also increasing lift from the motors. [Table 6] shows the initial conditions of the outbound transitions, as well as some transition characteristics observed based on [Figure 28-31]. Recommendations for improving the outbound transition are considered based on comparing the transition initial conditions and stability from several flights.

Table 6. Outbound Transition Initial Conditions

	Initial Pitch (deg)	Initial Throttle PWM (msec)	End Throttle PWM (msec)	Initial Climb Rate (ft/s)	Wing AoA @23 kts (deg)	Max Airspeed Deceleration Wing AoA/AS(deg/kts)	Maximum Throttle Delta (msec)	Max Sink Rate (ft/s)
Flight 14	-59	1.7	1.675	16	40	10/27	.15	-55
Flight 15	-45	1.675	1.625	23	40	12/28	.1	-65
Flight 16	-43	1.6	1.55	10	45	22/34	.05	-22
Flight 17	-39	1.6	1.525	12	47	37/32	.05	-24

Flight 18	-52	1.675	1.575	25	40	20/27	.125	-93
Flight 20	-35	1.6	1.525	15	36	31/27	.075	-30

Several characteristics were also recorded in the table to help identify trends that were associated with initial conditions that led to better transitions. The wing AoA at 23 kts indicates the wing AoA when the airspeed is in range of the airspeed sensor, this provides an indication of increased forward acceleration during the first half of the transition. The max airspeed deceleration indicates the wing AoA that had the most drag compared to the forward thrust from the motors, this provides an indication in the transition that requires more forward thrust. The maximum throttle delta indicates the maximum difference in PWM commands being sent to the wing motors and tail motors, which provides indication that wing and tail rotation schedule needs to be changed. The maximum sink rate indicates the severity of stalls during transition, which provides an overall grade of the transition with the ideal transition having no altitude loss. A method of single action transition (i.e. going from hover directly to FFF) was employed for this effort. An unbalance of thrust effects lead to significant challenges controlling the vehicle and very low vehicular accelerations in the early phases of transition. Given the test priorities for configuration control, no attempt was made to correct these thrust effects through adjustments of the tail angle or tail thrust schedule. The best outbound transition method developed herein was to start the transition at a low-thrust level just able to maintain level flight in hover, further decrease thrust through the transition, and use gravitational acceleration through shallow descents to gain airspeed. One recommendation form this effort would be to define a maximum speed and minimum wing angle for non-FFF flight and transition to this speed/wing angle combination and stabilize before progressing all the way to FFF. Another recommendation is to develop thrust schedules and tail angles to produce zero pitching moment on the vehicle for all wing/tail angles.

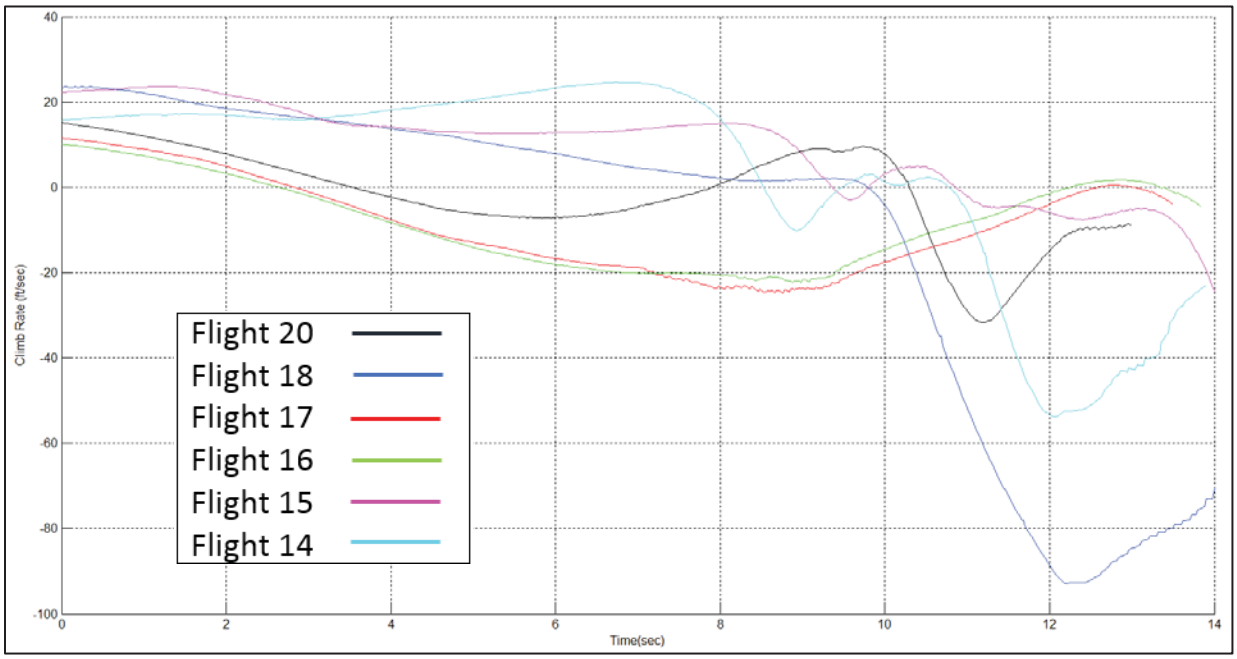

Figure 28. Outbound Transition Climb Characteristics

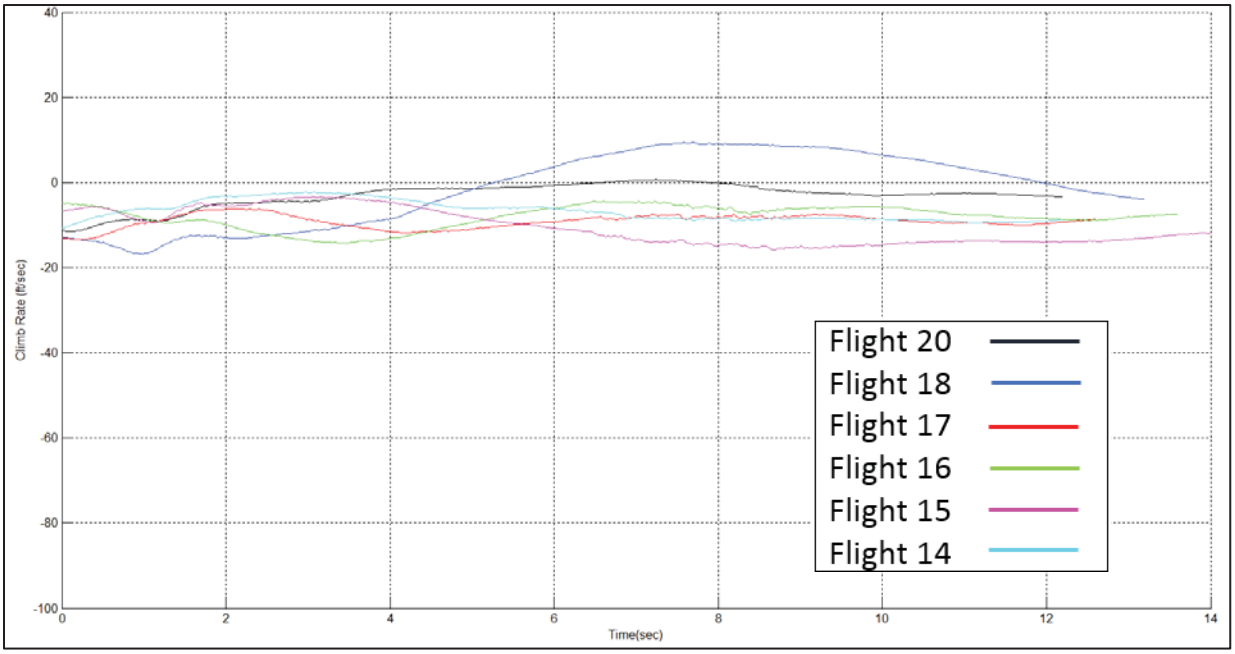

Figure 29. Inbound Transition Climb Characteristics

It is also worth noting there is also a differential thrust applied for pitch control which reduces forward thrust on 8 out of 10 motors to provide the pitching moments for control authority. The outbound transition motor commands indicate there is a nose up pitching moment which is being compensated for by a very large delta between wing and tail motor commands. A 1.8 msec command represents 100% power, while a 1.3 msec command represents 0% power. Flight 14 which had one of the least desirable outbound transitions used a 32% power delta between the tail and wing motor commands between 4 and 6 seconds after starting the transition. This large thrust delta between wing and tail motor commands indicated a significant nose up aerodynamic pitching moment was being applied during this portion of the transition. It is worth noting that even with this pitching moment applied from the motors differential thrust to counteract the aerodynamic pitch moment, the pitch attitude continued to nose up during this segment. Large pitching moments can be seen on Flight 14, 15, and 20 around T=5 with higher initial throttle values.

The wing and tail motor commands for each flights transition are indicated with a solid line for wing motors, and a dashed line for tail motors. This helps determine the pitching moment direction which the motors are generating.

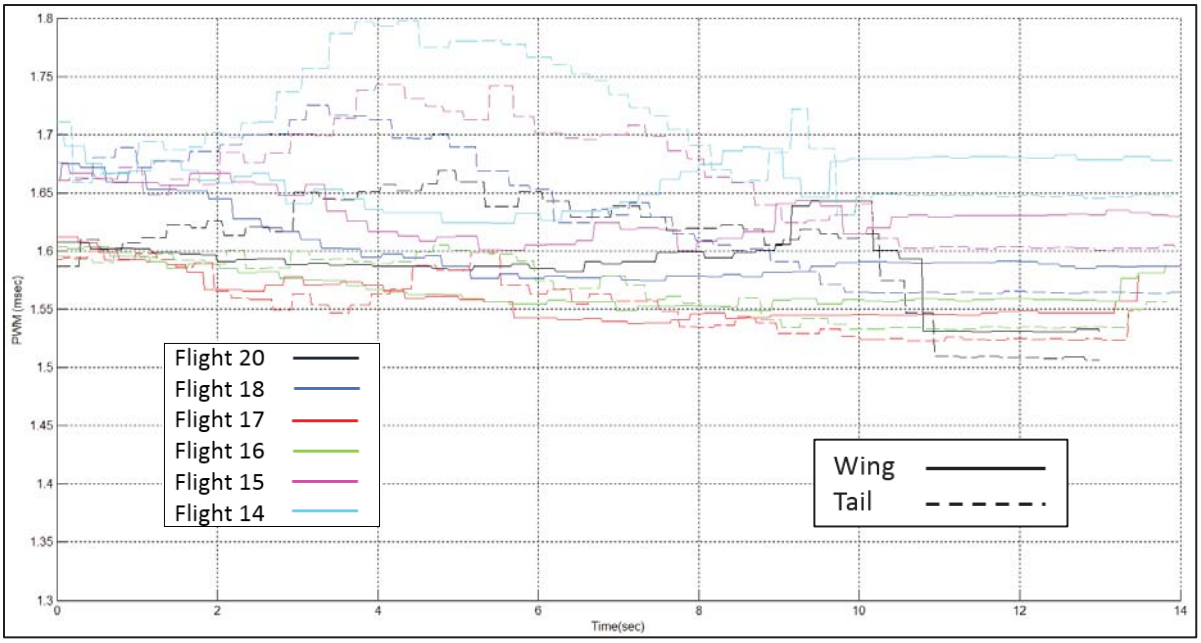

Figure 30. Outbound Transition Motor Commands

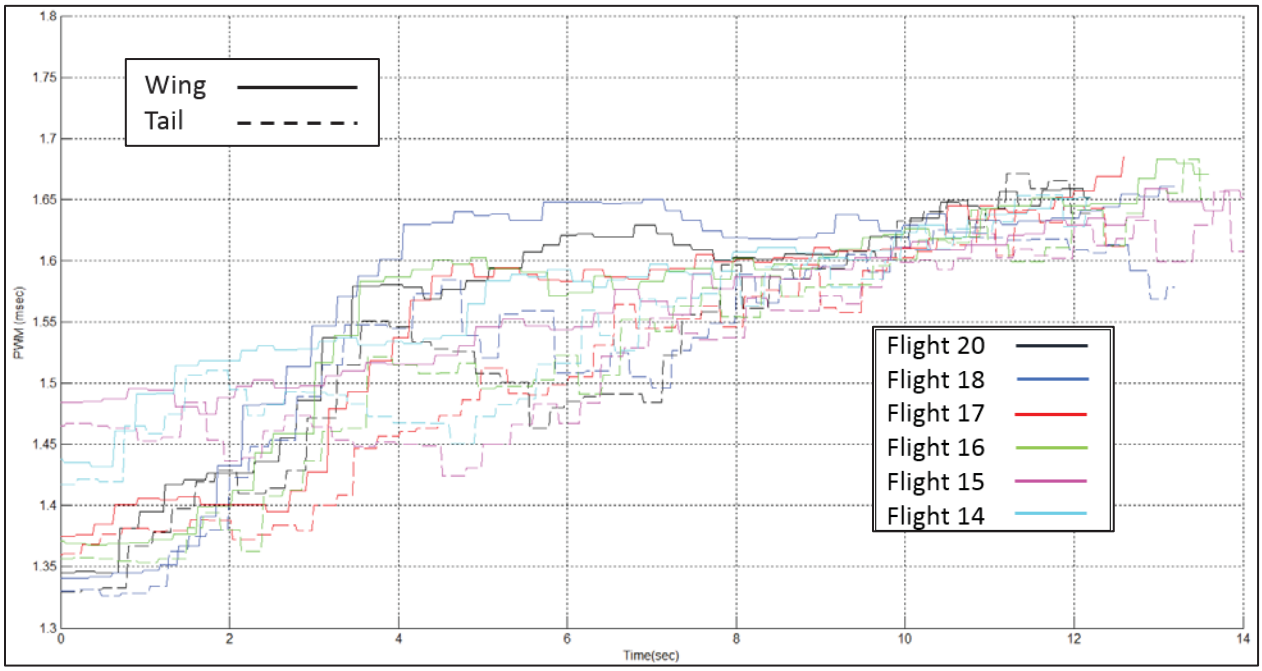

Figure 31. Inbound Transition Motor Commands

Flight 16 transition data in [Figure 32-36] provide a reference for the one of the best transition characteristics. All the transition data from the flights referenced for comparison can be viewed in [Appendix A] which can be useful for comparing the initial conditions, moments acting on the aircraft during transition, and understanding of the dynamics associated with the transition.

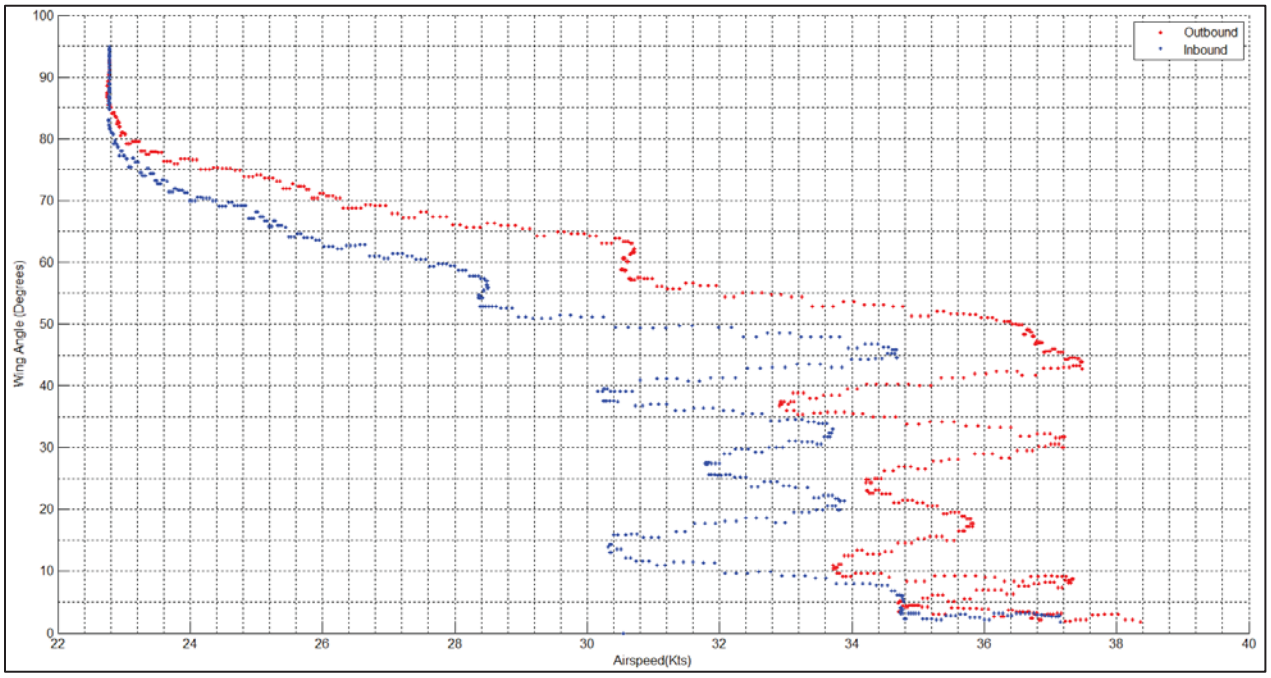

Figure 32. Flight 16 Transition Corridor W.R.T. Wing Angle Relative to the Fuselage

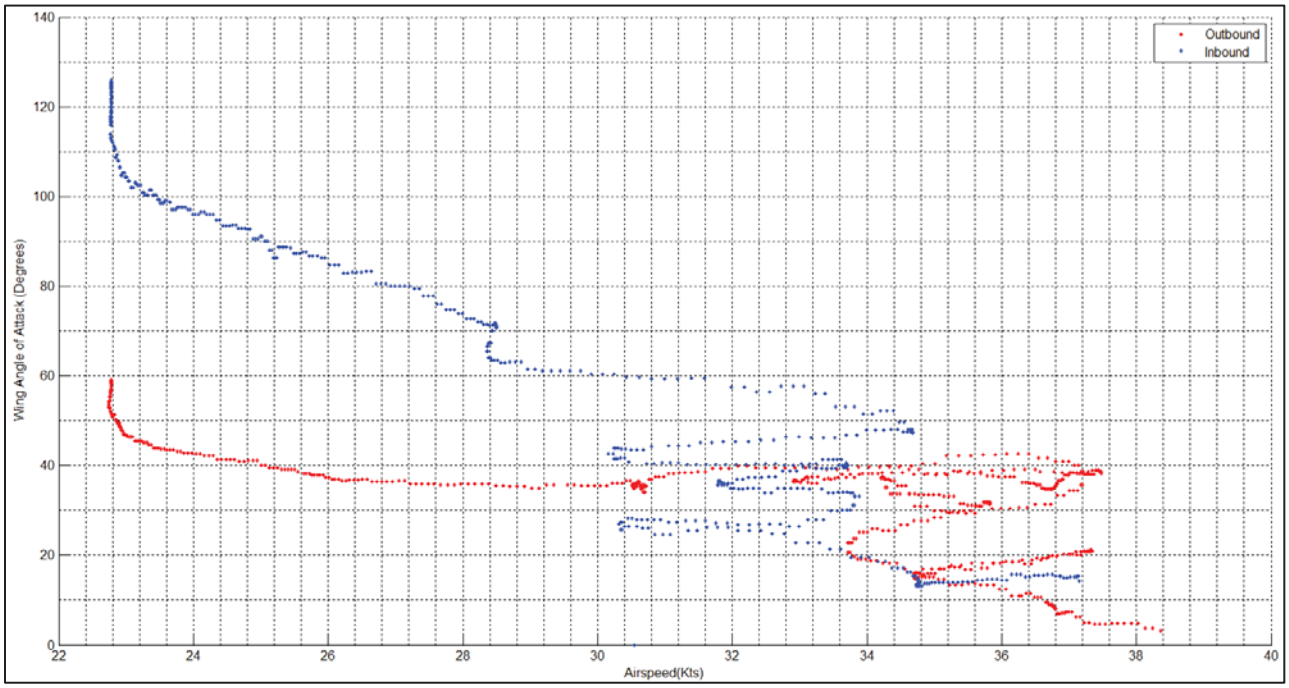

Figure 33. Flight 16 Transition Corridor W.R.T. Wing Angle of Attack Relative to the Freestream

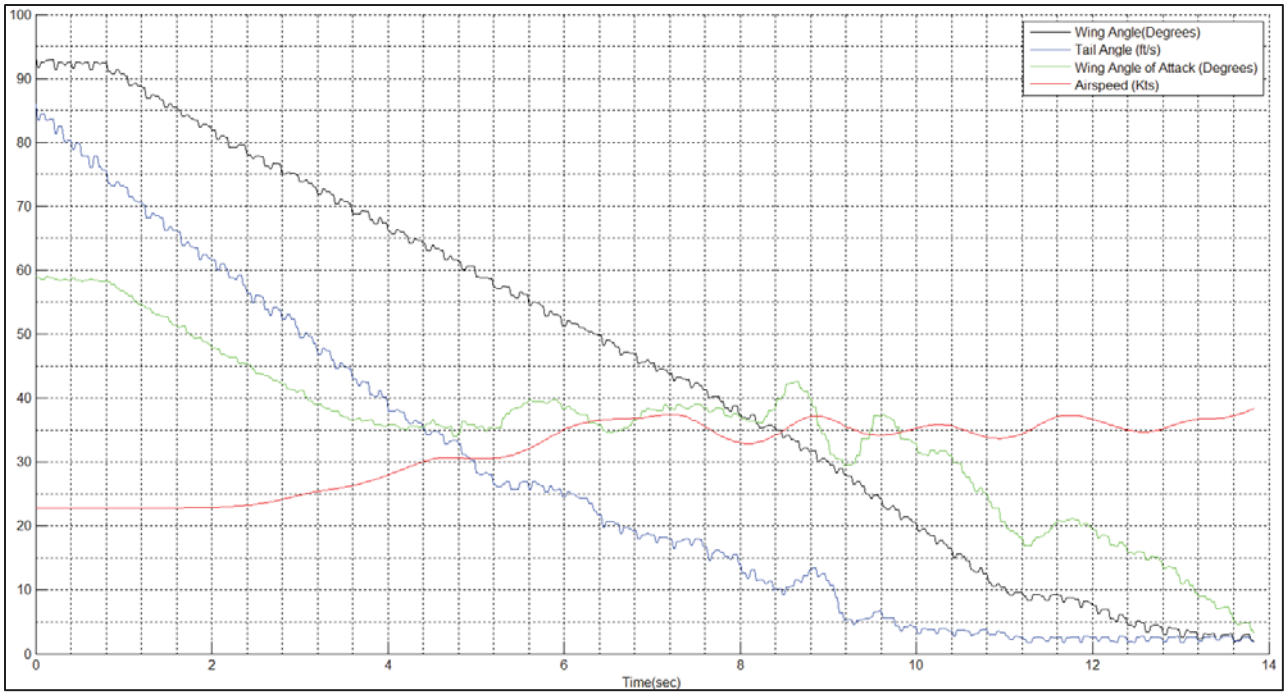

Figure 34. Flight 16 Outbound Transition Parameters W.R.T. Airspeed

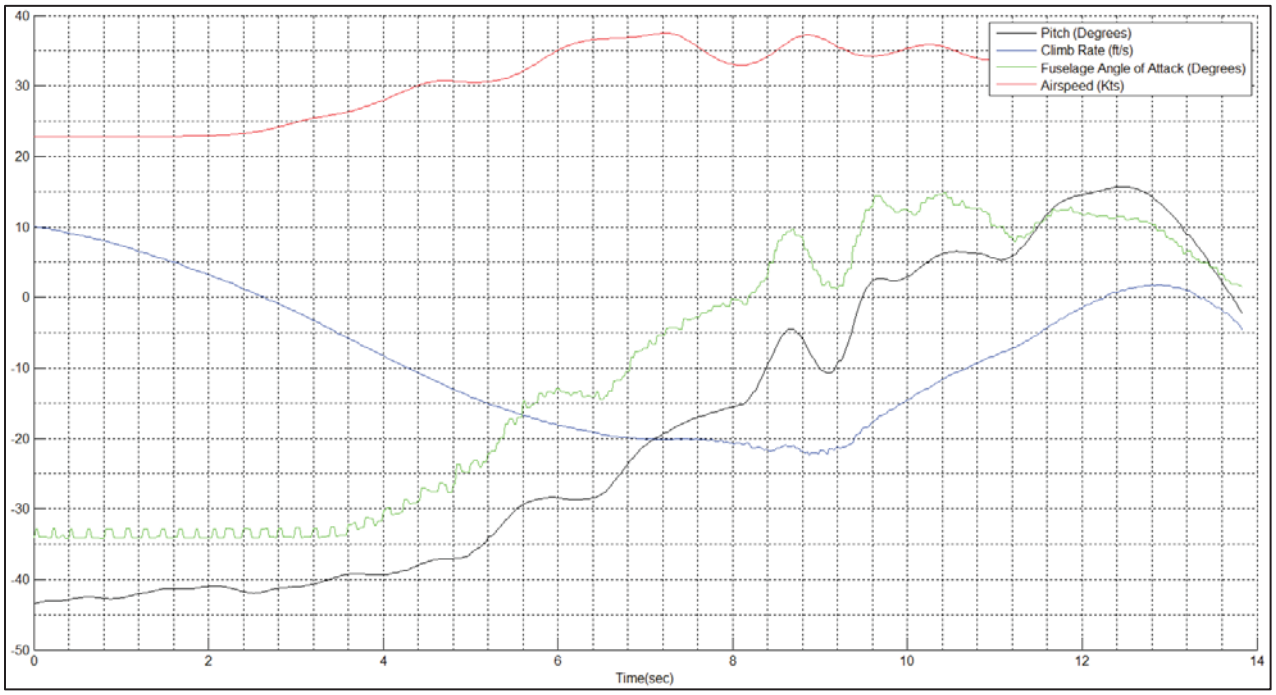

Figure 35. Flight 16 Outbound Transition Stability W.R.T. Airspeed

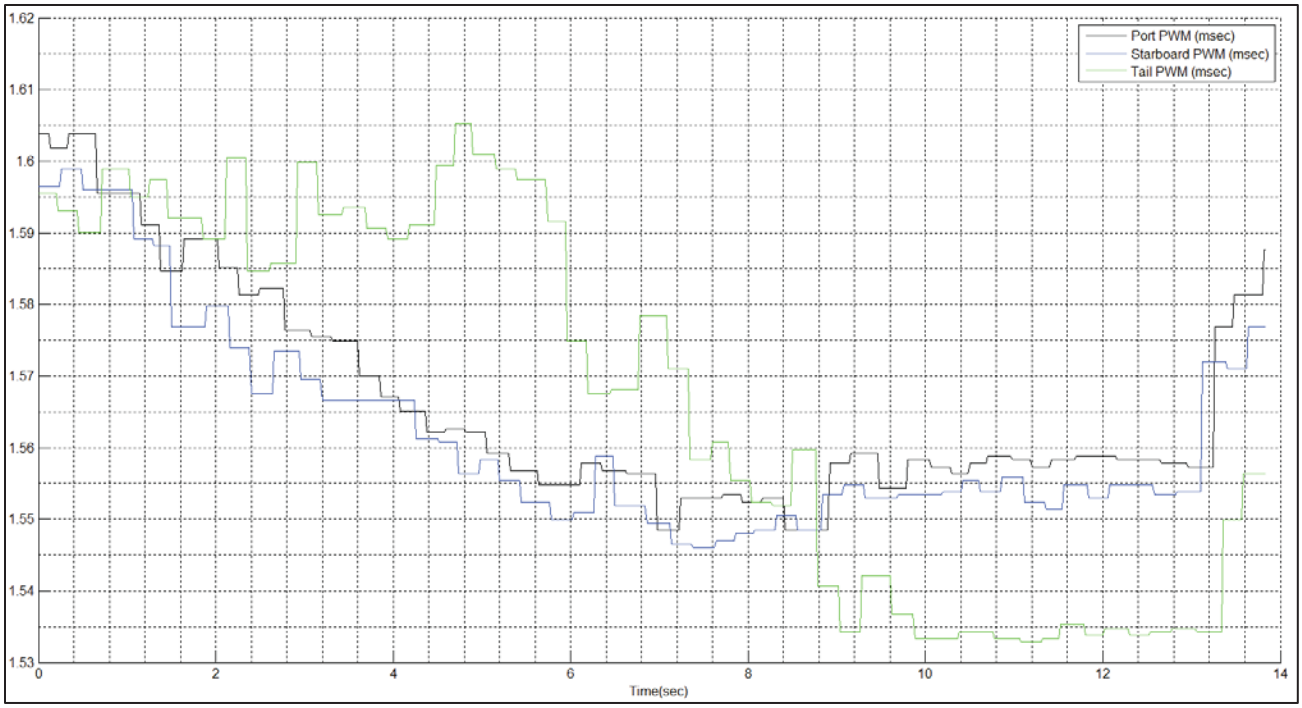

Figure 36. Flight 16 Motor Pitch and Thrust Characteristics

Powered Aerodynamic Performance

Aerodynamic performance can be measured looking at the Effective Lift to Drag Ratio (L/D_{eff}) [Equation 2] during level flight while maintaining a constant altitude. An example of this being used to calculate Flight 14 Data Run 1 is provided below. This assumes the lift generated is equal to the weight of the aircraft. This was measured during various flights by taking an average during straight and level flight data runs which can be seen in [Table 7-10]. The data plots for these mean values can be seen in [Appendix B]. The weight of the research aircraft was 57.5 lbs (255.8 N) for all flights and was constant throughout the entire flight since the power source was lithium polymer batteries.

$$L/D_{eff} = \frac{W_{Aircraft} V_{Cruise}}{P_{Required}} \quad (2)$$

Aircraft Weight	$W_{Aircraft}$ =255.8 kg*m*s^{-2}
Cruise Velocity	V_{Cruise} =22.7 m*s^{-1}
Power Required	$P_{Required}$ = 1140 kg*m^{2}*s^{-3}
Effective Lift to Drag Ratio	L/D_{eff} = 5.1

Table 7. GL-10 Experimentally Measured Effective L/D

	L/D_{eff}	Angle of Attack	Airspeed
Flight 14 Data Run 1	5	5	44
Flight 14 Data Run 2	6	4	47
Flight 14 Data Run 3	5	4	46
Flight 15 Data Run 1	4	2	49
Flight 18 Data Run 1	4	3	48

Although the best L/D_{eff} is 6, this data point has a 13 ft loss of altitude during the data run over 8 seconds. For the best data run we would want a height change of zero during the portion of data being averaged, and we would want the time period of the data collected to be as long as possible. Based on this consideration, the best measurement recorded for the GL-10 L/D_{eff} is 5 for an AoA of 5 and an airspeed of 44 kts. This indicates utilizing all motors during forward flight the aerodynamic performance of the GL-10 would be 25% better than the performance of a conventional helicopter. It is important to note this is the "dirtiest" form of the aircraft and it was not designed to be operated this way during long endurance missions when inboard motors would be turned off and only the wingtip motors would be used for forward flight. L/D_{eff} would be expected to increase with the limit of this increase being constrained by the "clean" aerodynamic performance without propellers deployed. This mode of operation with all motors on would only be used during short periods of time during take-off, climb out and landing.

Table 8. Flight 14 Powered Aerodynamic Data

Flight 14 Powered Straight and Level	Data Run 1	Data Run 2	Data Run 3
Mean AS (kts/mps)	44.1 / 22.7	46.7 / 24.0	45.9 / 23.6
Mean AOA(deg)	5.0	4.2	4.3
Mean Total Current (A)	40.8	35.4	43.2
Height Change(ft)	9.4	-13.6	-2.1
Time Change(sec)	17.3	8.6	3.3
Mean Port RPM	5400	5540	5680
Mean Starboard RPM	5530	5760	5820
Mean Tail RPM	5150	5390	5410
Mean Bus Voltage (V)	27.9	27.7	27.3
Mean Power(W)	1140	980	1180
Effective L/D	5.1	6.3	5.1

Table 9. Flight 15 Powered Aerodynamic Performance Data

Flight 15 Powered Straight and Level	Data Run 1
Mean AS (kts/mps)	48.6 / 24.98
Mean AOA(deg)	2.2
Mean Total Current(A)	56.3
Height Change(ft)	5.6
Time Change(sec)	9.1
Mean Port RPM	6140
Mean Starboard RPM	6220
Mean Tail RPM	5750
Mean Bus Voltage(V)	27.7
Mean Power(W)	1560
Effective L/D	4.1

Table 10. Flight 18 Powered Aerodynamic Performance Data

Flight 18 Powered Straight and Level	Data Run 1
Mean AS (kts/mps)	48.1 / 24.7
Mean AOA(deg)	3.1
Mean Total Current(A)	64.8
Height Change(ft)	2.1
Time Change(sec)	5.2
Mean Port RPM	6230
Mean Starboard RPM	6310
Mean Tail RPM	5820
Mean Bus Voltage(V)	27.7
Mean Power(W)	1800
Effective L/D	3.5

Flight Power Requirements

During flight testing power required for several modes of flight were recorded between zero and six kilowatts. The power required for all modes of operation of the GL-10 can be viewed in [Appendix C] for several flights.

For hover operations the maximum recorded power required was ~ 6 kW. This maximum power output was recorded during the beginning of take-off. During constant altitude hover operation prior to landing ~ 4.5 kW of power was recorded. This can be seen in the data run shown in [Table 11] which provides a mean value of variables. The data plots for these mean values can be seen in [Figure 36]. Throughout flight tests ~ 3.5 kW of power was required at times during descents.

Table 11. Hover Altitude Hold Data Run Values

Flight 16	Hover 1
Mean Lateral Velocity(ft/sec)	1.7
Mean Pitch(deg)	-6
Mean Roll(deg)	1
Mean System Current(A)	174.6
Height Change(ft)	-.6
Time Change(sec)	20.4
Mean Port RPM	5610
Mean Starboard RPM	5550
Mean Tail RPM	4820
Mean Bus Voltage (V)	25.3
Mean Power(W)	4412

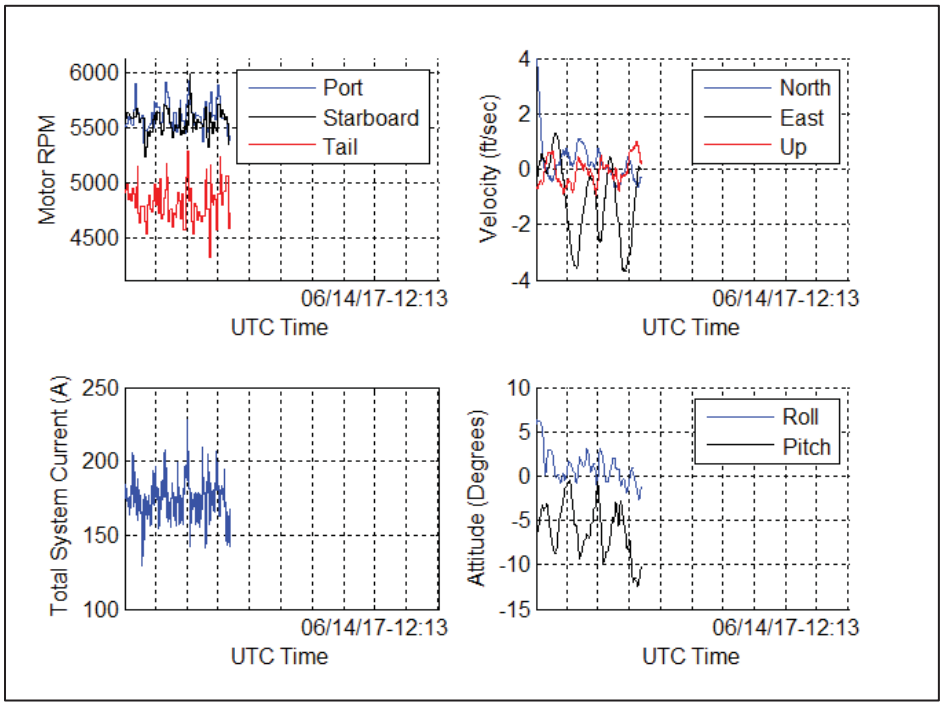

Figure 37. Flight 16 Hover Data Run 1

For forward flight operations with all motors providing thrust the maximum recorded power required was ~ 3 kW. This maximum power output was during climbs. Throughout flights approximately 1.5 kW was required to sustain straight and level flight. At various airspeeds this would change as indicated in the data runs provided. The lowest power observed during descent was .75 kW, not including unpowered glides. These recorded power levels provide the range of power required for all modes of operation with the aircraft at a take-off weight of 57.5 lbs (255.8 N).

Unpowered Aerodynamic Performance

The flight model during this flight test did not have the capability to shutdown individual motors. This is due to the original flight controller setup used for demonstrating the transition, which meant the "clean" aerodynamic performance would be measured with all motors off utilizing [Equation 3-5] which can be used during unpowered glides with a constant glide slope.

$$\frac{L}{D} = \frac{C_l}{C_d} = \frac{1}{\tan a} \tag{3}$$

$$a = \sin^{-1}\frac{h}{y} \tag{4}$$

$$y = V_{Airspeed} \cos \alpha_f \, t_{datarun} \tag{5}$$

Flight Path Airspeed	$V_{Airspeed}$ = 68.6 ft*sec^{-1}
Fuselage Alpha	α_f = .137881 rad
Data Run Time Period	$t_{datarun}$ = 14.06 sec
Height	h = 108.8 ft
Glide Angle	a = 6.54 °= .11414 rad
Lift to Drag Ratio	L/D = 8.7

Conducting unpowered glides introduced a new flight envelope for the aircraft since previous flight testing was focused on transitioning the aircraft from hover to forward flight. Due to this envelope expansion these flight were conducted after the required hover and forward flight research flights were completed. A build-up approach was used, which can be seen in Flight 21 and Flight 22 where several data runs had wind milling observed from the propellers. These two flights led to two configuration changes to enable folding propellers: 1) Increasing the brake power applied by the ESC when throttle was set to zero; 2) Loosening the folding propellers collar attachment screws. These two changes enabled the propellers to fold on Flight 22 when the motors were stopped using the electronic brake during the glide data runs. Flight 21 had wind-milling observed in the data shown in [Table 12], these measurements do not provide confidence in repeatability since there was variance in which propellers wind-milled on each glide. Propellers were observed to be folded during Flight 22 unpowered glides providing a more consistent measurement of the "clean" aerodynamic performance which can be seen in [Table 13].

Table 12. Propeller(s) Wind-milling Performance Measurements

Flight 21	Mean AS (kts)	Mean AOA (deg)	Mean L/D
Glide 1	40	8	4.8
Glide 2	45	4	7.5
Glide 3	41	8	8.7
Glide 4	43	6	6.5

Table 13. Propeller(s) Folded Performance Measurements

Flight 22	Mean AS (kts)	Mean AOA (deg)	Mean L/D
Glide 1	52	1	6.5
Glide 2	45	4	7.1
Glide 3	40	7	7.4

The mean values used for determining these flight performance measurements are indicated in [Table 14-15]. There are also plots for these averaged parameters which can be found in [Appendix D]. The plots found in the appendix gives insights on the data runs which provide measurements outside of expectations. For example in Data Run 3 there is a measured value of 8.7 L/D for an AOA of 8, this value does not fall within expected bounds because there is a large variation in the airspeed, angle of attack, and climb rate which can be observed in the appendix plots. This allows these measured values to have qualitative confidence assigned to them.

Table 14. Flight 21 Unpowered Glide Mean Measurements

Flight 21 Unpowered Glides	Data Run 1	Data Run 2	Data Run 3	Data Run 4
Propeller Wind-milling	Yes	Yes	Yes	Yes
Vertical Height(ft)	92.9	102.9	108.8	151.5
Mean AS (ft/s)	67.9	76.4	68.6	72.5
Mean GS (ft/s)	78.0	88	64.0	66.1
Time Change(sec)	6.82	10.3	14.06	13.9
AS Flight Path Distance(ft)	458.5	784.2	956.0	1000.2
Glide Slope(deg)	11.7	7.5	6.5	8.7
L/D	4.8	7.5	8.7	6.5
Mean AS (kts)	40.2	45	40.7	43.0
Mean AoA (deg)	7.8	3.7	7.9	6.1

Table 15. Flight 22 Unpowered Glide Mean Measurements

Flight 22 Unpowered Glides	Data Run 1	Data Run 2	Data Run 3
Propeller Wind-milling	No	No	No
Vertical Height(ft)	105	52.8	105
Mean AS (ft/s)	85.3	76.0	66.7
Mean GS (ft/s)	76.3	68.9	62.0
Time Change (sec)	7.84	5.02	-11.86
AS Flight Path Distance (ft)	694.7	380.5	785.2
Glide Slope (deg)	8.7	8.0	7.7
L/D	6.5	7.1	7.4
Mean AS (kts)	52.5	45	39.5
Mean AoA (deg)	.71	3.7	7

Conclusion

The flight data collected during DELIVER research flights provides a database to verify aircraft performance predictions tools currently used at NASA for small unconventional aircraft designs. In addition, the current effort provides a wealth of data regarding hybrid VTOL transition characteristics and flight dynamics. These data can also be used for mission planning of the GL-10 flight model, the estimated power required for a variety of flight modes can be seen in [Table 16]. These values can be used to determine power system benchmarks requirements for the operation of the GL-10 concept at a ~55lb vehicle scale.

Table 16. Power Required for Different Modes of Flight

Mode	Motors	Phase	Power
Hover	All Used	Take-Off	6 kW
Hover	All Used	Altitude Hold	4.5 kW
Hover	All Used	Descent	3.5 kW
Forward Flight*	All Used	Climb	3 kW
Forward Flight*	All Used	Level Flight	1.5 kW
Forward Flight*	All Used	Descent	.75 kW

*All 10 Motor Used, more efficient configurations possible

Power required for forward flight at 45kts has been measured at 1.2kW, this verifies that a 1.5kW generator could sustain the GL-10 in forward flight for long endurance missions provided the take-off weight could be maintained. Although the integration of the Genset would not be trivial, it is worth noting that the 1.2kW power required is for a “Dirty” aerodynamic configuration (All motors on) which would be used for take-off and landing phases of flight. The power required would go down if only the outboard wing motors were used for a long endurance cruise phase. Based on the experimentally measured L/D_{max} the power required for a long endurance cruise phase could go as low as 800W.

The best outbound transition method developed herein was to start the transition at a low-thrust level just able to maintain level flight in hover, further decrease thrust through the transition, and use gravitational acceleration through shallow descents to gain airspeed. One recommendation from this effort would be to define an airspeed and wing angle to transition to prior to FFF accounting for the expected deceleration before progressing all the way to FFF. Another recommendation is to develop thrust schedules and tail angles to produce zero pitching moment on the vehicle for all wing/tail angles.

Aerodynamic data collected during DELIVER indicates the GL-10 flight model has an L/D_{max} of 7.2 which is achieved at an angle of attack of 5° at a speed of 45 kts. Wind tunnel data which was collected for controls research provides a reference to compare the flight test measurements against [Figure 37]. Between both of these measurement methods the GL-10 concept has demonstrated a 75% increase in aerodynamic performance from a conventional helicopter design ($L/D_{max} = 4$).

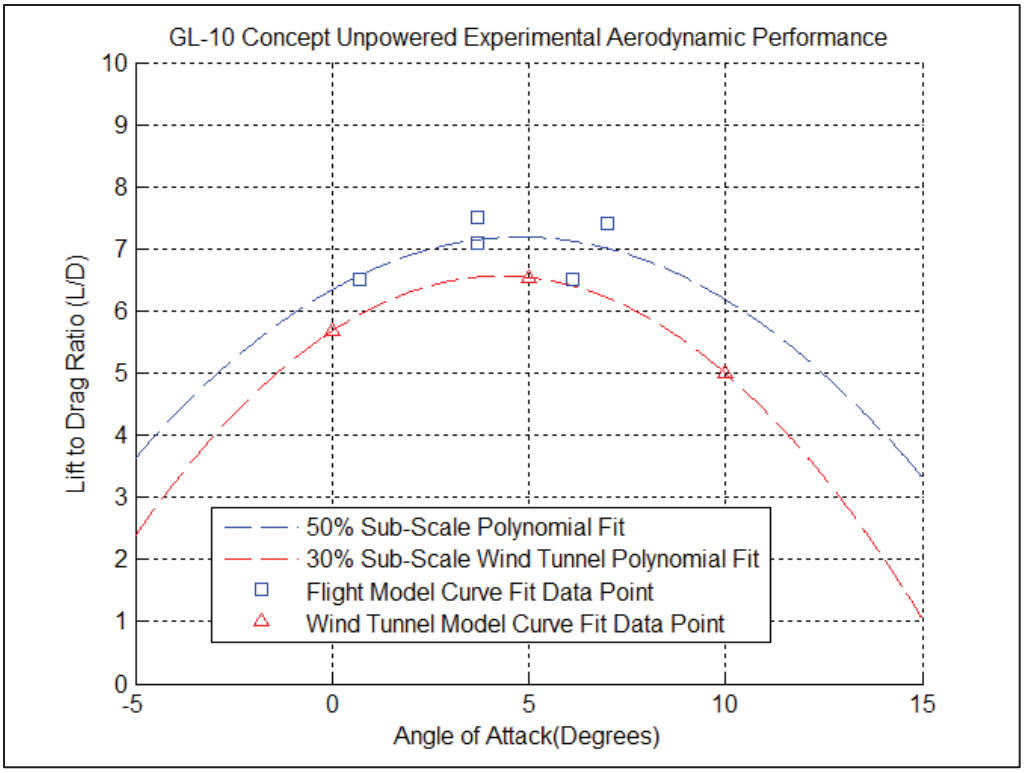

Figure 38. Experimental Unpowered Aerodynamic Performance Comparison

Two engine operation which would be required for enabling a long endurance cruise mode is feasible. This is based on the thrust required to sustain straight and level flight with wingtip motors would be approximately 8 lbs (L/D_{max} of 7.2); And the current motor and propeller combination can produce approximately 4 lbs of thrust each.

References

[1] Fredericks, W. J.; McSwain, R. G.; Beaton, B. F.; Klassman, D. W.; Theodore, C. R.: Greased Lightning (GL-10) Flight Testing Campaign. NASA/TM-2017-219643, 2017.

[2] Fredericks, W. J.; Agate, M. A.; Johns, Z. R.: NASA GL-10 Tilt-Wing VTOL UAS Flight Validation Experiments. AIAA Aviation 2015 Conference, Jun. 22-24, 2015, Dallas, Tx., 2015.

[3] Johnson, W.: NDARC NASA Design and Analysis of Rotorcraft. NASA/TP-2009-215402, 2009.

[4] Busan, R., Rothhaar, P., Croom, M., Murphy, P. C., Grafton, S., O'Neal, A.; Enabling Advanced Wind-Tunnel Research Methods Using the NASA Langley 12-Foot Low Speed Tunnel, AIAA AFM Conference, AIAA Aviation 2014, Atlanta, June 16-20, 2014. AIAA Paper No. 2014-3000.

[5] Rothhaar, P., Murphy, P. C., Bacon, B. J., Grauer, J.; NASA Langley Distributed Propulsion VTOL Tilt Wing Aircraft Testing, Modeling, Simulation, Control, and Flight Test Development, AIAA AFM Conference, AIAA Aviation 2014, Atlanta, June 16-20, 2014. AIAA Paper No. 2014-2999.

[6] Murphy, P. C., Landman, D.: Experiment Design for Complex VTOL Aircraft with Distributed Propulsion and Tilt Wing, AIAA AFM Conference, SciTech 2015, Kissimmee, FL, January 05-09, 2015. AIAA Paper No. 2015-0017.

APPENDIX A: TRANSITION COMPARISON PLOTS

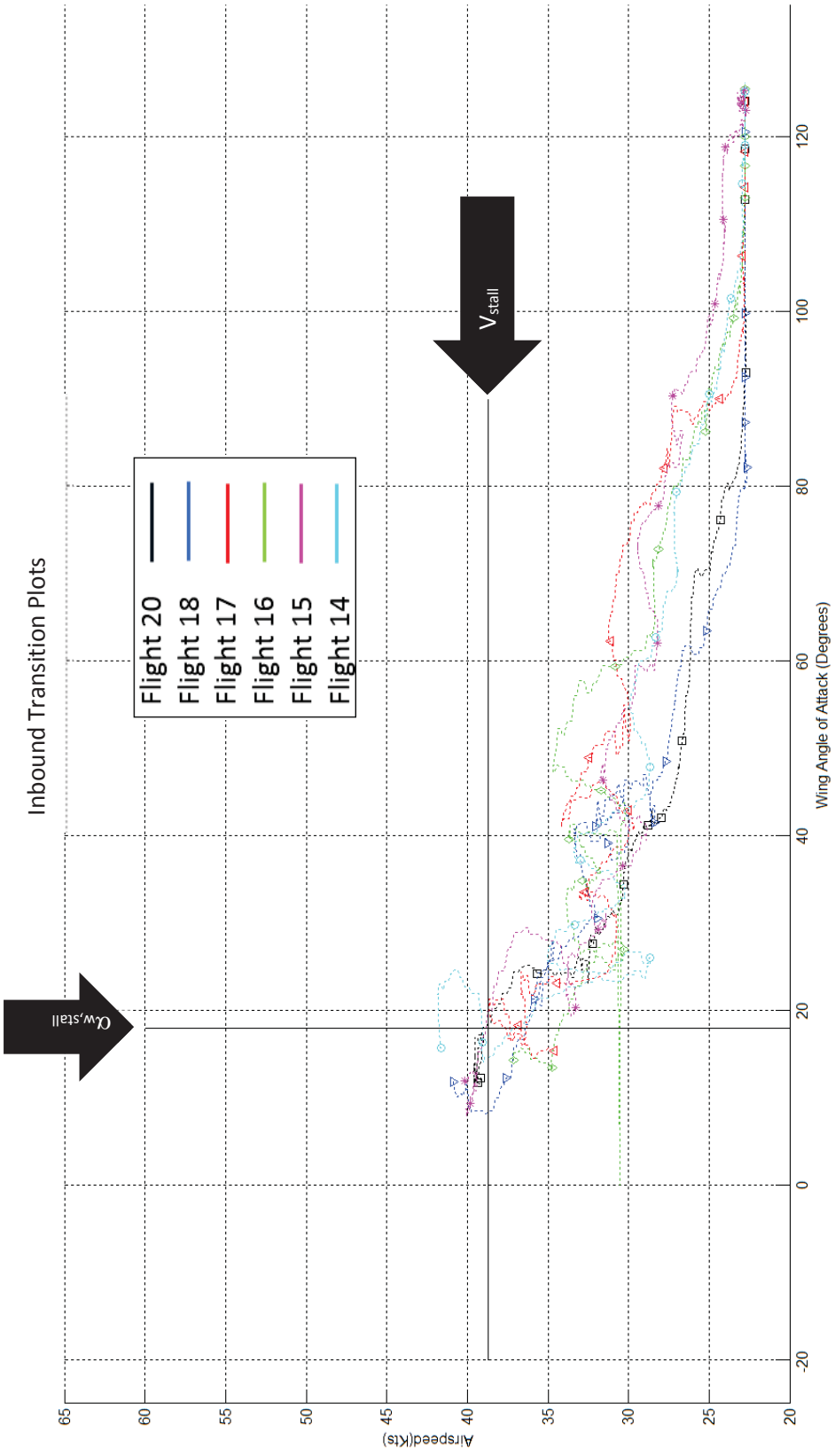

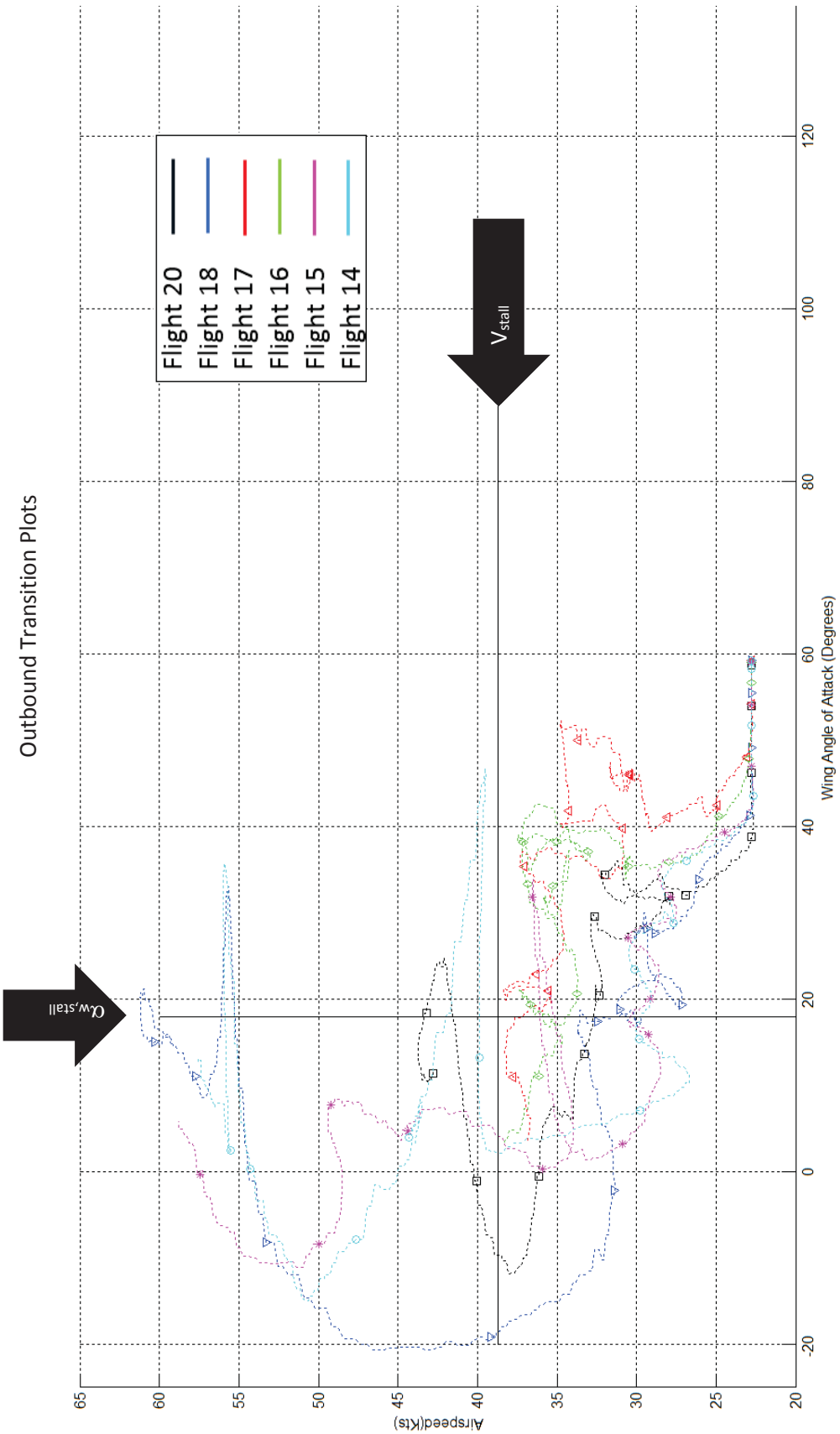
Outbound Transition Plots
Flight 20
Flight 18
Flight 17
Flight 16
Flight 15
Flight 14
V_{stall}
$\alpha_{w,stall}$
Airspeed(Kts)
Wing Angle of Attack (Degrees)
65
60
55
50
45
40
35
30
25
20
-20
0
20
40
60
80
100
120

APPENDIX B: TRANSITION DATA PLOTS

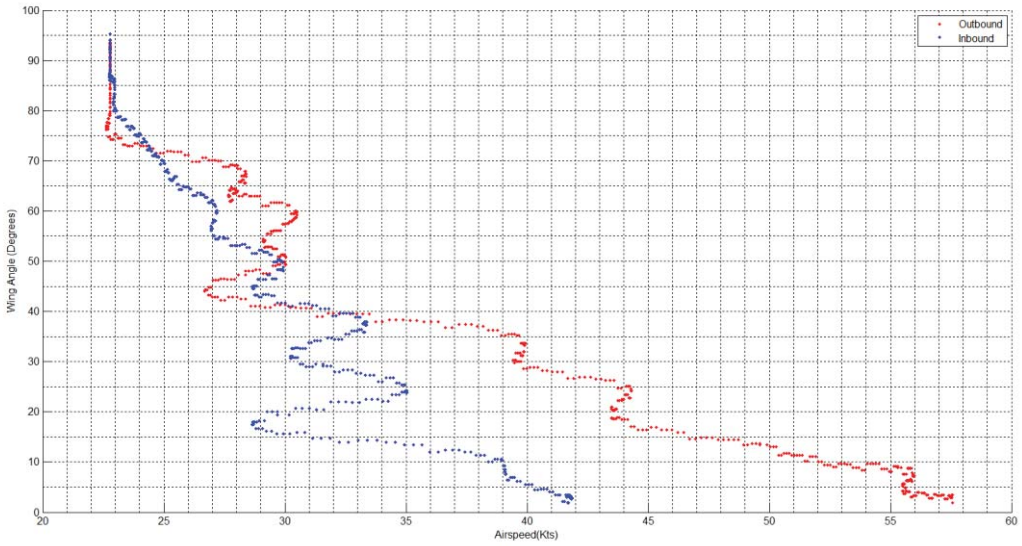

Flight 14 Transition Corridor W.R.T. Wing Angle

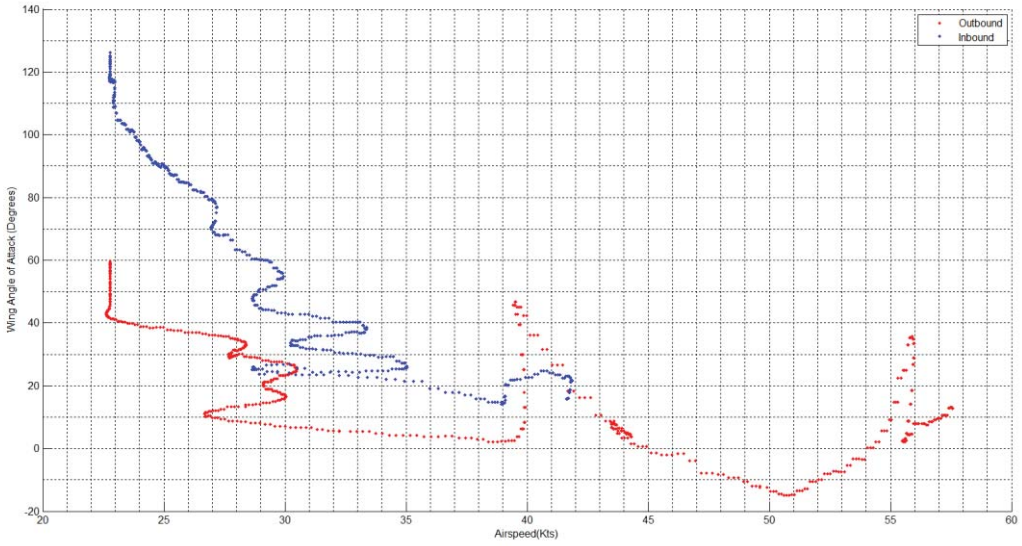

Flight 14 Transition Corridor W.R.T. Wing Angle of Attack

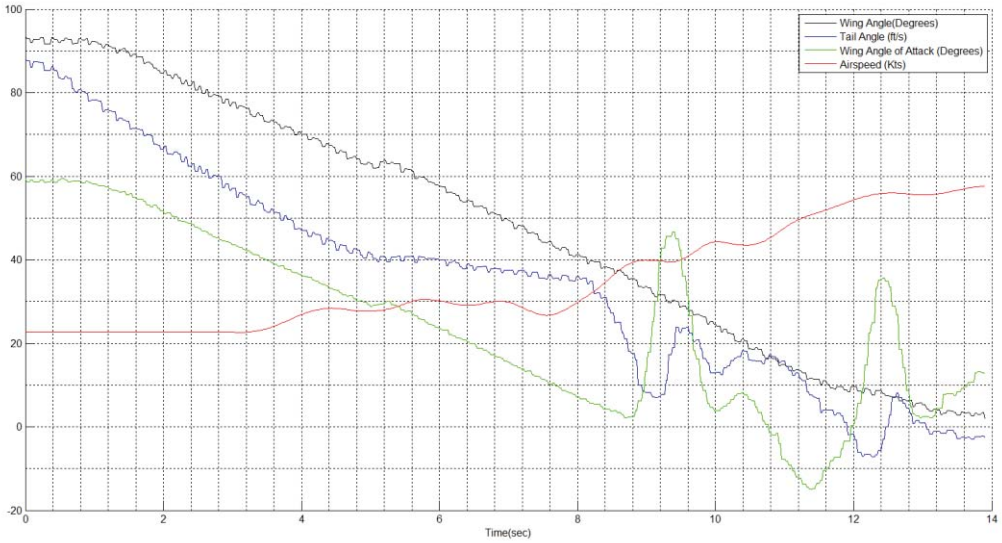

Flight 14 Transition Parameters W.R.T. Airspeed

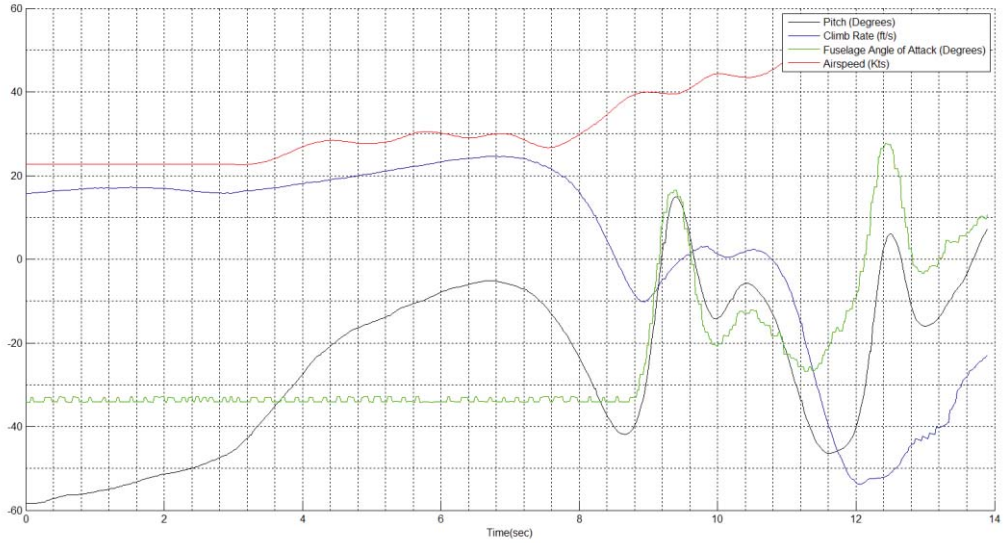

Flight 14 Transition Stability W.R.T. Airspeed

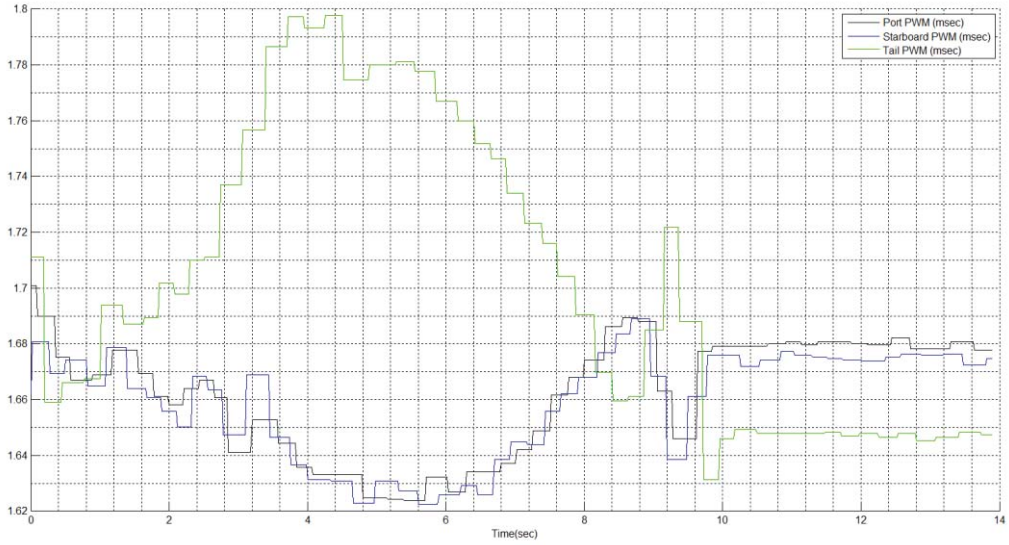

Flight 14 Motor Pitch and Thrust Characteristics

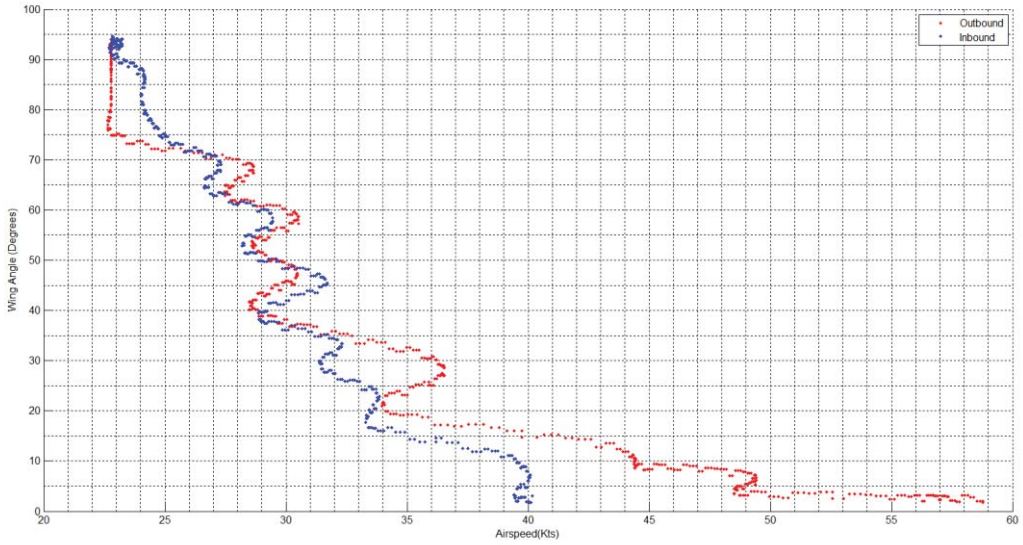

Flight 15 Transition Corridor W.R.T. Wing Angle

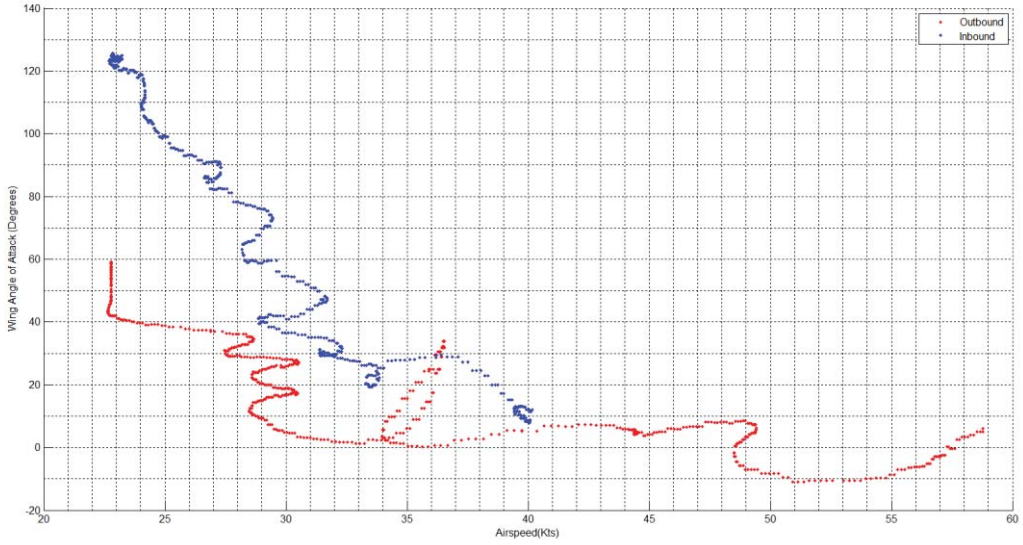

Flight 15 Transition Corridor W.R.T. Wing Angle of Attack

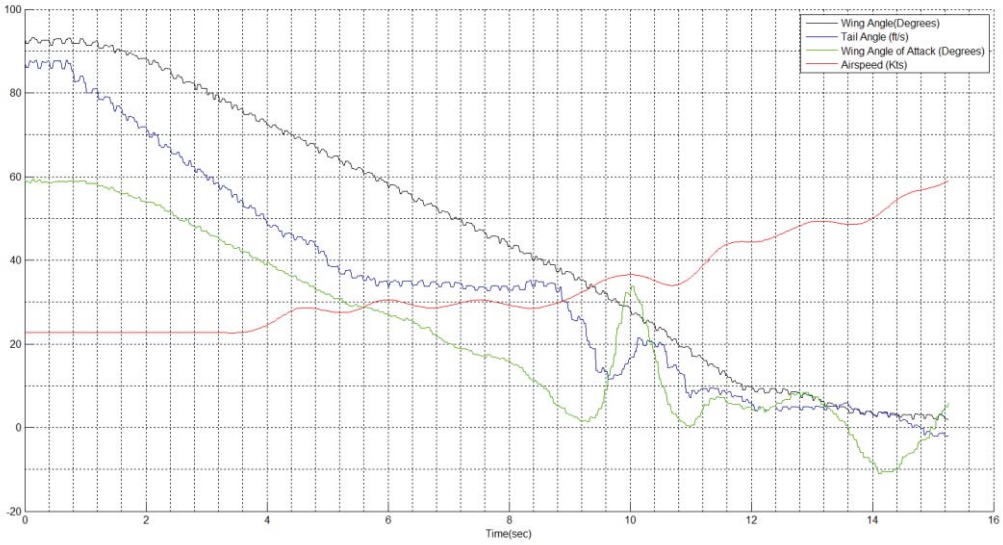

Flight 15 Transition Parameters W.R.T. Airspeed

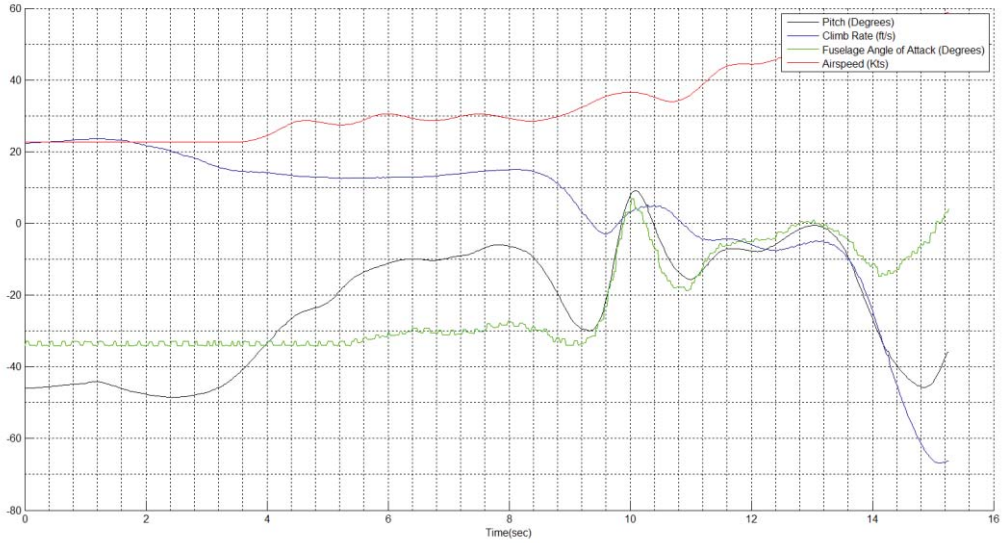

Flight 15 Transition Stability W.R.T. Airspeed

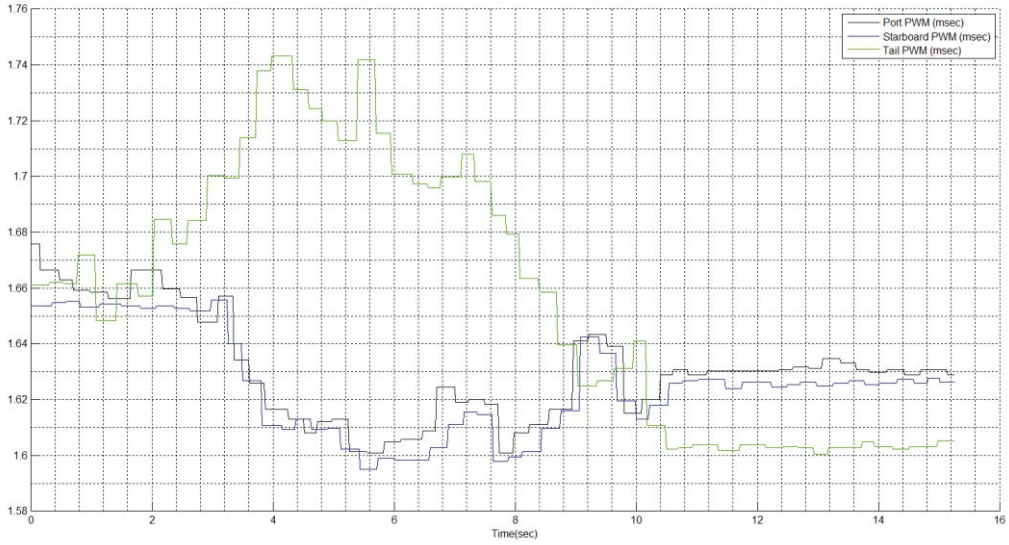

Flight 15 Motor Pitch and Thrust Characteristics

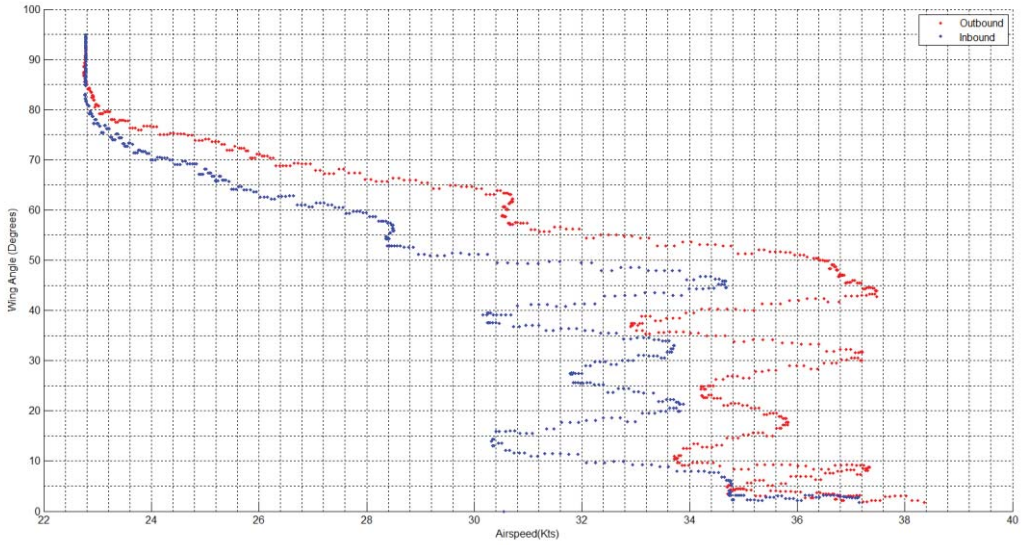

Flight 16 Transition Corridor W.R.T. Wing Angle

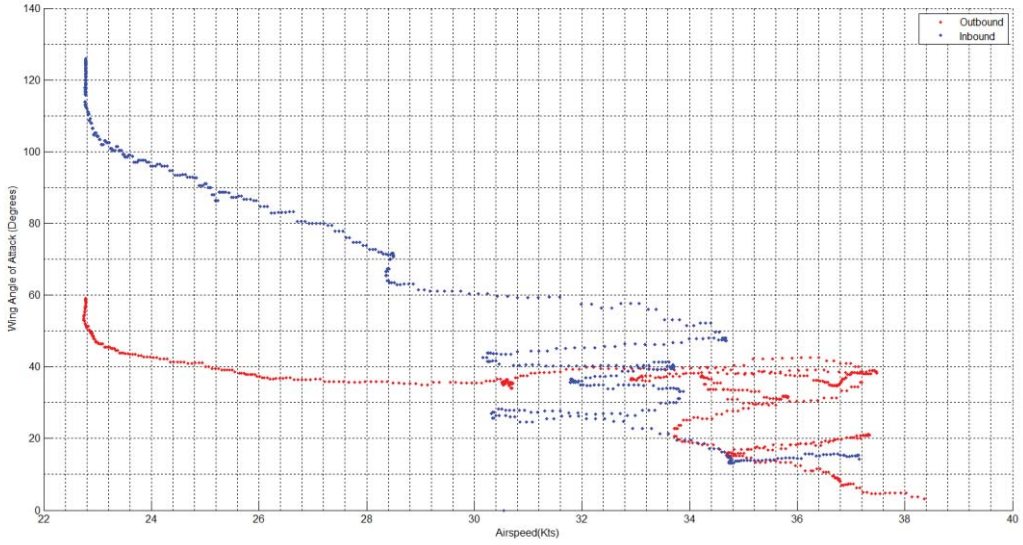

Flight 16 Transition Corridor W.R.T. Wing Angle of Attack

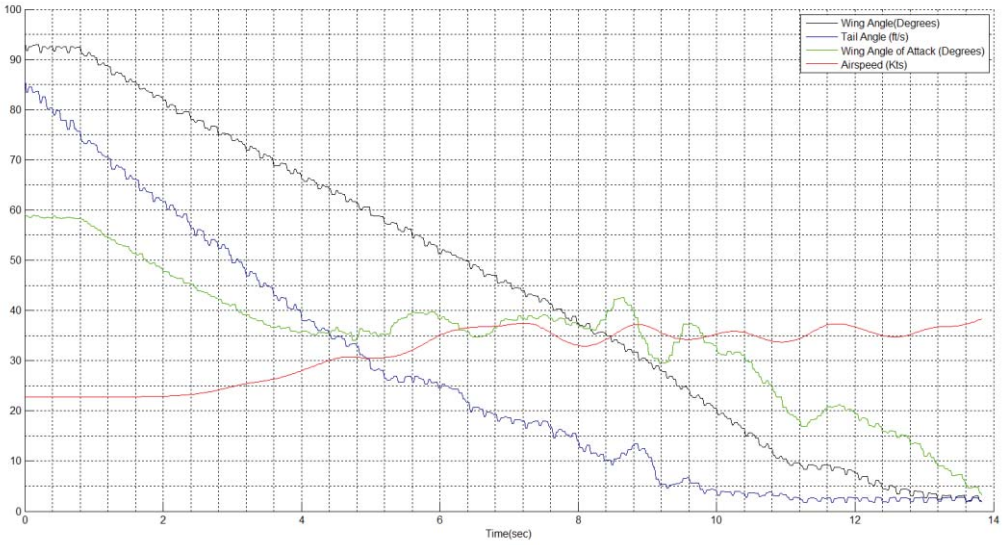

Flight 16 Transition Parameters W.R.T. Airspeed

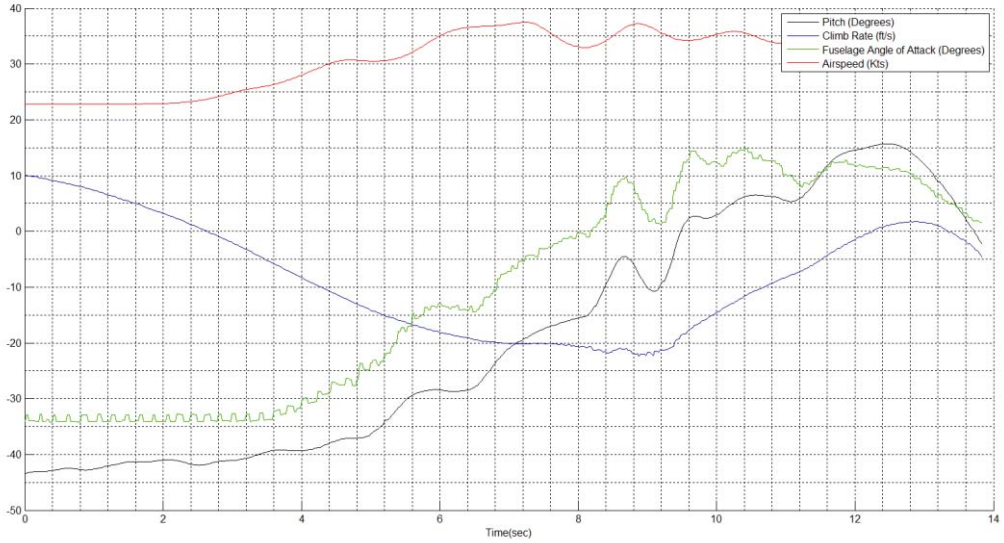

Flight 16 Transition Stability W.R.T. Airspeed

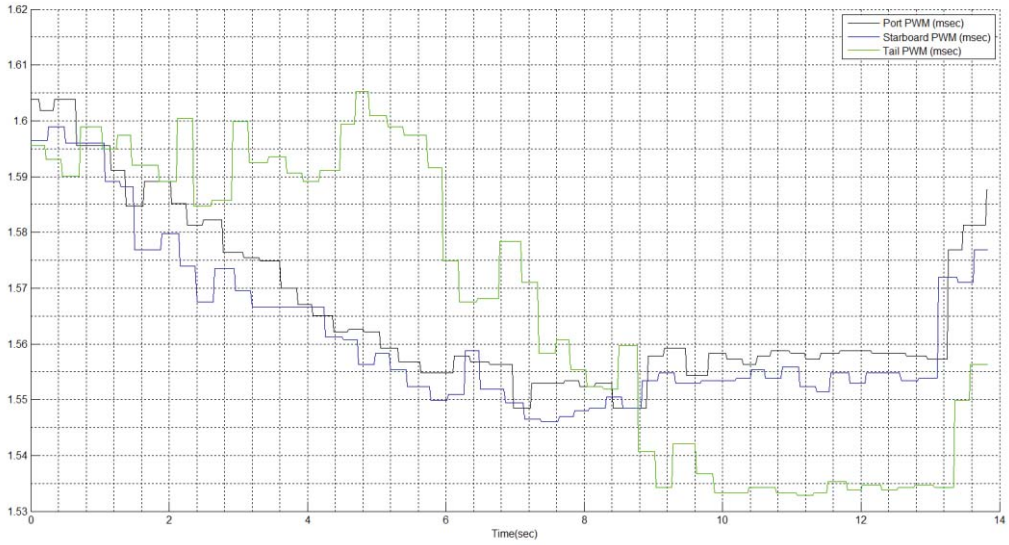

Flight 16 Motor Pitch and Thrust Characteristics

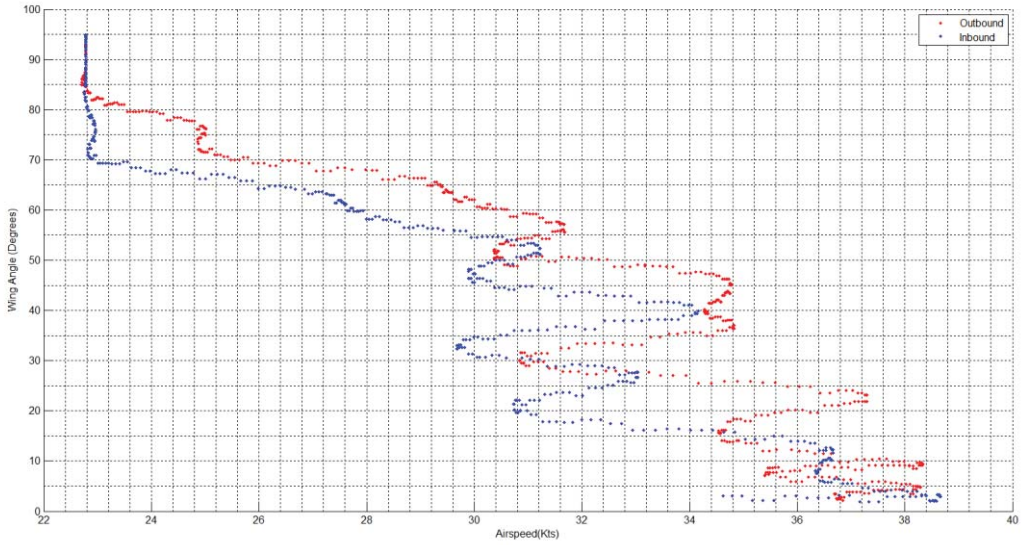

Flight 17 Transition Corridor W.R.T. Wing Angle

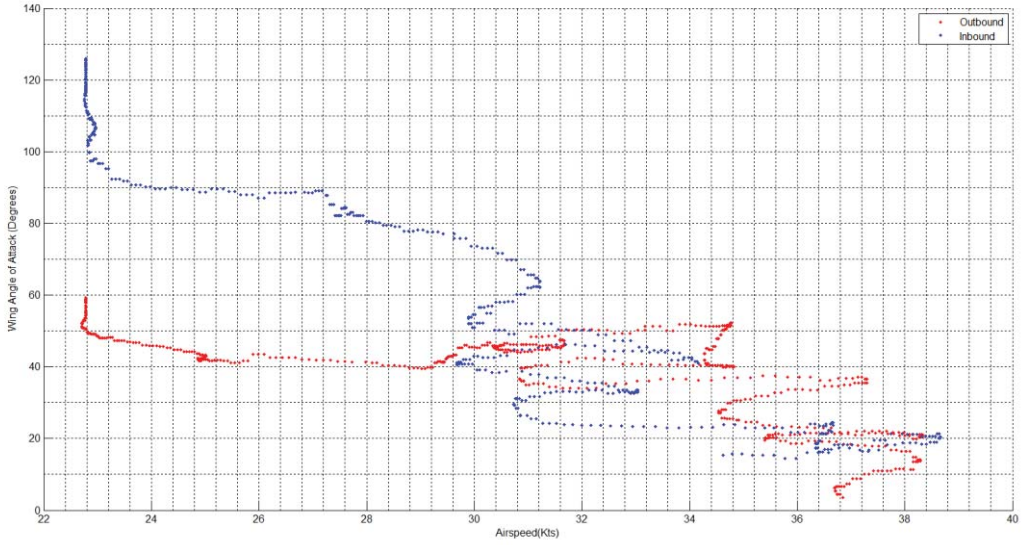

Flight 17 Transition Corridor W.R.T. Wing Angle of Attack

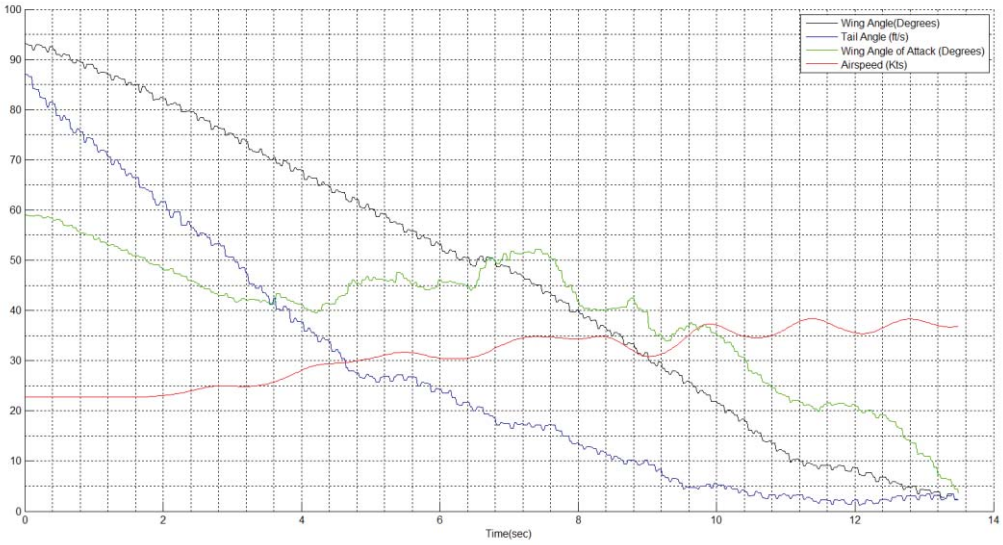

Flight 17 Transition Parameters W.R.T. Airspeed

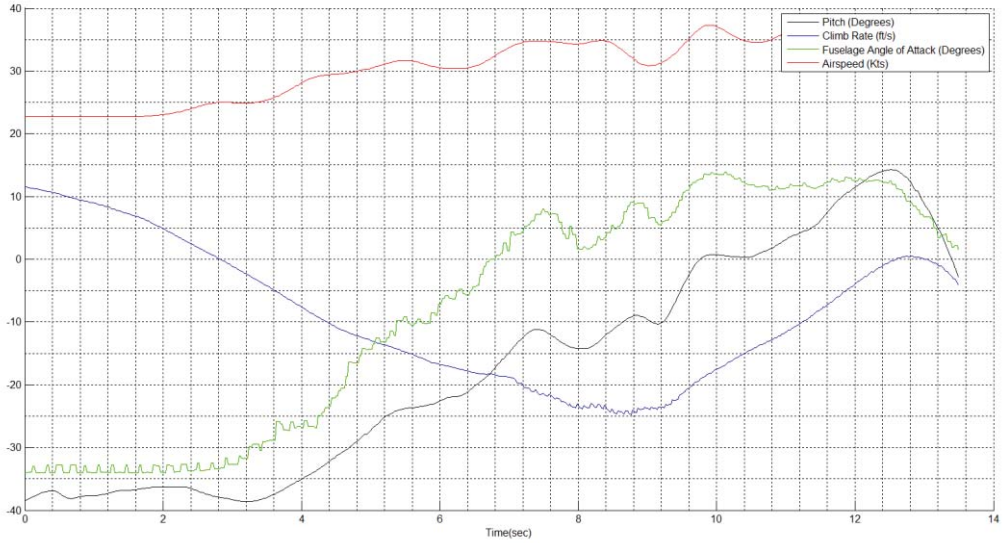

Flight 17 Transition Stability W.R.T. Airspeed

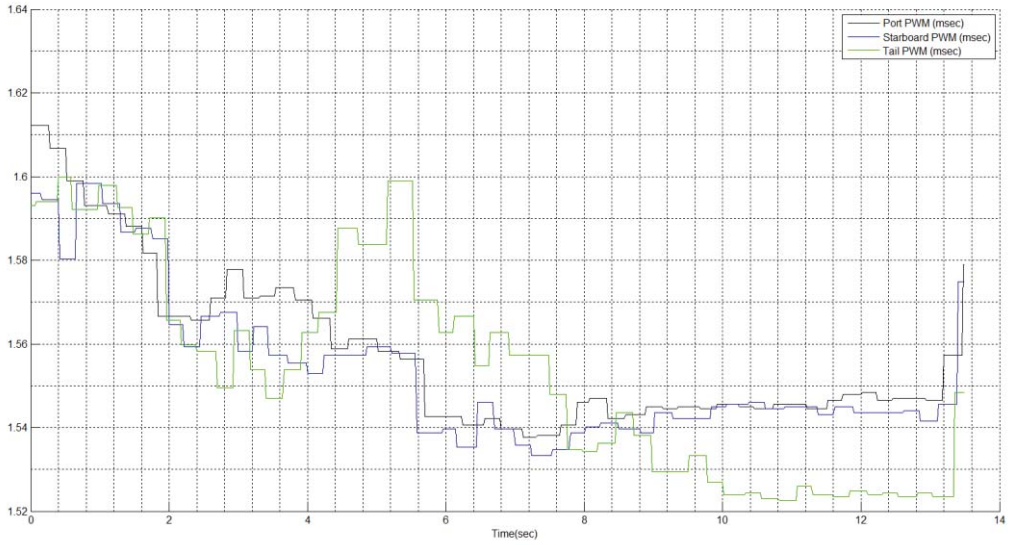

Flight 17 Motor Pitch and Thrust Characteristics

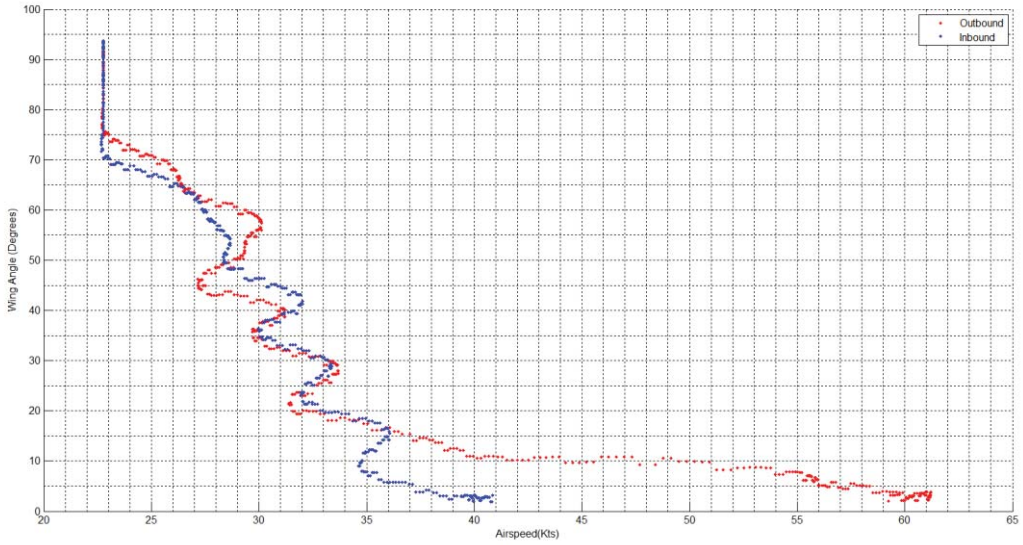

Flight 18 Transition Corridor W.R.T. Wing Angle

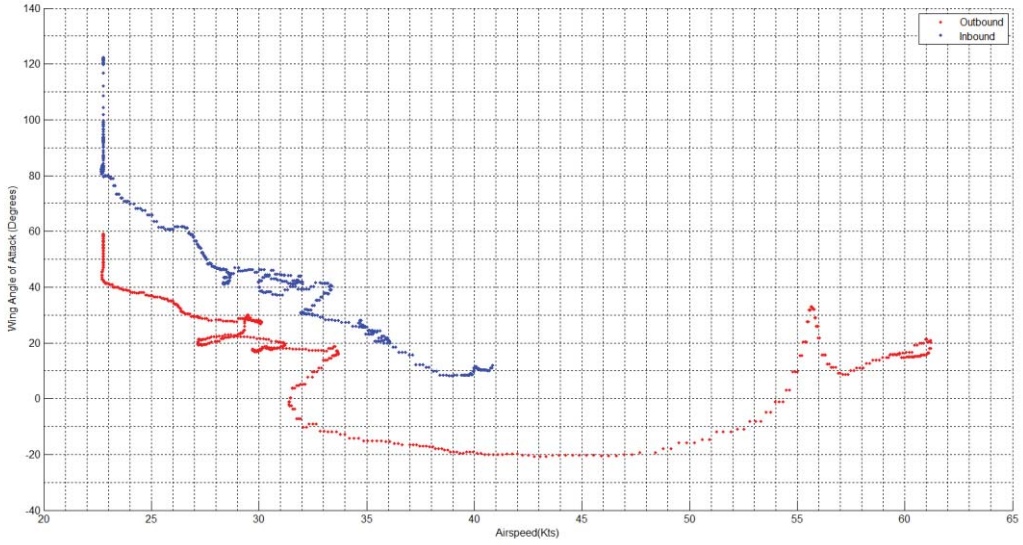

Flight 18 Transition Corridor W.R.T. Wing Angle of Attack

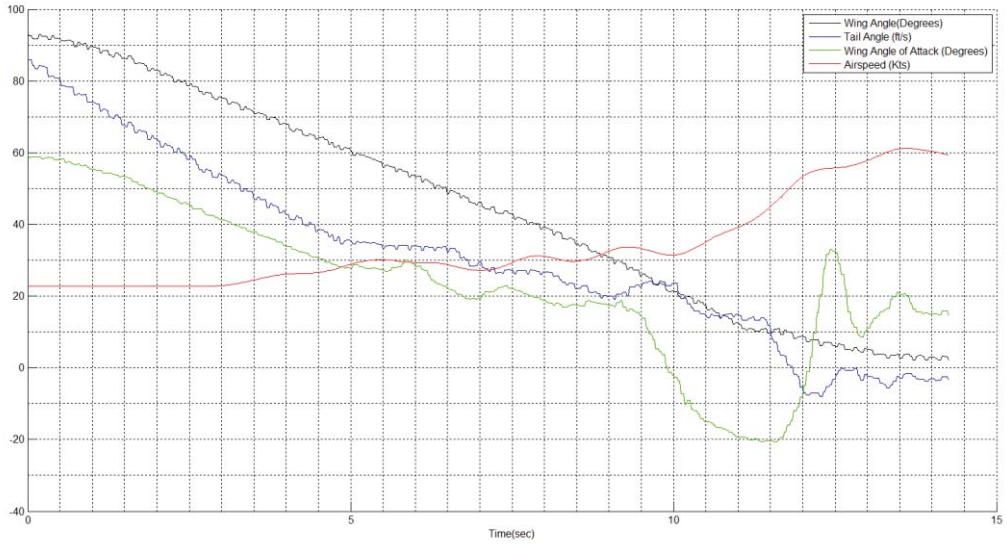

Flight 18 Transition Parameters W.R.T. Airspeed

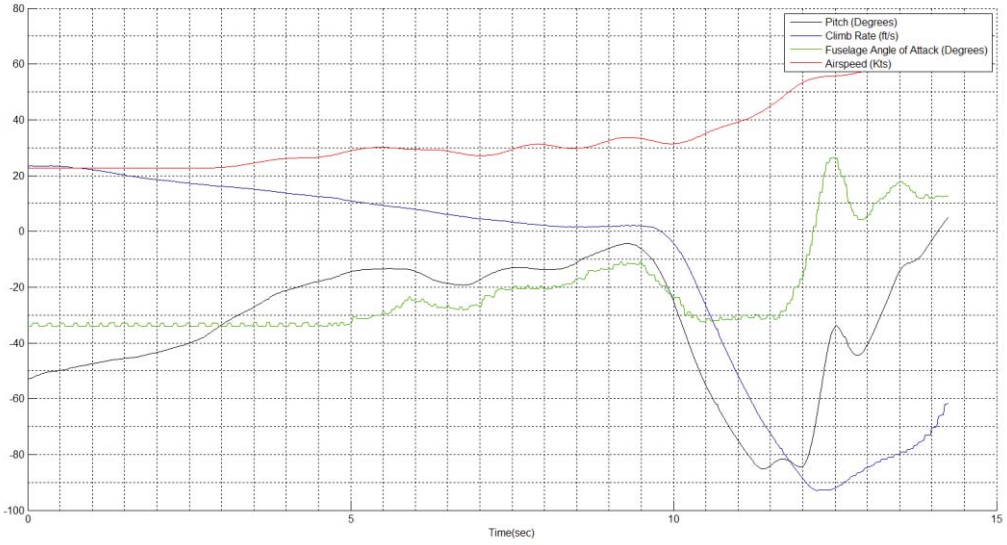

Flight 18 Transition Stability W.R.T. Airspeed

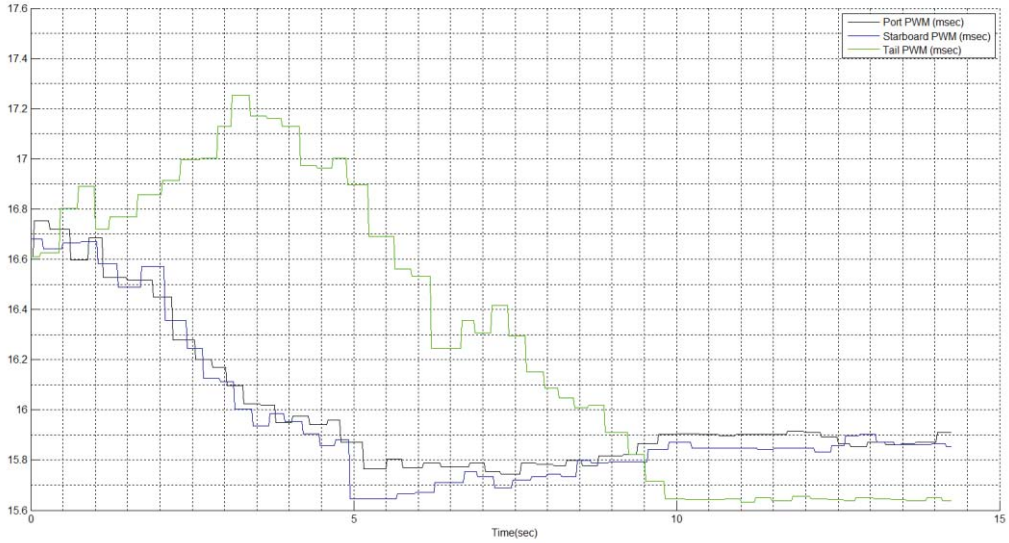

Flight 18 Motor Pitch and Thrust Characteristics

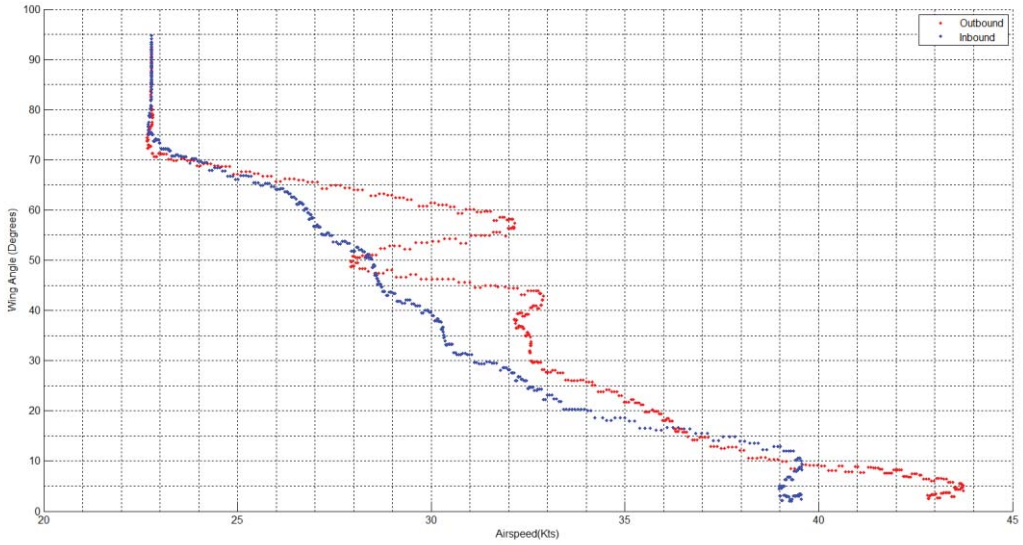

Flight 20 Transition Corridor W.R.T. Wing Angle

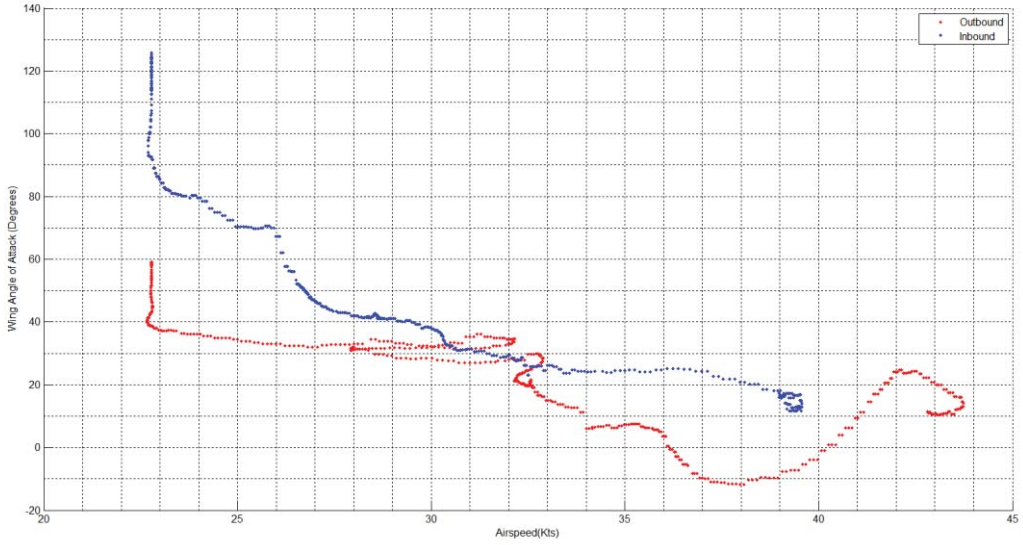

Flight 20 Transition Corridor W.R.T. Wing Angle of Attack

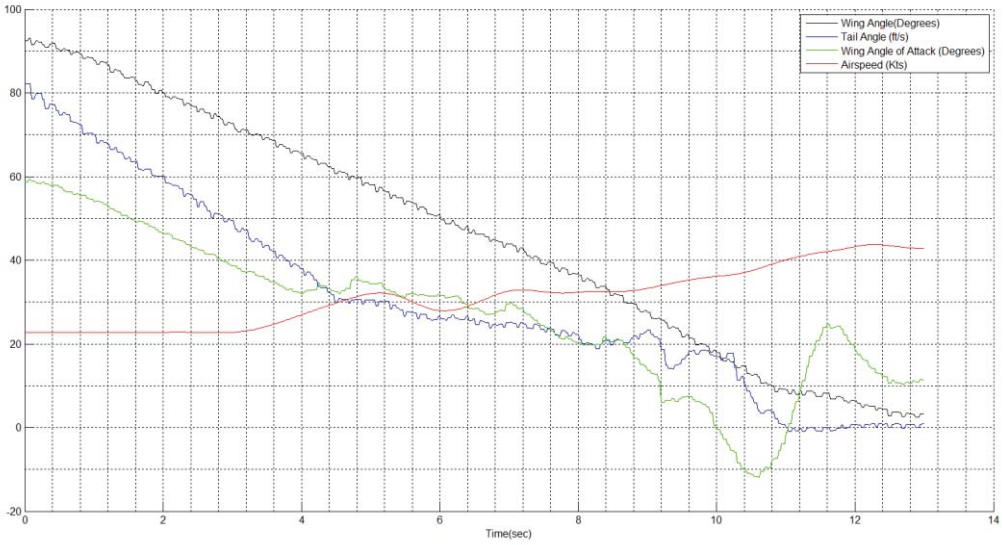

Flight 20 Transition Parameters W.R.T. Airspeed

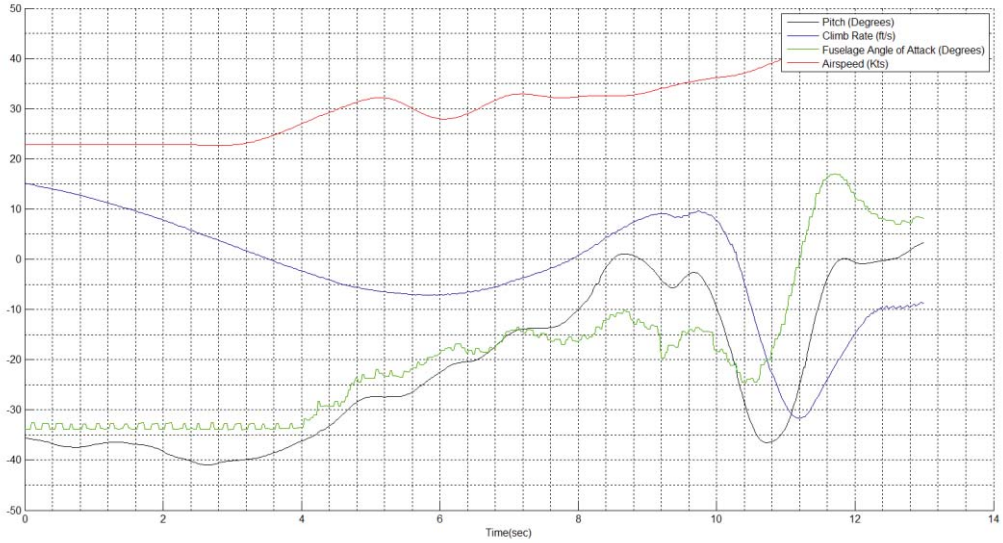

Flight 20 Transition Stability W.R.T. Airspeed

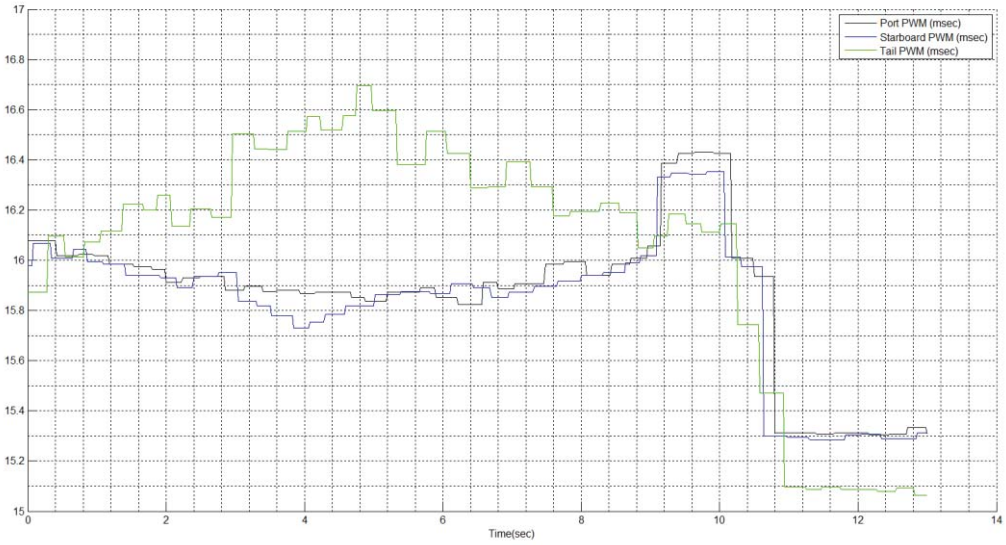

Flight 20 Motor Pitch and Thrust Characteristics

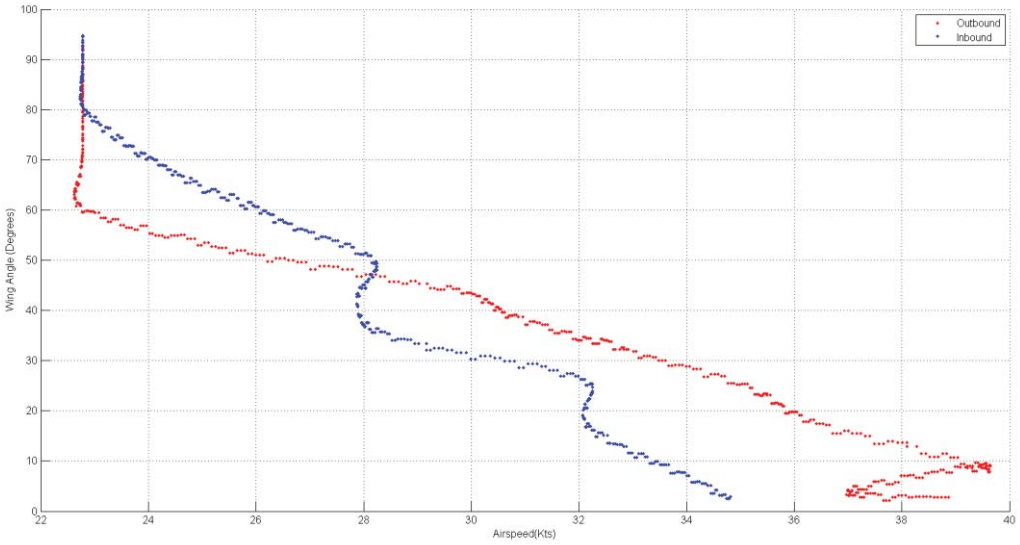

Flight 21 Transition Corridor W.R.T. Wing Angle

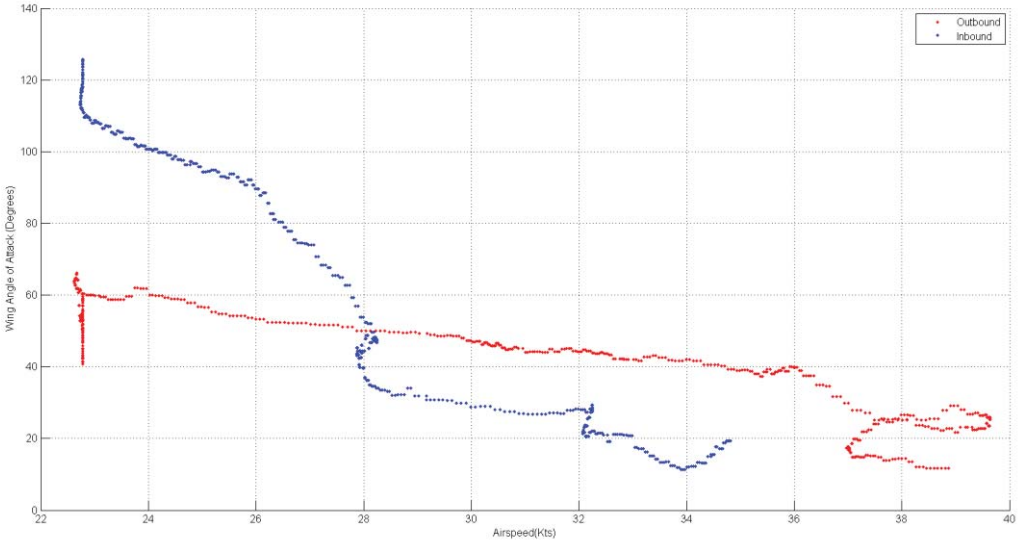

Flight 21 Transition Corridor W.R.T. Wing Angle of Attack

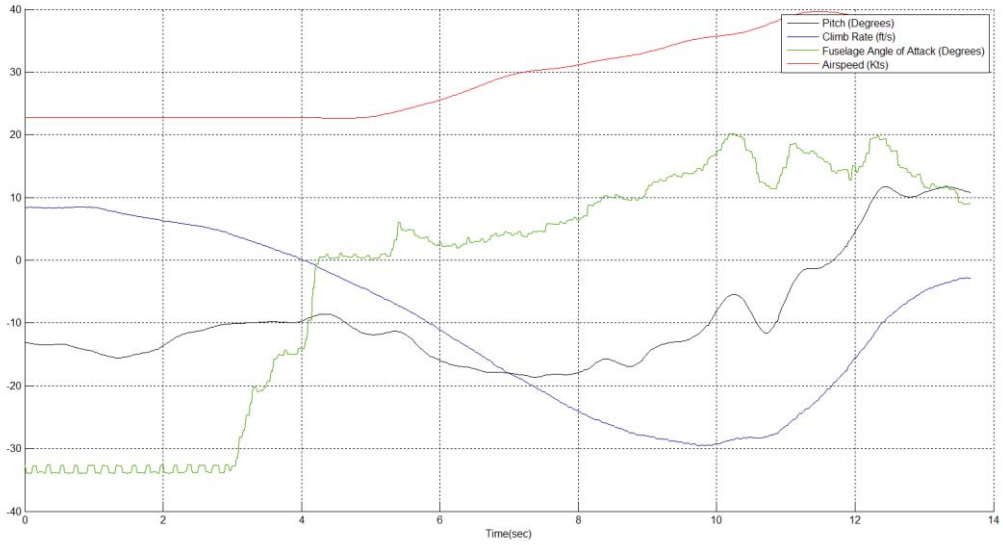

Flight 21 Transition Parameters W.R.T. Airspeed

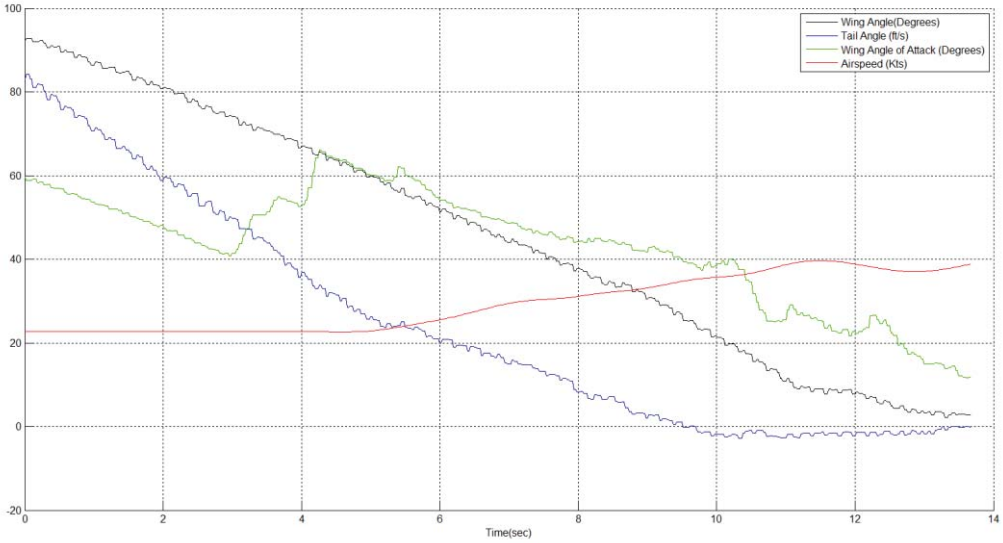

Flight 21 Transition Stability W.R.T. Airspeed

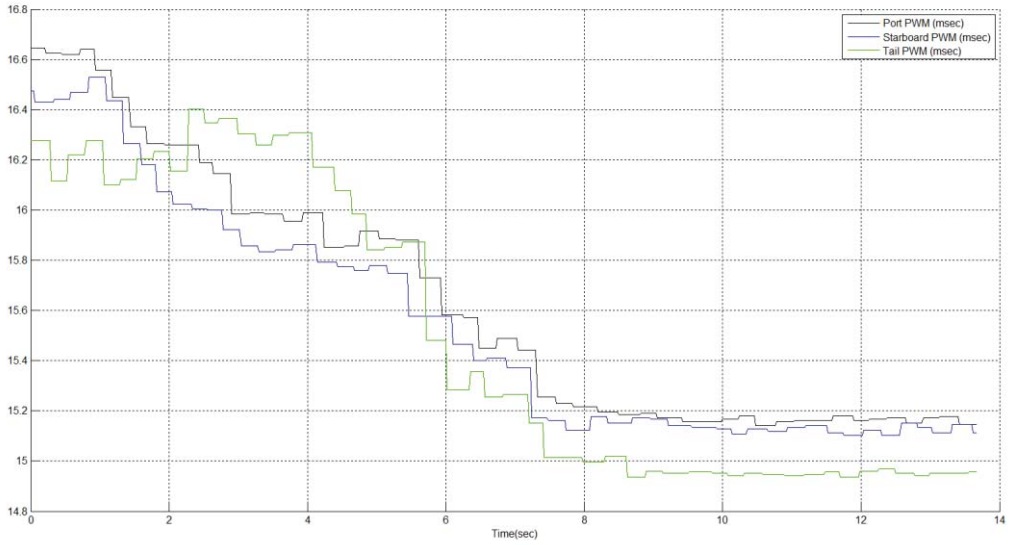

Flight 21 Motor Pitch and Thrust Characteristics

Appendix C: Powered Straight and Level Data Run Plots

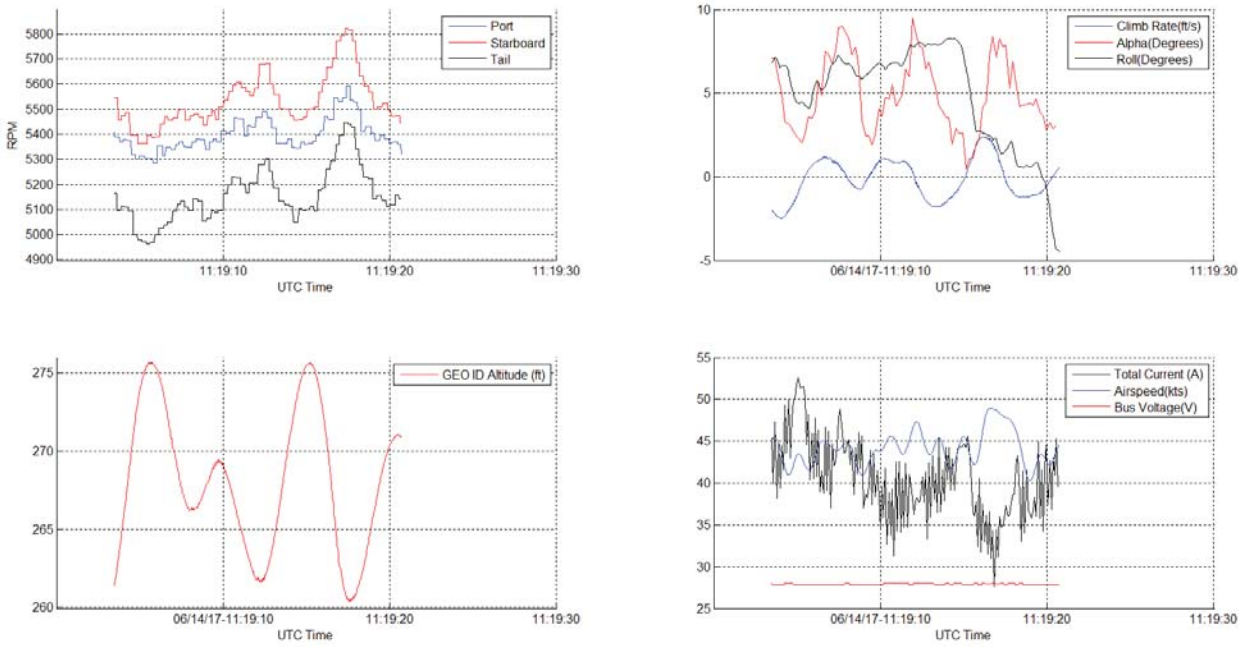

Flight 14 Powered Straight and Level Data Run 1

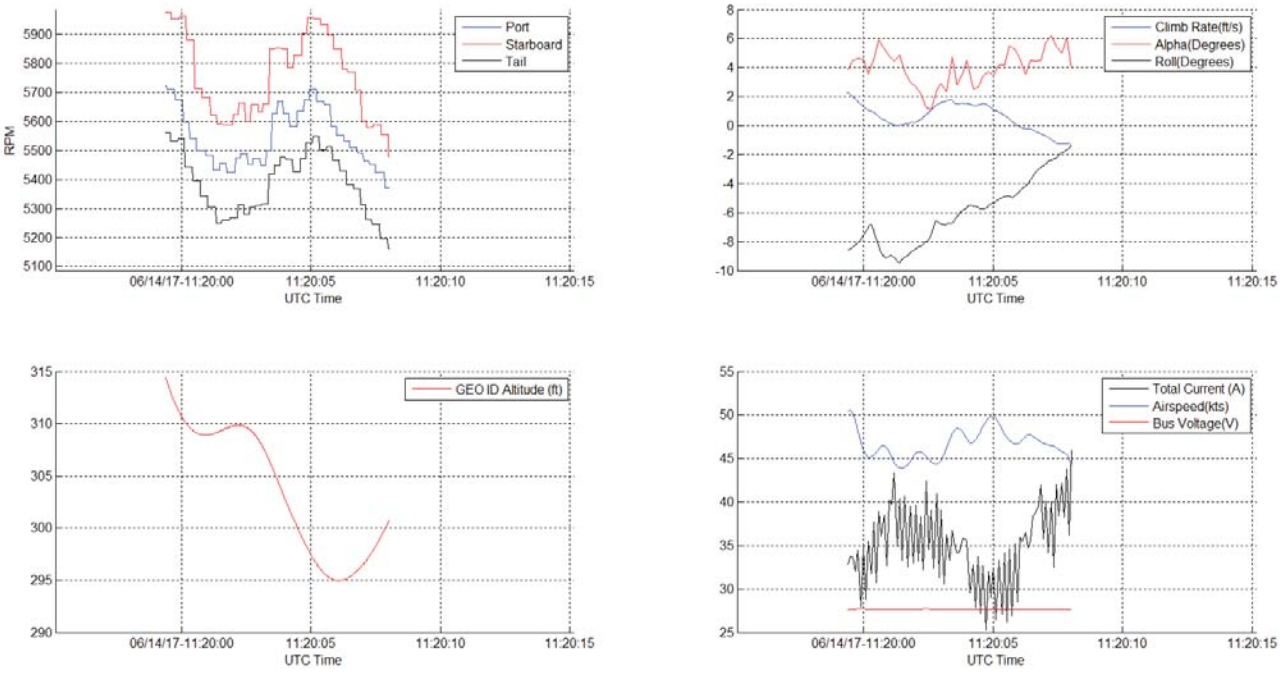

Flight 14 Powered Straight and Level Data Run 2

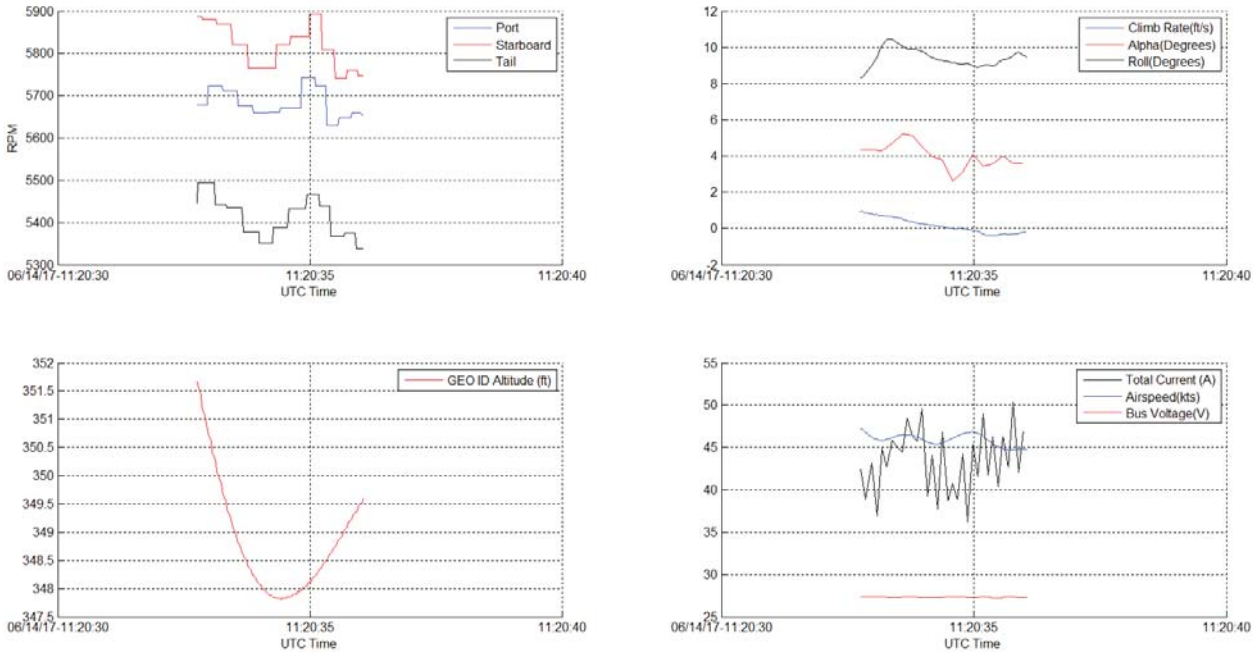

Flight 14 Powered Straight and Level Data Run 3

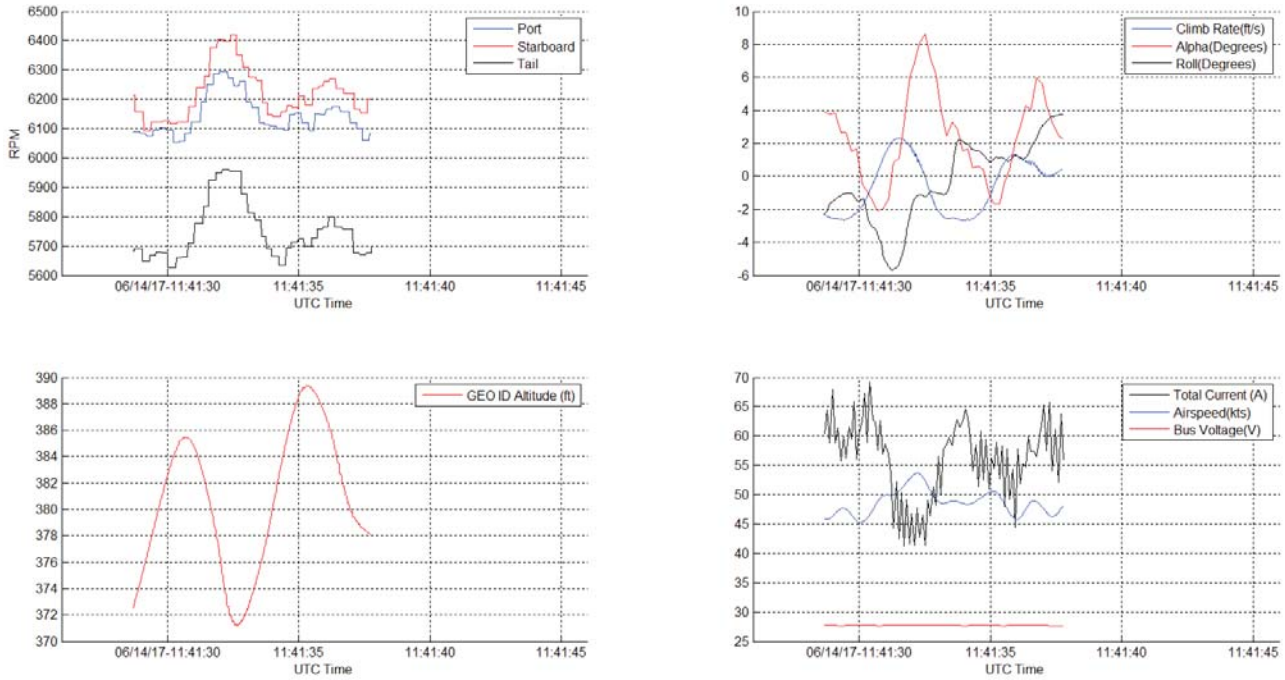

Flight 15 Powered Straight and Level Data Run 1

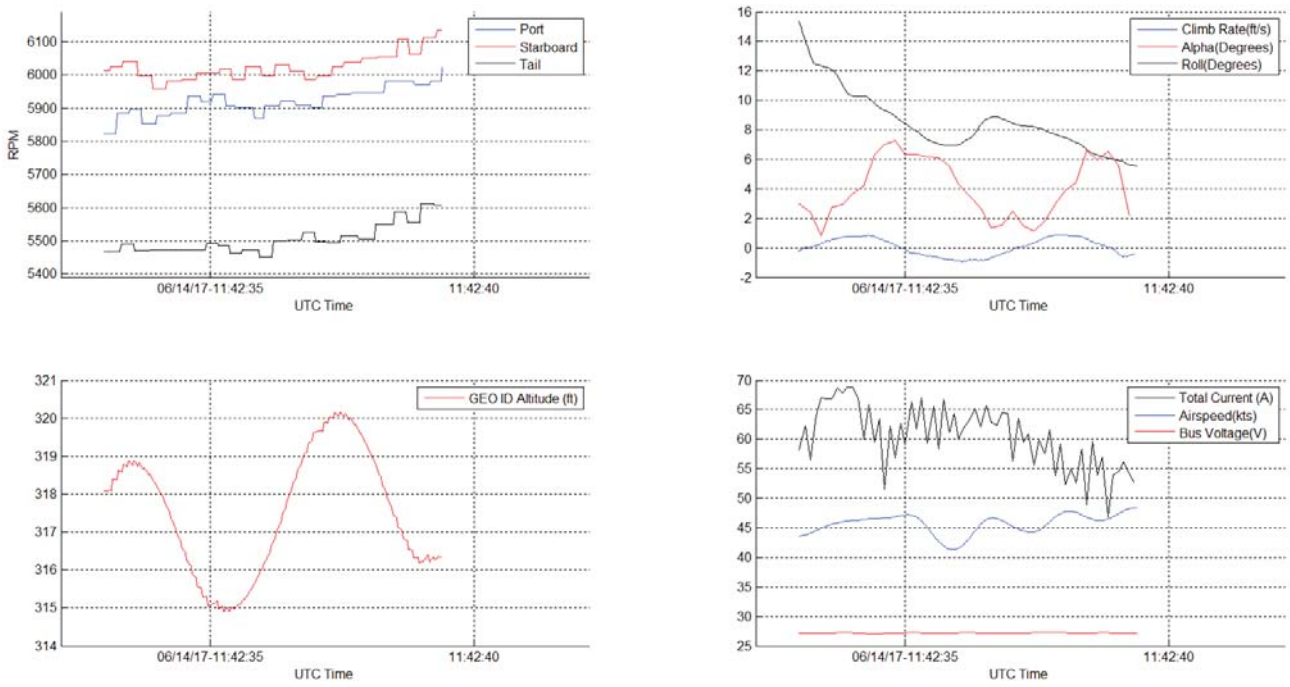

Flight 15 Powered Straight and Level Data Run 2

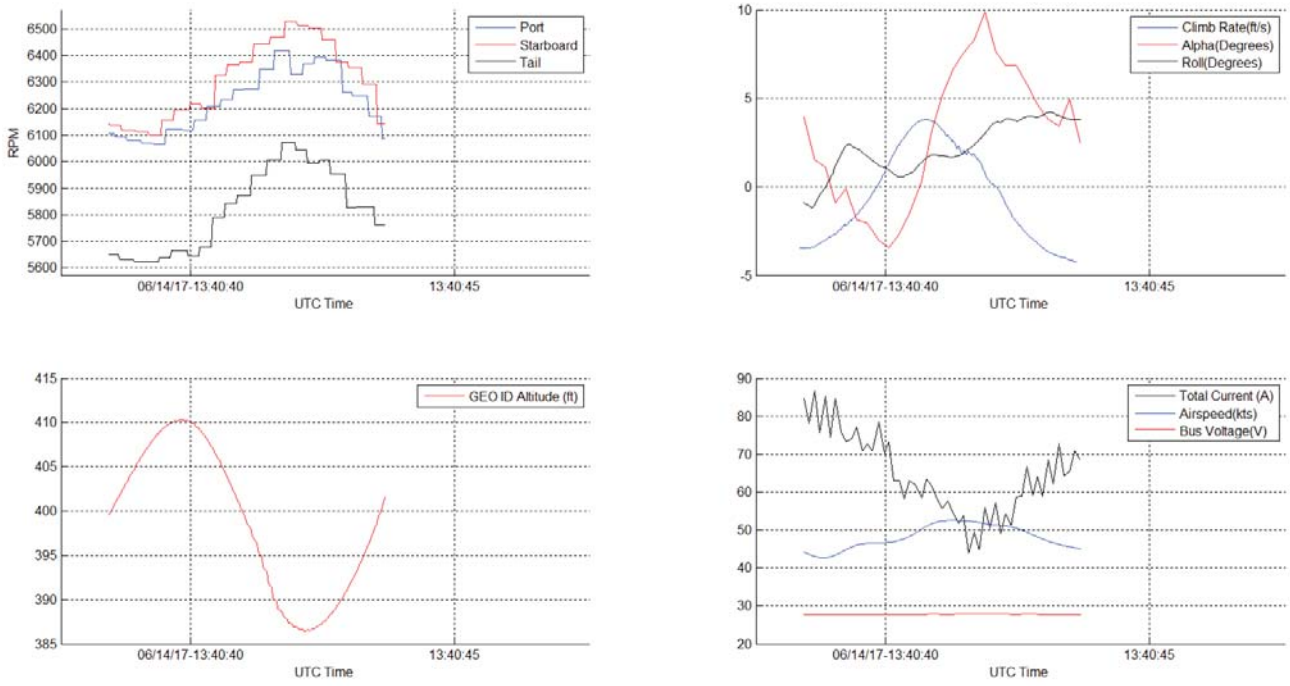

Flight 18 Powered Straight and Level Data Run 1

APPENDIX D: POWERED PERFORMANCE DATA PLOTS

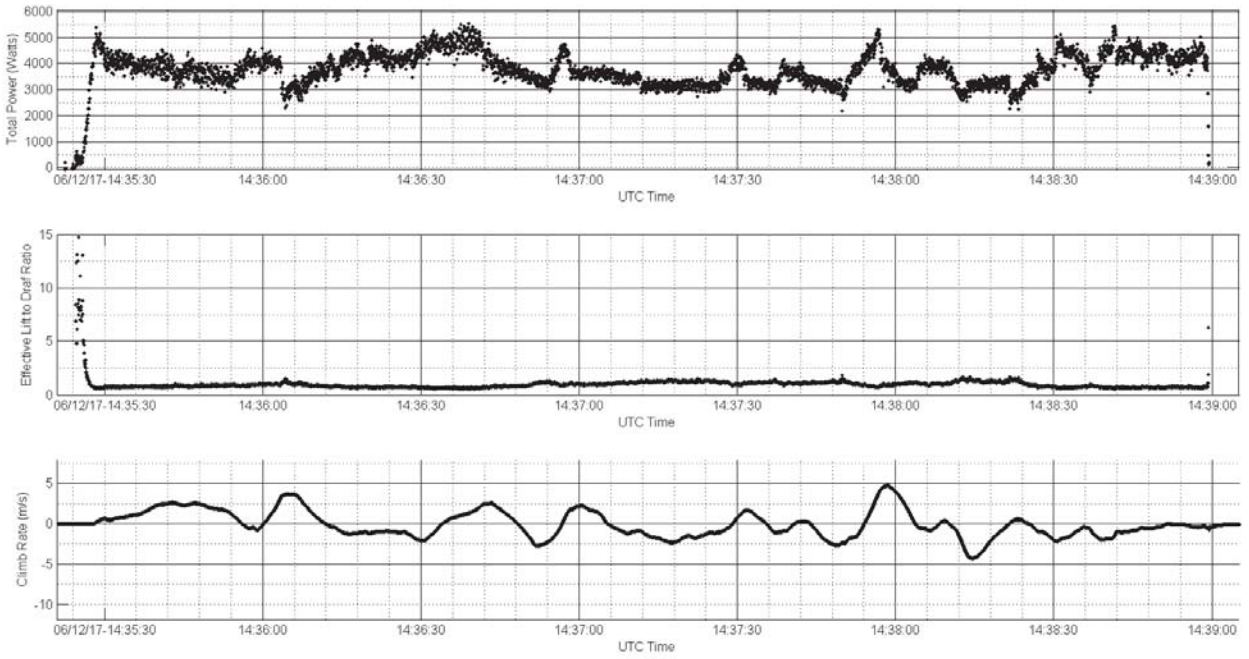

Flight 10 Powered Performance Plot

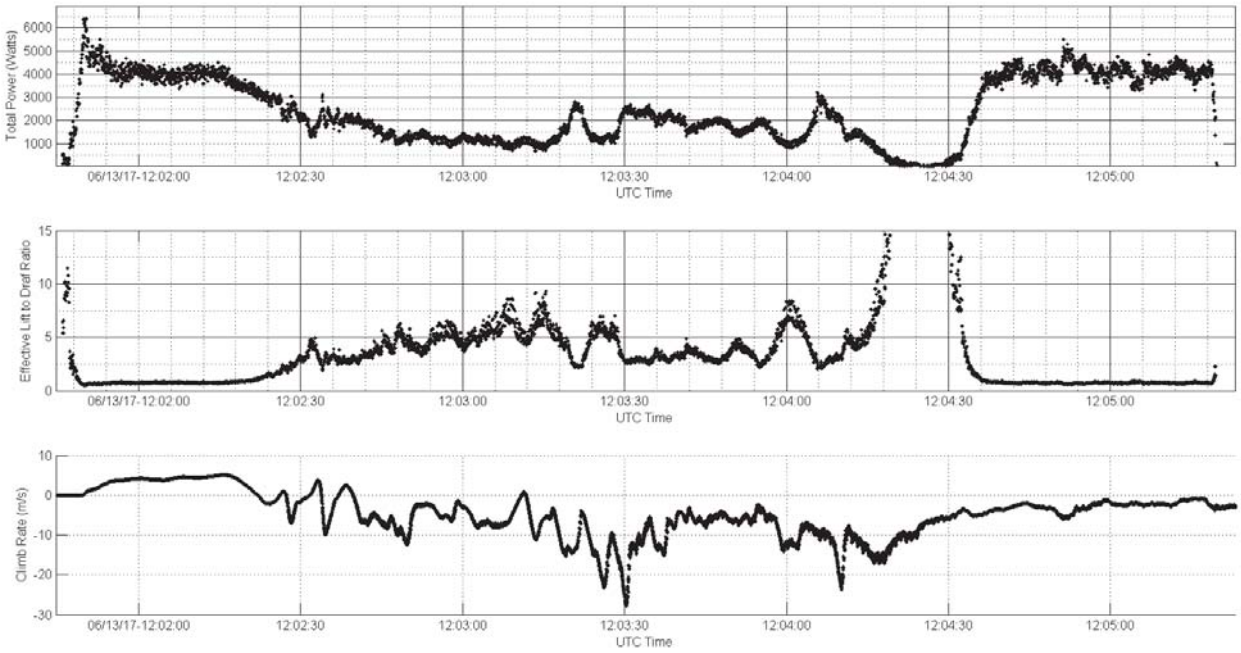

Flight 12 Powered Performance

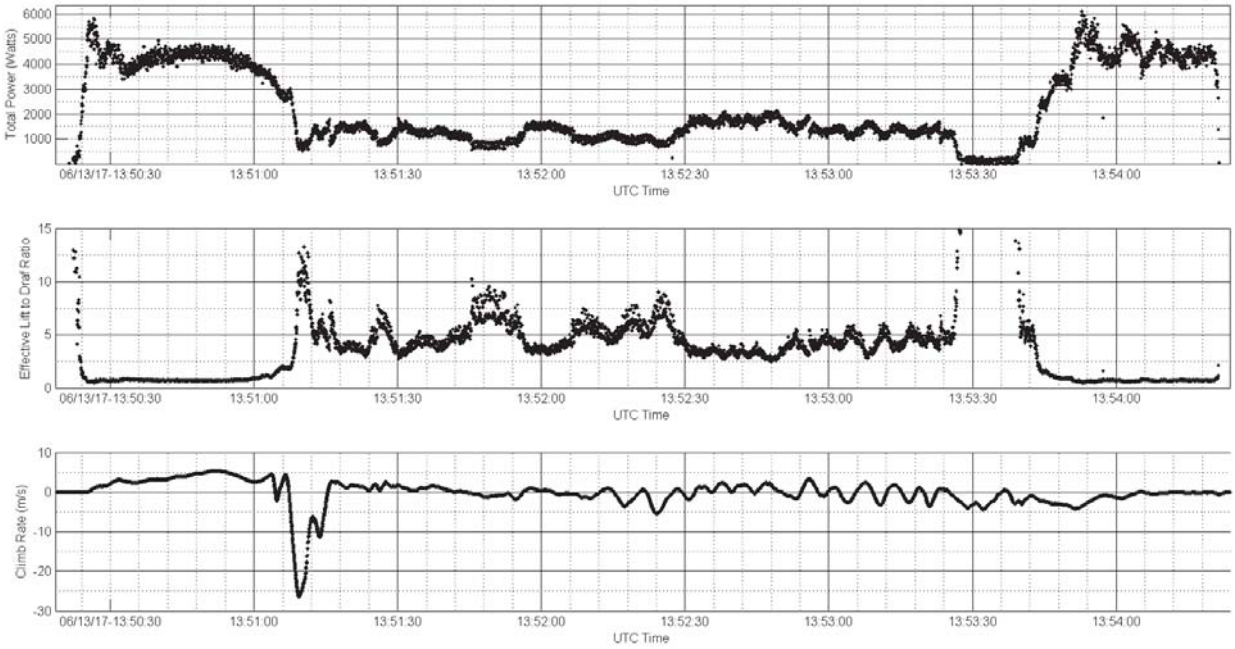

Flight 13 Powered Performance

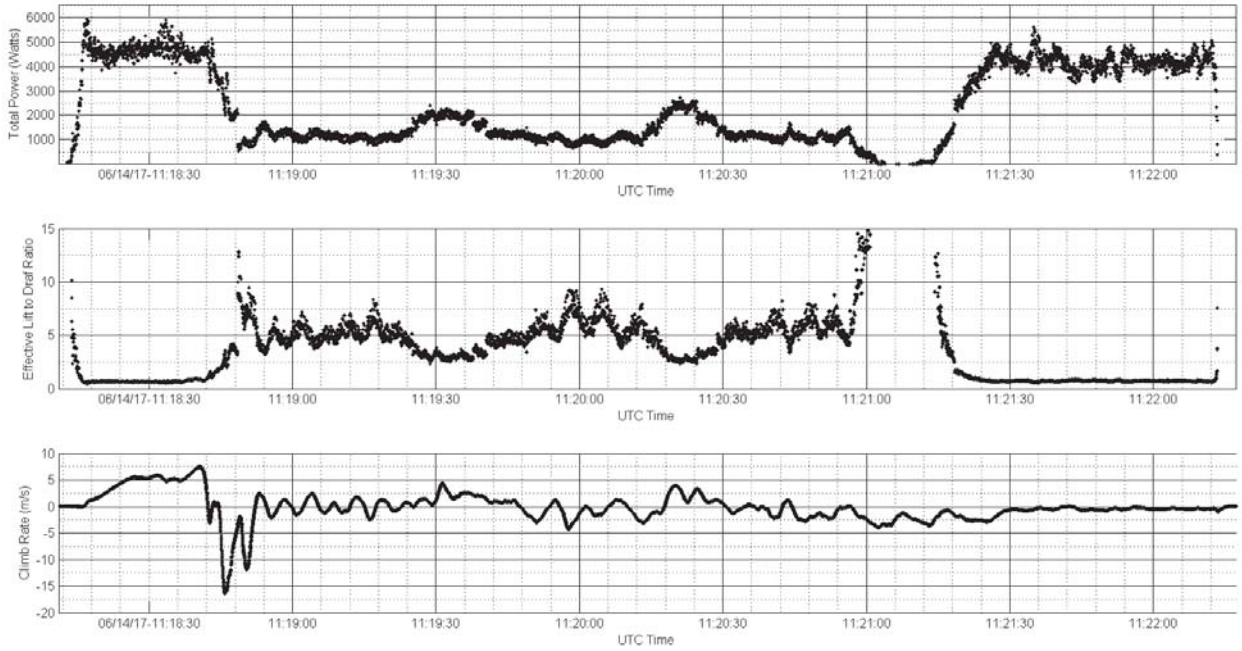

Flight 14 Powered Performance

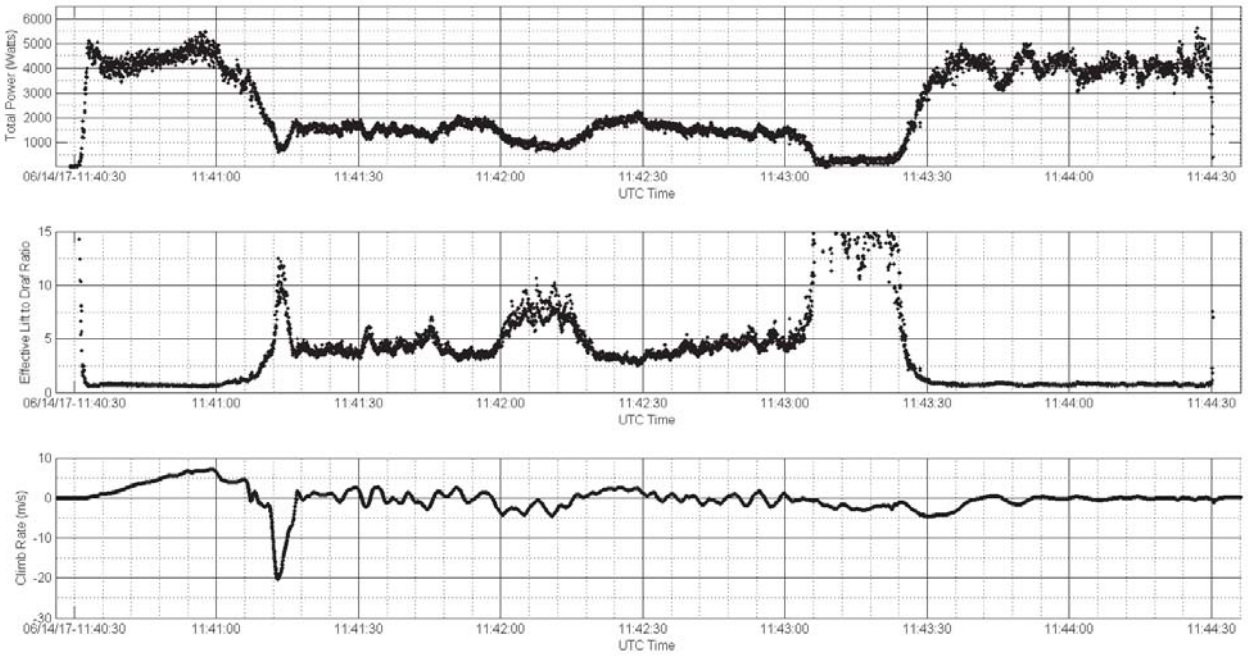

Flight 15 Powered Performance

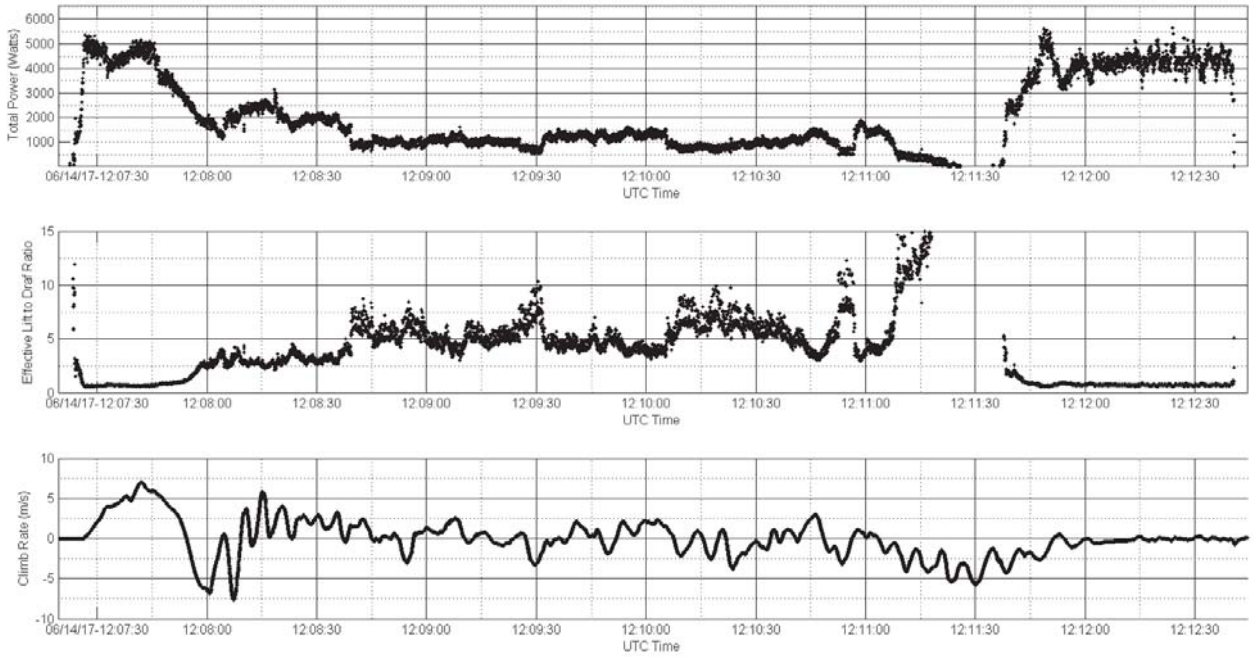

Flight 16 Power Performance

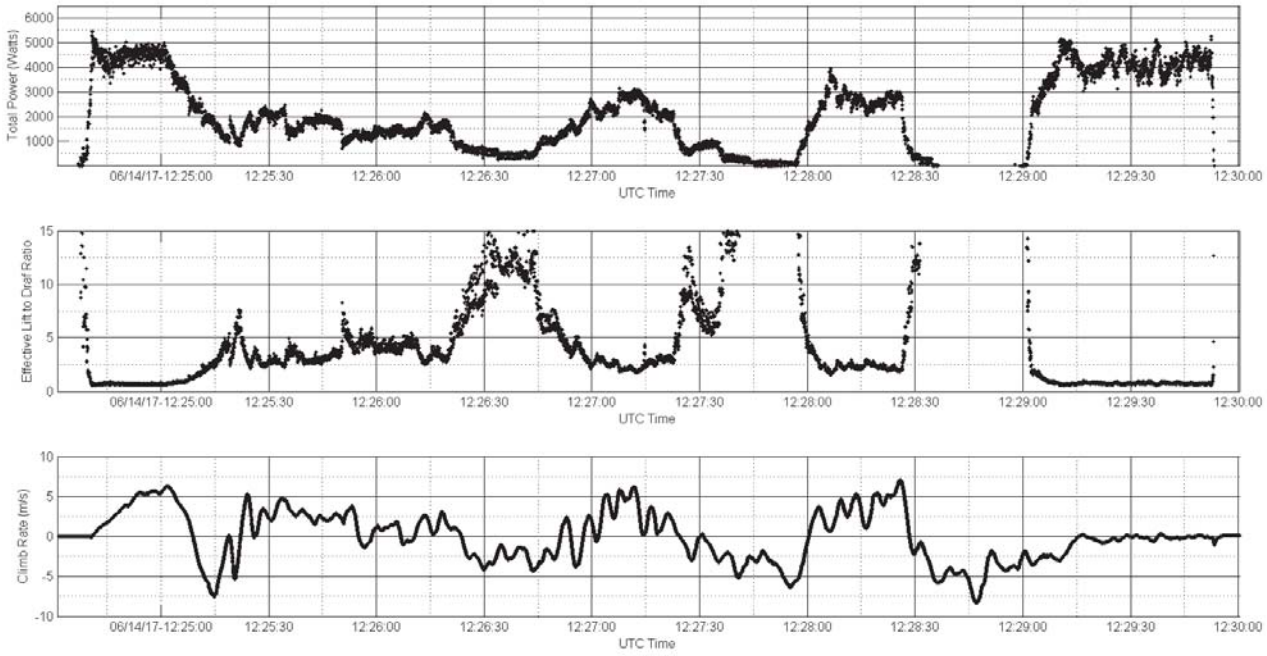

Flight 17 Power Performance

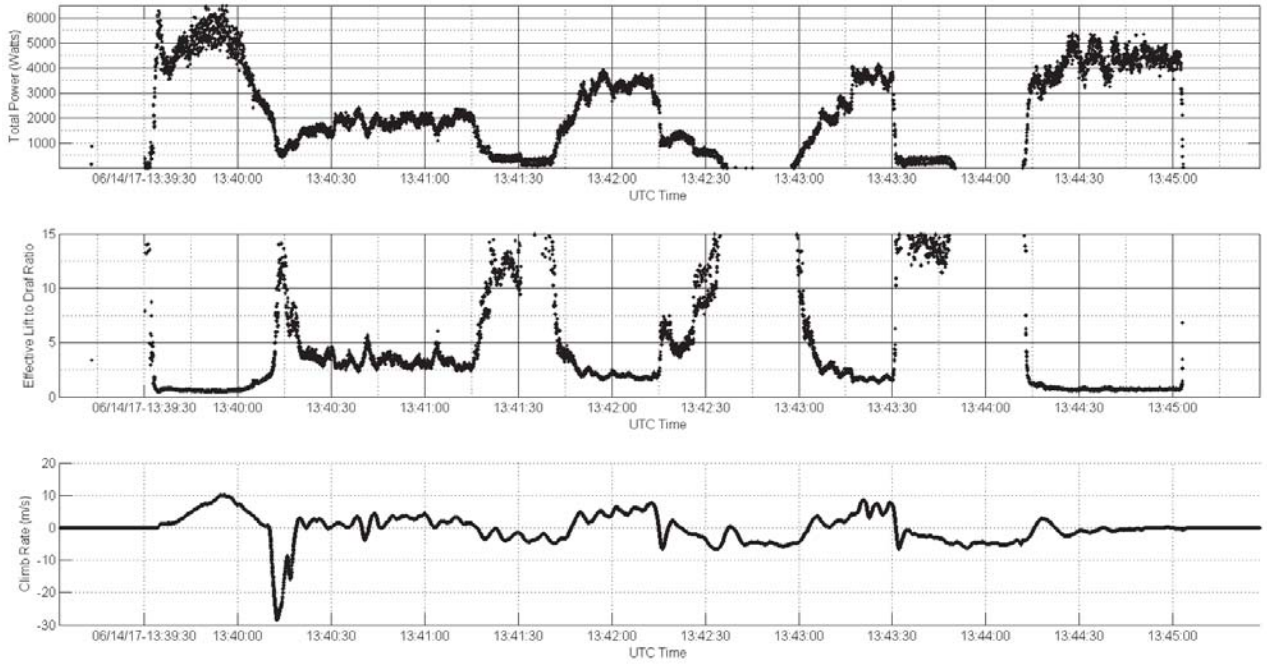

Flight 19 Power Performance

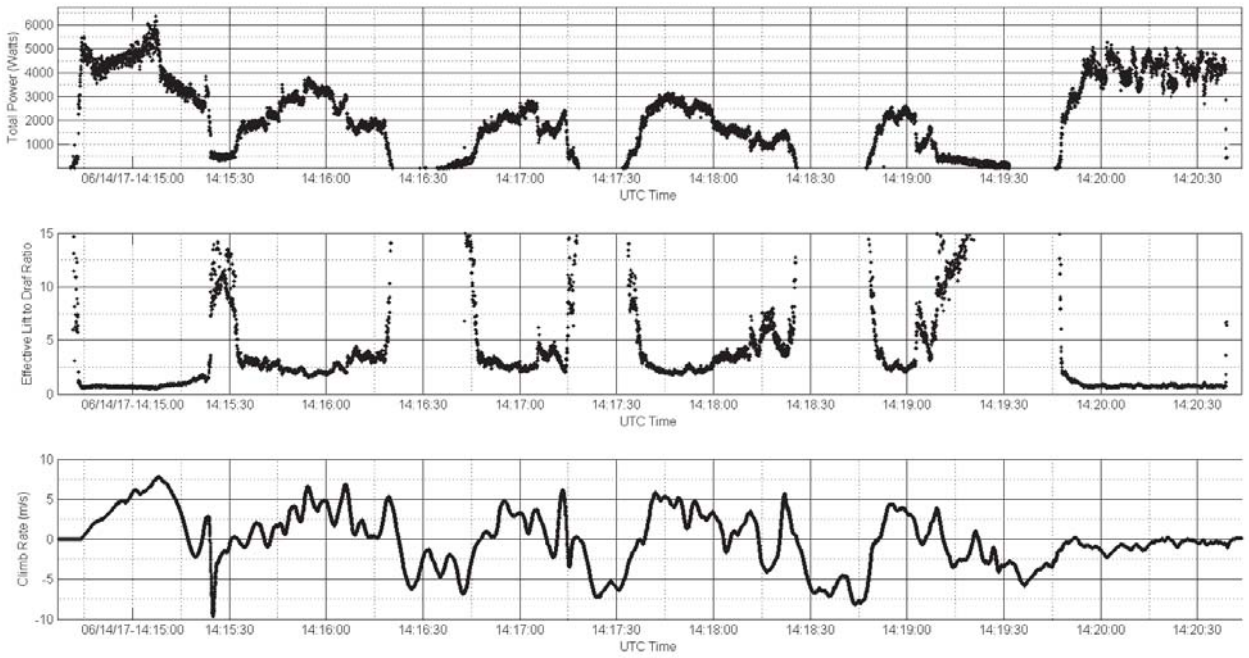

Flight 20 Power Performance

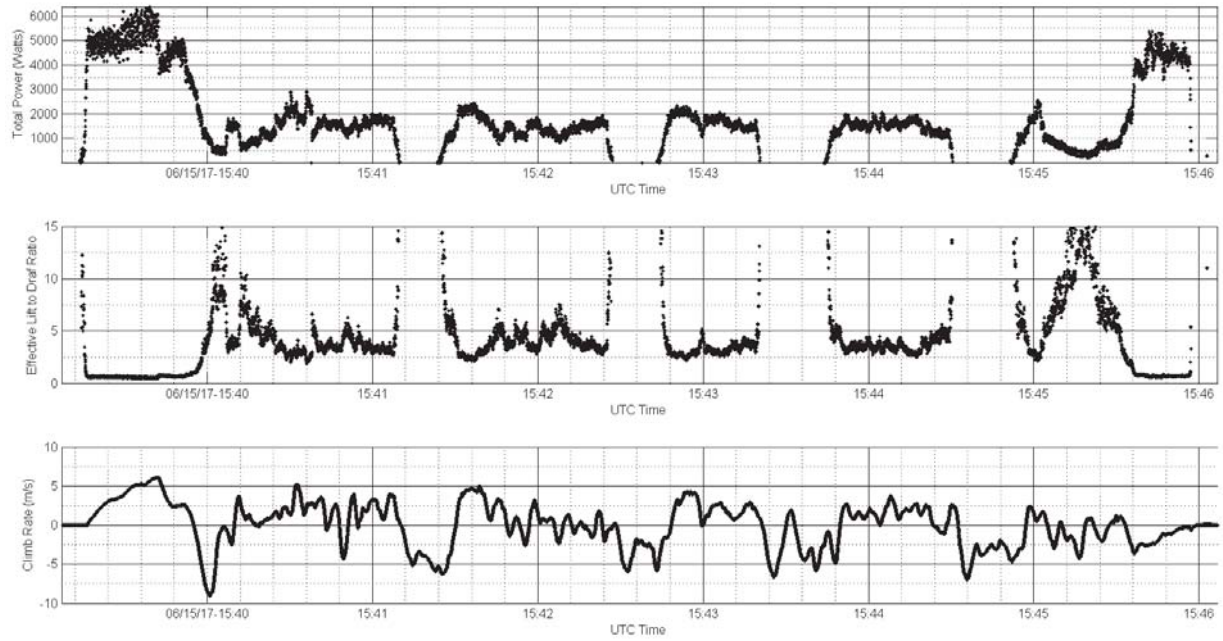

Flight 21 Powered Performance

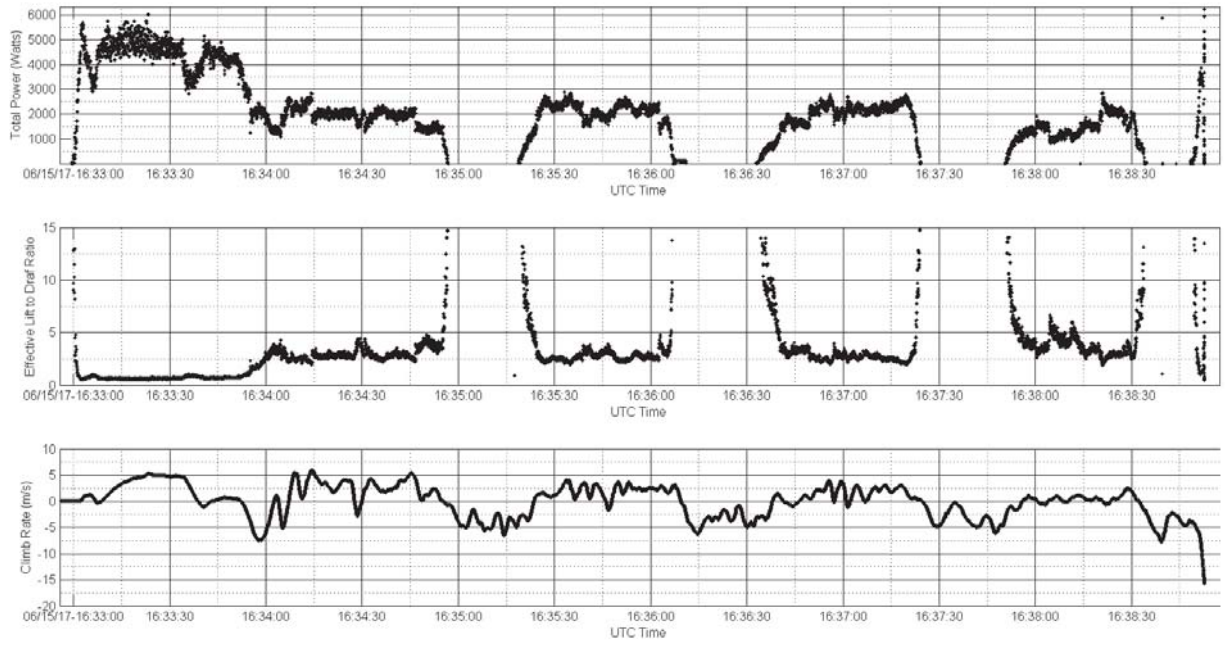

Flight 22 Powered Performance

APPENDIX E: UNPOWERED GLIDE AERODYNAMIC DATA RUN PLOTS

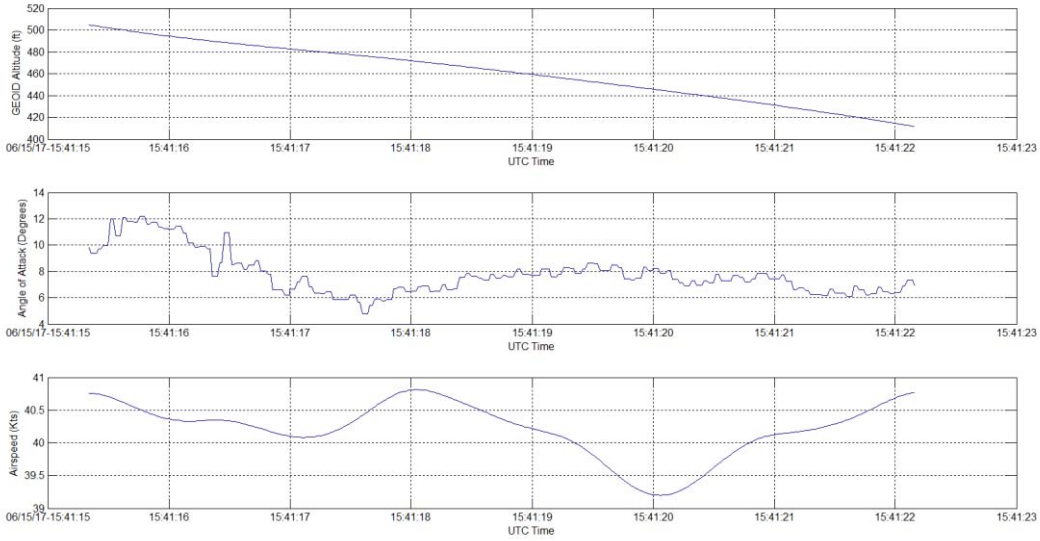

Flight 21 Data Run 1

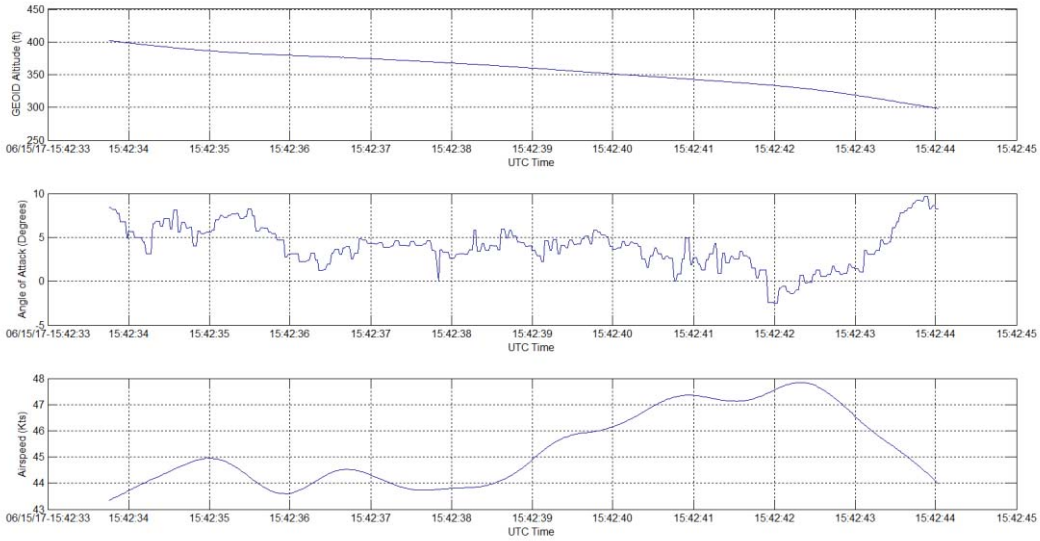

Flight 21 Data Run 2

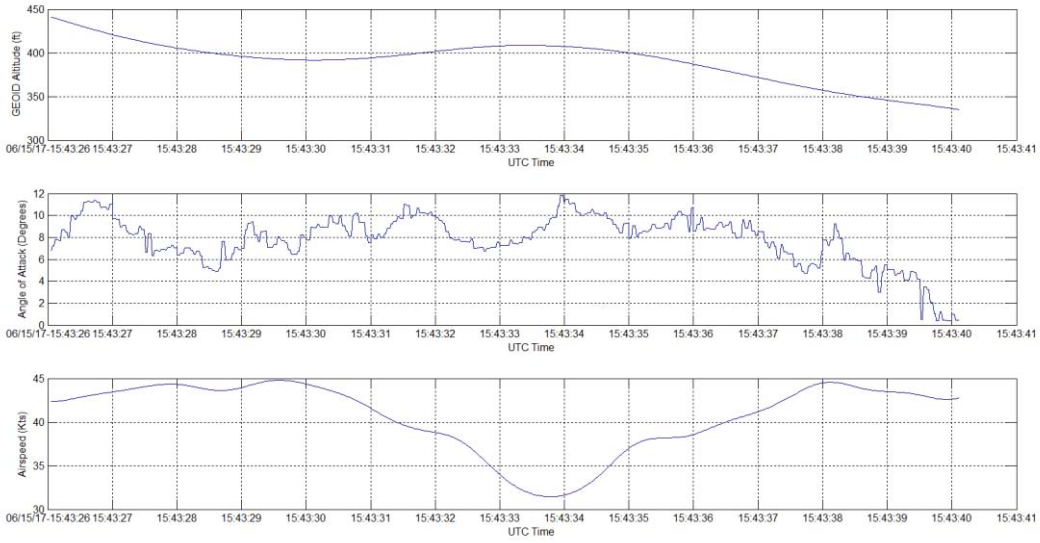

Flight 21 Data Run 3

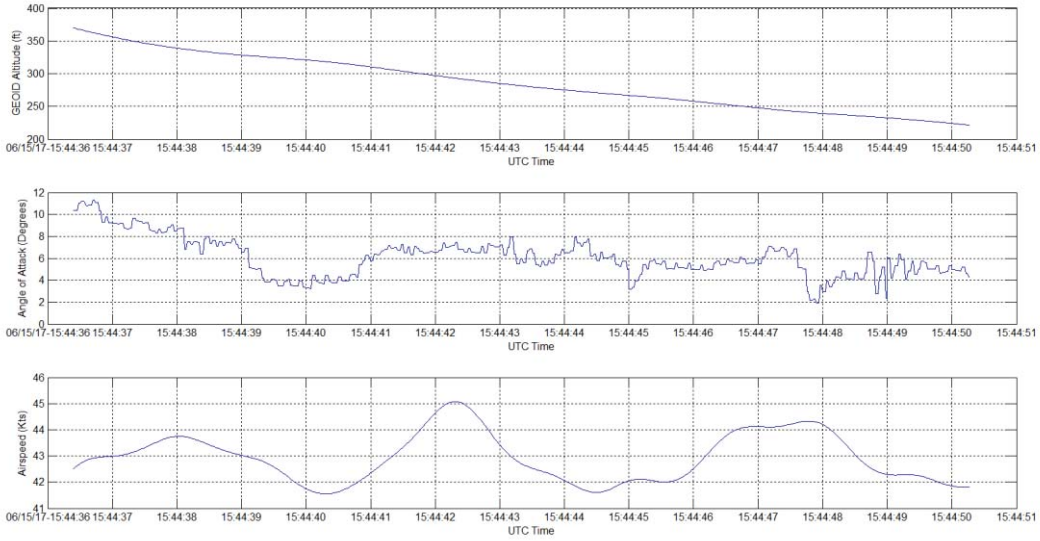

Flight 21 Data Run 4

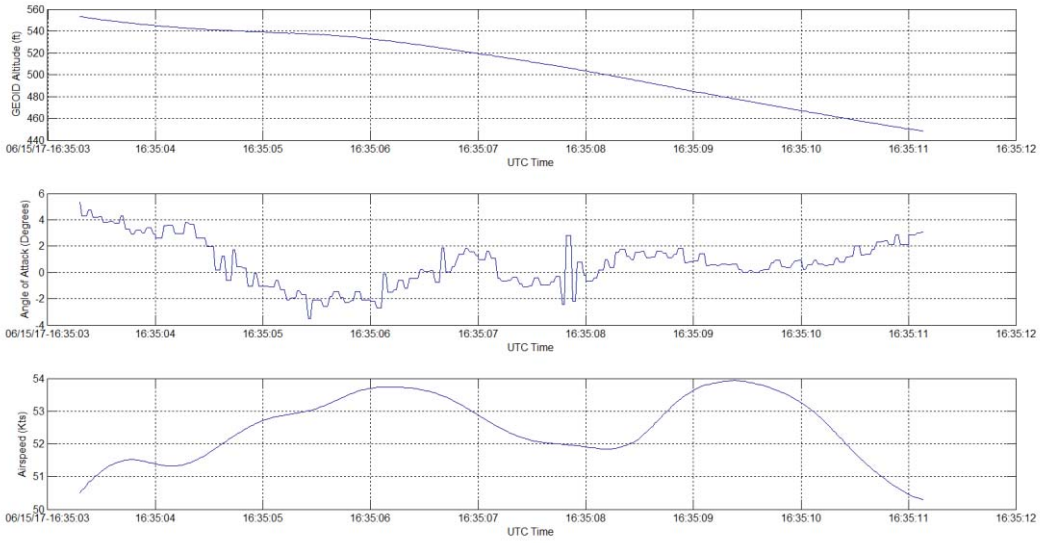

Flight 22 Data Run 1

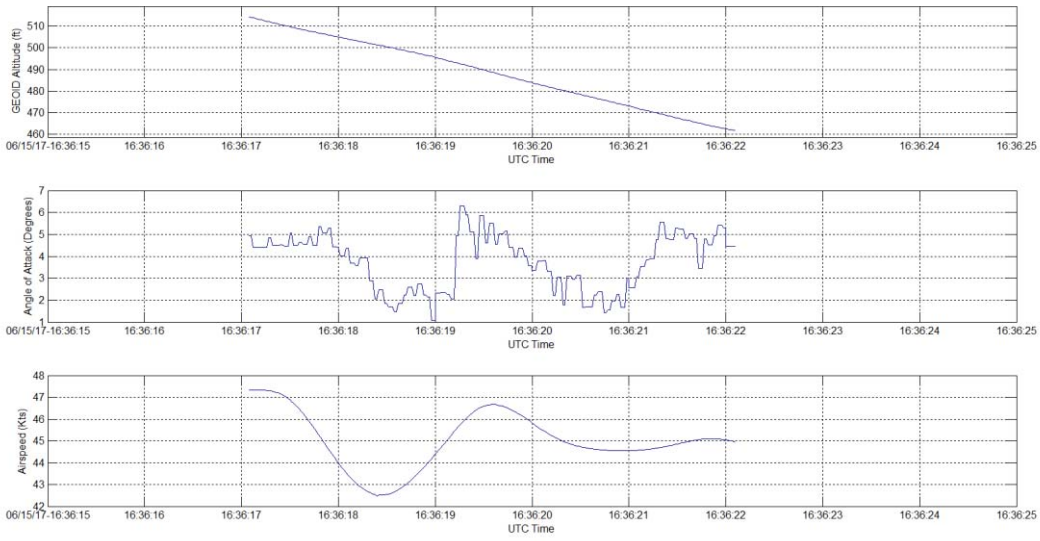

Flight 22 Data Run 2

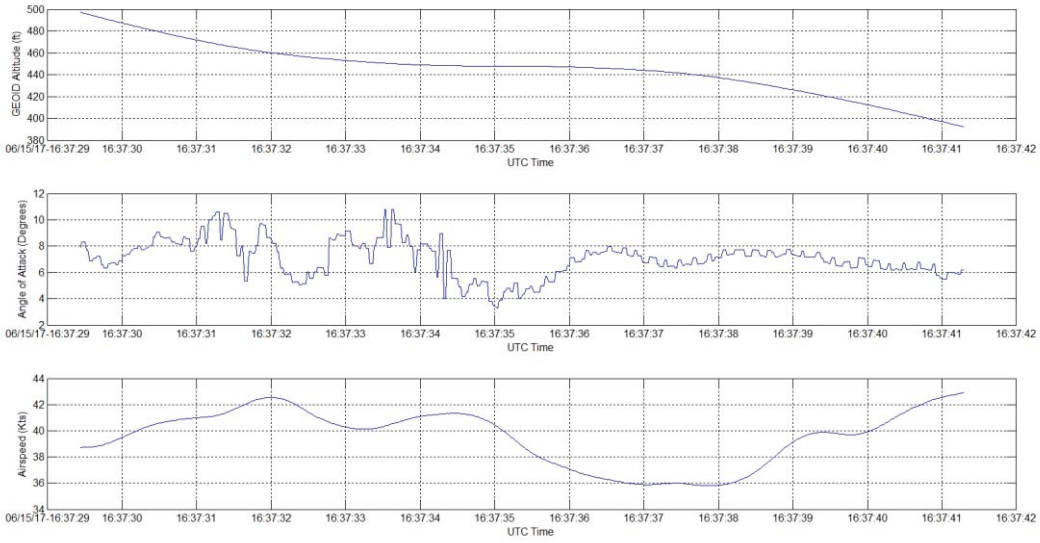

Flight 22 Data Run 3

REPORT DOCUMENTATION PAGE

Form Approved
OMB No. 0704-0188

1. REPORT DATE *(DD-MM-YYYY)*	2. REPORT TYPE	3. DATES COVERED *(From - To)*
01-11-2017	Technical Memorandum	

4. TITLE AND SUBTITLE

Greased Lightning (GL-10) Performance Flight Research - Flight Data Report

5a. CONTRACT NUMBER

5b. GRANT NUMBER

5c. PROGRAM ELEMENT NUMBER

6. AUTHOR(S)

McSwain, Robert G.; Glaab, Louis J.; Theordore, Colin R.; Rhew, Ray D.; North, David D.

5d. PROJECT NUMBER

5e. TASK NUMBER

5f. WORK UNIT NUMBER

533127.02.15.07.01

7. PERFORMING ORGANIZATION NAME(S) AND ADDRESS(ES)

NASA Langley Research Center
Hampton, Virginia 23681-2199

8. PERFORMING ORGANIZATION REPORT NUMBER

L-20888

9. SPONSORING/MONITORING AGENCY NAME(S) AND ADDRESS(ES)

National Aeronautics and Space Administration
Washington, DC 20546-0001

10. SPONSOR/MONITOR'S ACRONYM(S)

NASA

11. SPONSOR/MONITOR'S REPORT NUMBER(S)

NASA-TM-2017-219794

12. DISTRIBUTION/AVAILABILITY STATEMENT

Unclassified
Subject Category 05
Availability: NASA STI Program (757) 864-9658

13. SUPPLEMENTARY NOTES

14. ABSTRACT

Modern aircraft design methods have produced acceptable designs for large conventional aircraft performance. Throughout a long aviation history developing fixed wing aircraft and rotorcraft, many first principle models are built on simplifying assumptions to allow for performance metrics to be derived quickly and reliably for design trade studies. With revolutionary electronic propulsion technologies fueled by the growth in the small UAS (Unmanned Aerial Systems) industry, these same prediction models are being applied to new smaller, and experimental design concepts requiring a VTOL (Vertical Take Off and Landing) capability for ODM (On Demand Mobility). In 2013 NASA designed a hybrid electric VTOL concept aircraft called the Greased Lightning (GL-10). A 50% sub-scale flight model was then built and tested to demonstrate the transition from hover to forward flight utilizing DEP (Distributed Electric Propulsion)[1][2].

15. SUBJECT TERMS

CAS; DELIVER; Flight; GL-10; Performance; Test; UAS; VTOL; sUAS

16. SECURITY CLASSIFICATION OF:			17. LIMITATION OF ABSTRACT	18. NUMBER OF PAGES	19a. NAME OF RESPONSIBLE PERSON
a. REPORT	b. ABSTRACT	c. THIS PAGE			STI Help Desk(email help@sti.nasa.gov
					19b. TELEPHONE NUMBER *(Include area code)*
U	U	U	UU	79	(757) 864-9658